UNIVERSITA' DEGLI STUDI DI MILANO-BICOCCA

Facoltà di Scienze Matematiche, Fisiche e Naturali

Dipartimento di Scienze dell'Ambiente e del Territorio e di Scienze della Terra

LITHOPHYLLUM SPP. AS PROXY OF CLIMATE VARIABILITY IN THE NW INDIAN OCEAN

Relatore: Prof. Daniela BASSO

Candidato:

Annalisa CARAGNANO

Matr. N. 734501

Dottorato in Scienze della Terra

XXV Ciclo

ACKNOWLEDGEMENTS

There are many people I would like to thank both for this work and for these scientific research years. It was also their presence and their advice that allowed me to achieve this important goal. From the point of view of work I have to thank for their patience and availability all those who have worked with me.

Firstly I thank Prof Daniela Basso for introduce me to the wonderful world of coralline red algae, and who believed with me in this project. I am grateful to her great experience who shared with me over the years of working together, and that allowed me to do a better job.

Thanks to Dr Graziella Rodondi for introduce me to biological support on coralline algae, and for her patience and moral support.

Thanks to Francesca Benzoni, my "sister on fieldwork" to share with me joys and pains of these three years, and to allow me to reach the wonderful tropical place involved in this venture.

I am very grateful to Robert Hirst and Yemen LNG, Claude Chaineu and Total E&P, for allowing fieldwork and sampling, and to Eric Dutrieux and Creocean for logistic and organization support. I thank S. Basheen (Professional Divers Yemen) help in different parts of the field work, and to the Environment Protection Authority (EPA) of Socotra for logistic support and for sampling permit.

Thanks to Sébastien Thorin for support and the nice time spent during the fieldwork in Balhaf (Yemen).

In the course of research I had a pleasure to open a collaboration with David Storz from the Institut für Geowissenschaften, Goethe-Universität of Frankfurt, who I am very grateful for suggestions, tips, patience and for his availability shown me.
I am grateful to Jacob Dorrit for teaching in the use of LA-ICP-MS in Mainz and for her sustain in my research.

I wish to thank Federica Ragazzola, Valentina Bracchi and my family that I had been close during this period.

INDEX

1. Introduction

Predictions of future climate trends, and assessment of human impact on climate and ecosystems require knowledge of former climates, especially from the most recent geological past (Alverson et al. 2001). Geochemical signals extracted from carbonate skeletons or shells of marine organisms have been used as paleoenvironmental indicators for reconstructing temperature and salinity variations of surface water masses (Jones 1983; Ganssen and Kroon 1991; Cole et al. 1993). For such an aim, shallow-water corals (mostly massive *Porites* sp. colonies) are commonly used as high-resolution paleoenvironmental archives in tropical marine environments. *Porites* sp. colonies are well suited for geochemical studies due to average growth rates of 10-15mm/y (Tudhope et al. 1996; Storz and Gischler 2011a). Long-living bivalves, such as *Arctica islandica* are commonly used in boreal seas. The main constraint in using shallow water corals as well as *A. islandica* is their limited geographical range. Although non-tropical corals such as *Cladocora caespitosa* are recently used as climate archive from the Mediterranean Sea (Montagna et al. 2007), corals are confined to tropical and subtropical seas, and *A. islandica* to the North Atlantic. Moreover, bivalves are influenced by an ontogenetic, asymptotic growth trend, which lead to a decreased resolution during the later stages of growth (Goodwin et al. 2003), and are often biased by vital effects (Schöne et al. 2011), as well as corals (Cohen and McConnaugey 2003).

Coralline red algae (non-geniculate algae of the order Corallinales) are a major calcifying component of marine benthos from tropical to polar oceans at all depths within the photic zone in almost every habitat type (Fabricius and De'ath 2001; Kuffner et al. 2007). Hence, they have no restriction in geographical distribution, unlike the above mentioned biogenic archives. Additionally, occurring in hard bottom benthic photic zones throughout the world ocean, the many genera and species of non-geniculate corallines are important

framework builders, framework cementers, and infill elements in coral reef environments (Bjork et al. 1995; Basso 2012). Reefs (and portions of reefs) are structured by wave energy, with coralline algae dominating at highest energies (algal ridges), corals dominating at intermediate hydrodynamics (Adey 1998). Coralline red algae can also dominate on deep banks and in fore reef zones (>60 m), if slopes are moderate (Dullo et al. 1990).

Laboratory experiments have shown that the Mg/Ca ratio of abiotic calcite precipitated from artificial seawater is determined by the temperature and Mg/Ca ratio of the precipitating solution (Berner 1975). Chave and Wheeler (1965) found that the amount of magnesium in the skeleton of the red algae *Clathromorphum compactum* varies seasonally in response to changes in sea surface temperature (SST). Additionally, experiments on *Neogoniolithon* sp. have also shown that the amount of Mg incorporated in the calcitic thallus varies as a function of Mg/Ca ratio of the seawater in which the algae is grown (Ries 2006). Although secular variations in the Mg/Ca ratio have occurred in seawater, the modern ocean has a constant value of 5.2 molar (Ries 2006). Until now, only few studies on corallines as potential climate archive exist, and they are mainly concerning species from boreal-subarctic environments (Chave and Wheeler 1965; Halfar et al. 2007; Halfar et al. 2008; Kamenos et al. 2008; Hetzinger et al. 2009; Hetzinger et al. 2011; Halfar et al. 2011). Frantz et al. (2000) found in a sub-tropical rhodolith of *Lithothamnion crassiusculum*, evidence for El Niño-Southern Oscillation (ENSO). Halfar et al. (2000) found a good correlation of Mg/Ca with $\delta^{18}O$ and SST for the same species. However, it is not clear how much algal metabolism exerts control on Mg-carbonate chemistry. Ries (2006) and Kamenos et al. (2008) suggest no significant vital effect for the Mg-fractionation in coralline algae and suggest that SST is the dominant factor controlling Mg-carbonate chemistry. In a phylomolecular study of 191 coralline specimens from New Zealand, in contrast, Smith et al. (2012) report that latitude (as

a proxy for SST) has only a slight relationship to Mg content. Fragoso et al. (2010) speculate on phylogenetic control on small biomineralogical variations within the Corallinales. Moberly (1968) suggested that the Mg content in calcite of coralline red algae depends on growth rates, which is a function of water temperature, light intensity and physiological cycle.

The Li/Ca ratio has a constant concentration in the present day ocean (Delaney et al. 1985). The major marine Li sources are rivers and hydrothermal activity (Edmond et al. 1979; Stoffyn-Egli and Mackenzie, 1984). The application of Li/Ca ratio as paleoceanographic proxy in carbonate skeletons or shells of marine organism is limited and controversially discussed. An inverse correlation between Li/Ca and temperature is seen in studies on inorganic calcite and in aragonite skeletons of corals and brachiopod shells (Marriott et al. 2004; Montagna et al. 2008; Delaney et al. 1989), while other studies on planktonic foraminiferal tests and corals found no significant correlation between Li/Ca and temperature yet and suggested that the incorporation of Li is controlled by non-SST factors (Delaney et al. 1985; Hall and Chan 2004; Rollion-Bard et al. 2009; Hall and Chan 2004). Since Li/Ca ratio was never investigated in the coralline algae thallus, nothing is known on the incorporation of this element into algal skeleton, and a relationship with temperature might be found in agreement with Marriott et al. (2004), Montagna et al (2008) and Delaney et al (1989).

Barium content of foraminifera shells and coral aragonite was used to reconstruct oceanic Ba distribution and as nutrient proxy (Lea and Boyle 1989, 1993; Lea and Martin 1996; Tudhope et al 1996). Ba substitutes Ca into the lattice of carbonate of coral skeleton and foraminiferal shell in equilibrium with seawater content (Lea and Boyle 1989). Hence, these works suggest that also coralline red algae could provide a quantitative record of seawater Ba content and an archive of upwelling intensity.

The predominant climate phenomenon of the subtropical sampling area is the Asian Monsoon system, which is characterized by seasonal reversals of the surface wind system and a distinct seasonality of precipitation. It is driven by the seasonal shift of the Inter-Tropical Convergence Zone (ITCZ), due to different heating of the Eurasian subcontinent and the Indian Ocean (Webster et al.1998; Al Saafani and Shenoi 2004; Al Saafani 2008). Upwelling of deep water occurred during the summer monsoon season, in the northwest Indian Ocean, and with different intensity in the Gulf of Aden (Al Saafani and Shenoi 2007). The hydrography and oceanography of the South Red Sea are strongly influenced by the south Asian monsoon system (Edwards 1987; Al Saafani and Shenoi 2004). Additionally, the Indian Ocean climate is affected by the El Niño-Southern Oscillation (ENSO) phenomenon, centered in the tropical East Pacific (Torrence and Webster 1999). It force the south Asian monsoon. In fact, warmest SSTs in the Indian Ocean are found in non-El Niño years in the eastern part of the Indian Ocean, with above-average precipitation during the SW monsoon season, and strong El Niño years cause higher than normal SSTs in the western equatorial Indian Ocean (Bhatt 1989; Webster et al. 1998).

Coralline red algae are slow growing and, some of them are long living species that can live more than 800 yrs (Halfar et al. 2007). Among crustose coralline algae, the genus *Clathromorphum* is particularly suitable for geochemical reconstruction of the paleoclimate, because it is one of the few encrusting coralline algae genera forming thickness individuals, even up 5 cm thick (Halfar et al. 2007). Indeed, rhodoliths (free-living coralline algae), as the thick long-lived nodules formed by the genera *Lithothamnion* and *Phymatolithon*, are considered the more suitable for paleoclimate reconstruction (Foster 2001). Moreover, these genera show clear growth banding in longitudinal section of the thallus, which are interpreted

as annual growth bands (Adey and McKibbin 1970; Basso 1994; Basso et al. 1997; Foster 2001).

The aim of this study is to contribute to a better understanding and application of coralline red algae as paleoclimatic archive. Although coralline red algae are widely distributed in the world oceans and resilient to a variety of environmental disturbances, rhodoliths are not common in some environments or confined to specific depth range. Additionally, *Clathromorphum* is geographically restricted and encrusting coralline algae are not usually so thick, rather, their strategy is often a marginal growth. Therefore there is a need to improve our knowledge on the potential of coralline algae as biogenic archive of paleoenvironmental signals across different environments, and thus to enlarge these studies on other coralline genera or families. In this study, the thalli of two forms of *Lithophyllum kotschyanum* f. *affine* (rhodolith and attached crust) from South Red Sea and Gulf of Aden, and a rhodolith of *Lithophyllum* sp. from west Arabian Sea, were analyzed geochemically on high-resolution with respect to their Mg/Ca, Li/Ca and Ba/Ca ratios, as well the algal extension rates, to investigate their application for paleoclimatic reconstructions. Contrarily to previous studies of geochemical proxies in corallines, *L.kotschyanum* f. *affine* and *Lithophyllum* sp. belong to a different phyletic line and their validity as paleoclimatic archive has not been explored yet.

2. Biomineralization in coralline red algae

Biomineralization is the process whereby organisms form minerals, and research in this field provides an excellent example at the interface between the earth and life sciences. The term biomineral refers not only to the mineral itself, but also to the organic components associated with the process of biomineralization (Weiner and Dove 2003). These processes, reflecting the degree of biological control, are divided into two fundamentally different groups (James and Austin 2008): “biologically induced” and “organic matrix-mediated”. In the first case, it is recognized a process of secondary precipitation of minerals resulting from the interactions between biological activity and the environment (McConnaughey 1989). In biologically controlled mineralization, a generalized term for organic matrix-mediated mineralization adopted by Mann (1983), cellular activity locates and controls the nucleation, growth and morphology of the biomineral. As such, both, biological processes and environmental signals are encoded into biominerals, the former often know as “vital effects” (James and Austin 2008). One of the major challenges now facing the palaeoceanographic community is the need to improve our understanding of some of the fundamental controls on the mechanisms of biomineralization and an understanding of vital effects is central to this effort (James and Austin 2008).

Calcification can occur in the red algae either as a constant and characteristic systematic feature of a group (Corallinaceae) or as a variable character according to the genera and species (Peyssonneliaceae). Calcification within the red algae was only observed in the subclass Florideophycideae. The orders of the Sporolithales and Corallinales are always calcified (Pueschel and Cole 1982, Le Gall et al. 2009). The subfamily of Lithophylloideae, considered in this study, belong to the family Corallinaceae, order Corallinales.

The thallus of Corallinales and Sporolithales develops from a thin crust, is composed of cell filaments that are connected together, and growth by division of the filaments and by addition of one new cell at the tip of each filament (Johansen 1981). The cell walls of the coralline thallus are completely calcified, with two exceptions: the reproductive cells (meristematic cells) and the superficial wall of the outermost epithallial cells in contact with seawater (Fig 2.1A).

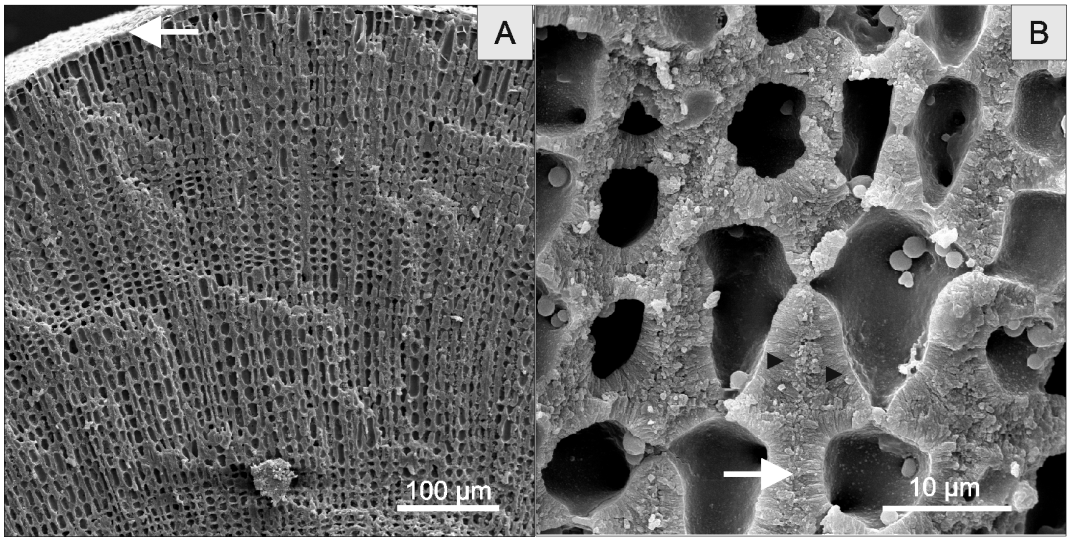

Fig. 2.1 SEM photos of longitudinal section of coralline thallus: A) *Lithophyllum kotschyanum* from Nabq (Gulf of Aqaba, North Red Sea) showing epithallus (arrow) and inward the perithallus structure. Hypothallus of coralline algae is inward the perithallus, on base of algae; B) *Lithophyllum* sp. from Socotra (DB635) showing transversal section of thin needles of Mg-calcite crystals (arrow) and the plate crystals perpendicular to the cell wall (arrowheads).

The calcification in these calcified algae occurs directly in the vegetative cell wall. The calcification appears to be controlled by a polysaccharide matrix. In the first stages of the young superficial cells (initial hypothallial and young perithallial cells), calcification occurs as two successive processes:

1) In the outer zone the general envelope contains thin needles arranged tangential to the cells and to parallel to the polysaccharide fibrils. Towards the base of the outer cells needles change progressively into plates. Among the epithallial cells, in the youngest part, only tangential crystals can be observed and they are regularly arranged in the lateral walls (Fig. 2.1).
2) Inwards, from the perithallial meristem and directly under the epithallus, calcification increases and a second phase can be observed in the form of crystallization perpendicular to the cell wall (Fig. 2.1B). These secondary crystal are very closely juxtaposed and form in contact with the plasmalemma.

The thickness of the cell-wall may vary either within a species or from one species to another (Cabioch and Giraud 1986). Although Walker and Moss (1984) found that some species of coralline algae repair damage to their substrate attachment with granules of aragonite, the cell-walls of coralline algae are composed of Mg-calcite, with [Mg] increasing in the calcite lattice as the temperature increases, in seawater with present-day Mg/Ca mole ratio (Chave 1954, Chave and Wheeler 1965, Basso 1992, Halfar et al. 2000, Basso 2012). The most important parameter controlling the precipitation of a solid from solution is the degree of supersaturation. The incorporations of elements into the structure and their dependence on the environmental parameters have to be known. Partition laws quantify distribution of an element between bulk solid and aqueous solution (empirically). The homogeneous partitioning coefficient D for a trace element T is given relative to the major element C it replaces:

$$\frac{[T_{bulk}]}{[C_{bulk}]} = D\frac{[T_{sol}]}{[C_{sol}]}$$

The substitution of cations in carbonates is mainly controlled by ion size, and charge plays only a secondary role. Thus Sr, which has a larger ionic radius than Ca, fits better into the orthorhombic structure of aragonite than into the hexagonal structure of calcite. Partitioning coefficients are strongly dependent on temperature. Trace element concentrations are therefore, often used as temperature proxy, but also other parameters such as precipitation rate or presence of other trace elements are influencing the partitioning coefficient.

3. Regional Setting

3.2. Balhaf (Yemen, Gulf of Aden)

Balhaf is located on the coast of Yemen at 13°58.5N; 48°10.5E (Fig. 3.1). This area is characterized by coral carpets of few centimeters to 1 m thick, with living coral cover of 24-78% (Benzoni et al. 2003). The coralline cover by attached forms is more than 16% (Benzoni et al. 2011), although the technique used by Benzoni et al. (2011) may underestimate the algae cover (Caragnano et al. 2009). Very few and small specimens of rhodoliths were observed during the same study.

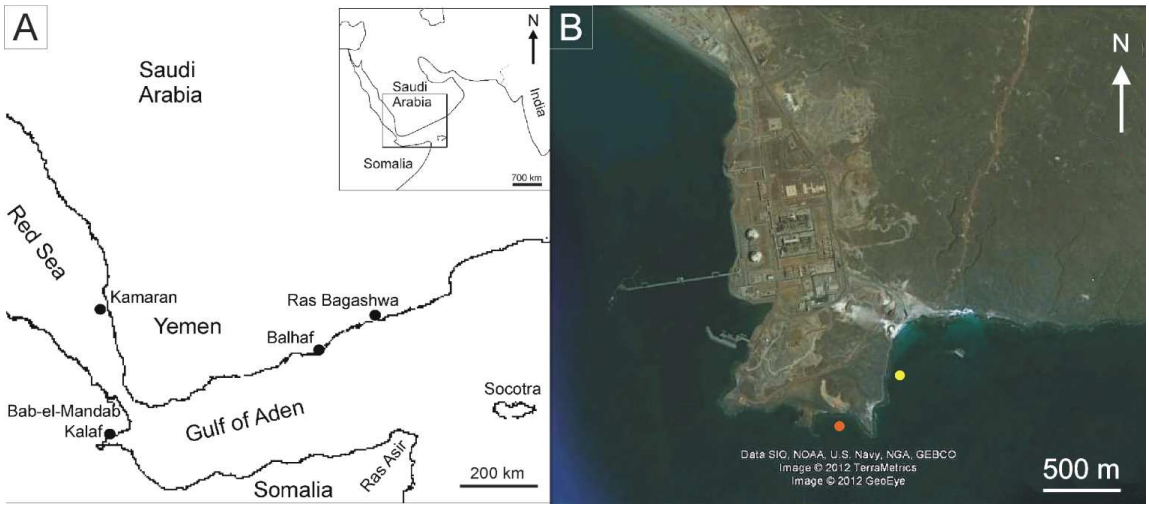

Fig. 3.1 Map of the study area: A) location map of the Gulf of Aden between the Red Sea and the north-west Indian Ocean; B) satellite photo of Balhaf by the software google earth 7.0.2, the circles indicate the sampling sites (yellow for DB659 specimen, and red for DB657 specimen).

The Gulf of Aden is 900 km long, it spreads over an area of about $220x10^3$ km^2, and up to about 1800 m deep and connects the Red Sea with the north-west Indian Ocean (Al Saafani and Shenoi 2007). It extends from west-northeastward from the Strait of Bab-el Mandab to an

imaginary line connecting Ras Baghashwa (Yemen coast) and Ras Asir (northern corner of the Somalia Peninsula, Fig. 3.1A). Its hydrography and climate is strongly affected by the Indian monsoon system (Al Saafani and Shenoi 2004; Al Saafani 2008). About 37% of the total volume of water mass in the Gulf of Aden is the Red Sea water, one of the most saline water masses in the world oceans (Al Saafani 2008). Four water masses are identified from salinity by Al Saafani and Shenoi (2007). The surface water (between 0 and 100 m depth) reaches a salinity maximum near the surface, and it is a mixture of local water and western Arabian Sea water during winter, and with Red Sea surface water during summer (Al Saafani and Shenoi 2007; Al Saafani 2008). Between 120 and 420 m depth the water mass is characterized by low salinity due to the northward spread of sub-tropical surface water from the south (Al Saafani and Shenoi 2007; Al Saafani 2008). The third water mass (350-1050 m depth) is the Red Sea water that shows a salinity maximum (Al Saafani and Shenoi 2007). The bottom water mass (1200-1600 m depth) is characterized by a mixture of Red Sea water and water of southern origin. Upwelling of deep water occurs during the summer monsoon season, in the northwestern Indian Ocean, and with different intensity in the Gulf of Aden (Al Saafani and Shenoi 2007; Fig. 3.2).

In situ regular records of the oceanographic parameters from Balhaf are not available. Therefore, have been used gridded instrumental climate records, that averaged over a geographical range and include various marine settings. Sources and references of all climate datasets used in this thesis are given in Table 1.

Table 1 Instrumental records of Sea Surface Temperature (SST), Sea Surface Salinity (SSS), precipitation, sea level pressure (SLP), wind speed, zonal surface currents, used in this study. Abbreviations used here and in the text: HadiSST: Hadley Centre Global Sea Ice and Sea Surface Temperature; SODA: Simple Ocean Data reanalysis project; ICOADS: International Comprehensive Ocean-Atmosphere Dataset; CRU: University of East Anglia Climate Research Unit.

Record	Grid	Reference
HadISST1	1°x1°; 47-48°E, 12-13°N; 54-55°E, 13-14°N	Rayner et al. (2003; http://www.metoffice.gov.uk/hadobs/hadisst/)
Zonal surface currents	0.5°x0.5°; 46-46.5°E, 12-12.5°N; 53-53.5°E, 12-12.5°N; 40-40.5°E, 16-16.5°N	SODA, Carton et al. (2005; http://apdrc.soest.hawaii.edu/)
SLP	2°x2° 40-42°E, 14-16°N	ICOADS v2.5 Woodruff et al. (2011; http://www.icoads.noaa.gov/)
Wind speed	1°x1° 46-48°E, 12-14°N; 53-54°E, 13-14°N	ICOADS v2.5 Woodruff et al. (2011; http://www.icoads.noaa.gov/)
SSS	0.5°x0.5°; 46-46.5°E, 12-12.5°N; 53-53.5°E, 12-12.5°N; 40-40.5°E, 16-16.5°N	SODA, Carton et al. (2005; http://apdrc.soest.hawaii.edu/)
Precipitation	1°x1°; 46-47°E, 13-14°N; 29-30°E, 30-31°N	CRU TS3.10, Mitchell and Jones (2005; http://www.cru.uea.ac.uk/cru/data/)
Seasonal South India rainfall (June-Sept)	0.5°x0.5°; 74-74.5°E, 13-13.5°N	IMD (CCCR; http://cccr.tropmet.res.in/cccr/home/index.jsp)

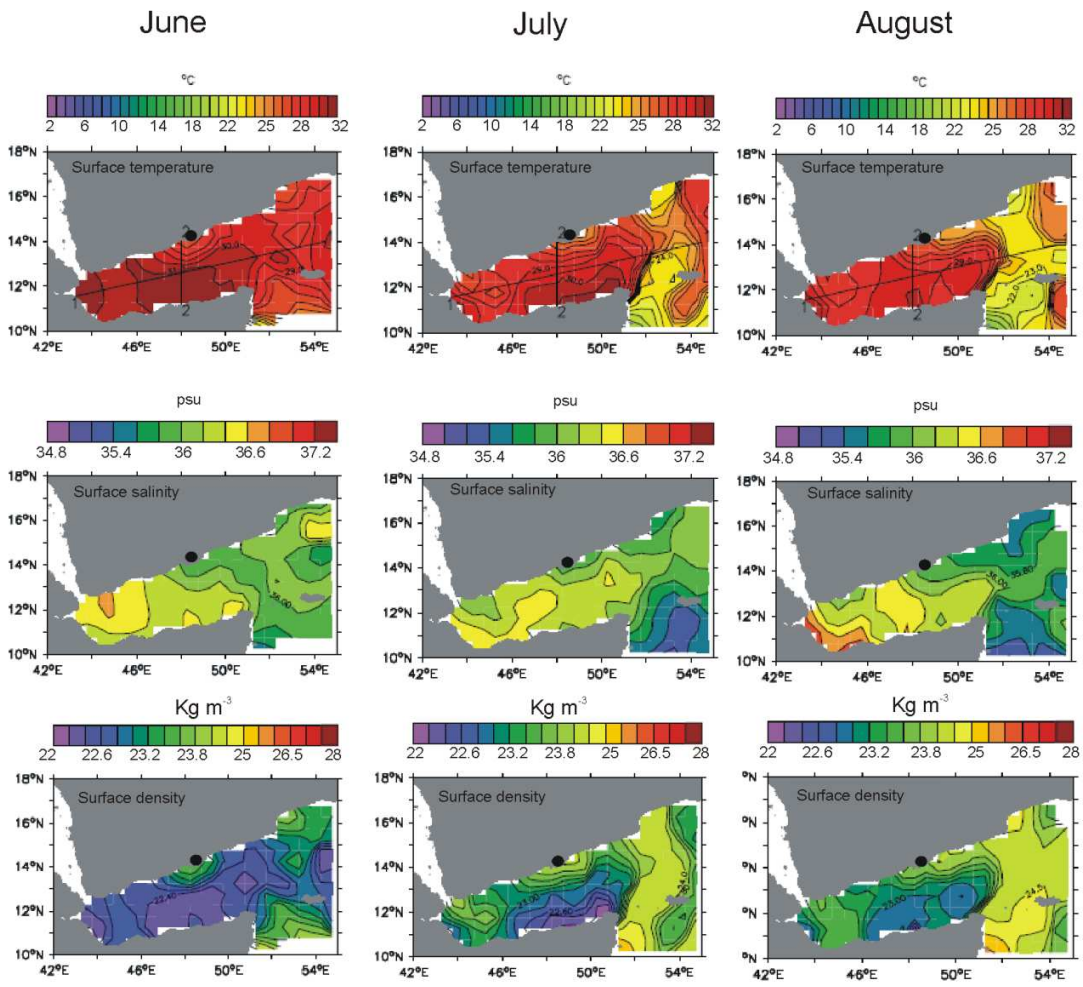

Fig. 3.2 Horizontal distribution of sea surface temperature, salinity and density in the Gulf of Aden during the SW monsoon. The black circle indicates Balhaf (from Al Saafani 2008).

During the winter monsoon season (November-March), the net flow in the gulf is westwards and during the summer monsoon (June- September) eastwards along the northern side of the gulf, westward along the southern side, and an anticyclonic eddy is seen at the center of the gulf (Al Saafani 2008; Fig. 3.3). The wind speed record in Balhaf (Fig. 3.4A) does not show a bimodal seasonal pattern with the highest values in July at the onset of the wet SW monsoon. The seasonal reversal of the monsoon winds force the reversal of sea surface currents (SSC) at zonal of Balhaf (Fig. 3.4B).

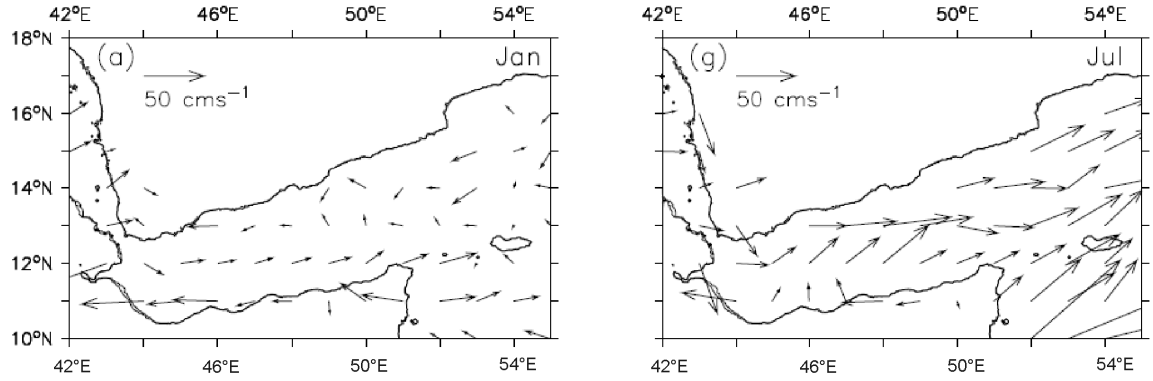

Fig. 3.3 The surface currents derived from ship drifts (cm s^{-1}) during the NE monsoon (on the left) and the SW monsoon (on the right). The surce for the ship drifts is the Ocean Current Drifter Data CDROMs NODC-53 and NODC-54 (NODC, Department of Commerce, NOAA) (from Al Saafani 2008).

Monthly zonal surface currents from Simple Ocean Data reanalysis project (SODA) gridded over 46-46.5°E, 12-12.5°N was used in this study as an indicator of monsoon current strength in Balhaf. South Indian precipitation from Indian Meteorological Department (IMD) dataset was usedas further indicator of the strength of the summer monsoon. Salinity (SSS) fluctuates between 36.05 (January) and 36.57 psu (October) in the gridded SSS record, and it exhibits a bimodal pattern (Fig. 3.5B). Although, precipitation in Balhaf shows a bimodal pattern as found for SSS, both records are not in phase (Fig. 3.5A and B). This may be due to the fact that hydrological cycle in the Gulf of Aden is coupled to atmosphere (monsoon system) and the Red Sea water mass cycle (Al Saafani and Shenoi 2007). During summer Red Sea water mass, one of the most saline water masses in the world oceans, inflow into the Gulf of Aden. Additionally, during summer monsoon, the currents induce upwelling of deep water mass, that is a mixture of Red Sea water and water of southern origin. Moreover, wind stress evaporation during summer may also contribute to higher salinity during the wet summer monsoon season.

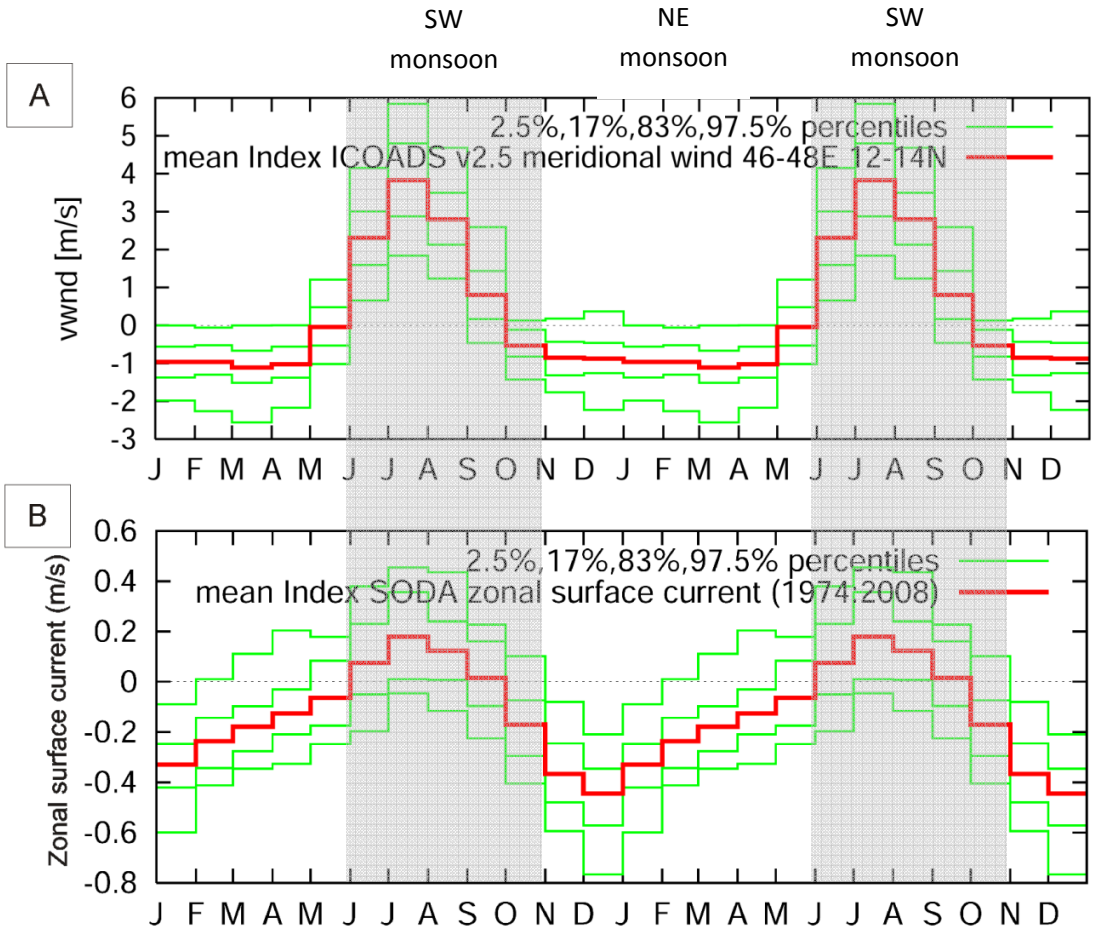

Fig. 3.4 Two mean seasonal cycles to Balhaf of A) the monthly gridded ICOADS wind speed records since 1974 (Woodruff et al. 1998), B) the monthly gridded SODA zonal currents record since 1974 (graphs was run with the KNMI climate explorer web application, www.climexp.knmi.nl). Note that positive velocities correspond to zonal velocity vectors orientated towards west, predominant during SW monsoon season, while negative velocities accordingly correspond to vector oriented towards east, predominant during the NE monsoon season.

The SST shows distinct seasonal variability in Balhaf (Fig. 3.5C). It is highest in May-June (31-32 °C), and undergoes a cooling during the summer monsoon in July-August (29-30 °C) depending on the strength of the westerly monsoon winds. Due of the weakening of the summer monsoon winds in September, a heating of sea water surface takes place (up to 30 °C). Afterwards, it cools again in October-January (24-25 °C) in response to winter monsoonal north-

easterly winds (Al Saafani 2008). The westerly winds during summer monsoon season cause upwelling of cooler water along the northern part of the gulf that are rich in nutrients (Sheppard et al. 1992; Al Saafani 2008). The gridded SST record shows a mean seasonality of 5.5 °C (HadiSST1 dataset, Fig. 3.5C), and exhibits a bimodal pattern, which is in phase with SSS (Fig. 3.5B and C).

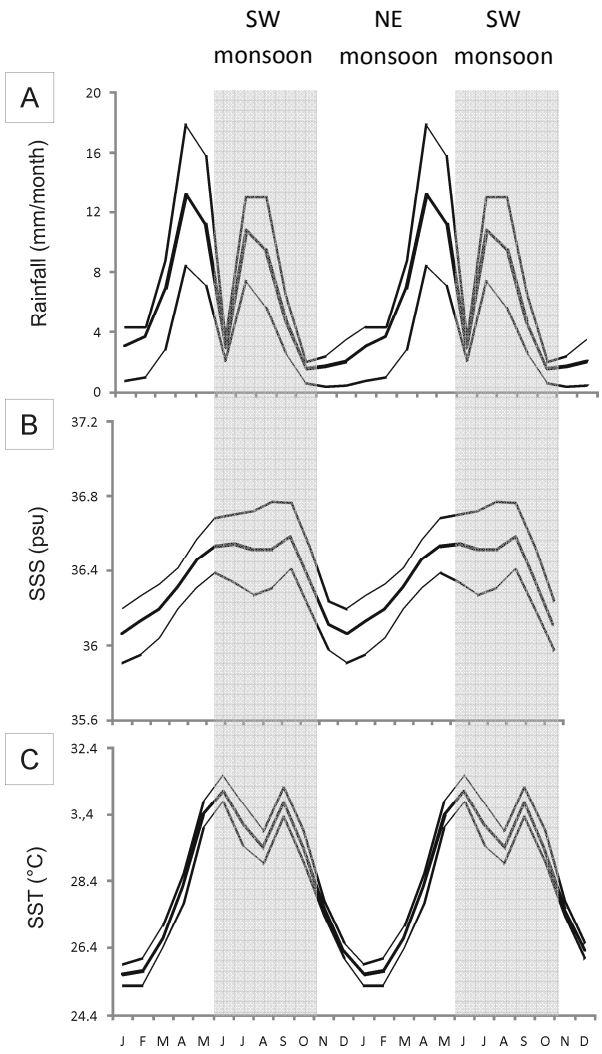

Fig. 3.5 Two mean seasonal cycles to Balhaf of A) the local monthly gridded CRU precipitation records since 1974 (Mitchell and Jones 2005), B) the monthly gridded SODA SSS records since 1974 (Carton et al. 2005), C) the monthly gridded HadiSST since 1974 (Rayner et al. 2003). Note that the highest values are during the SW monsoon.

The predominant climate phenomenon in the Indian Ocean climate north of 10°S is the Indian monsoon system, but the last decades of research showed that climate variability in the Indian Ocean are mainly triggered by the Pacific. Thus the Indian Ocean climate is affected by the El Niño-Southern Oscillation (ENSO) phenomenon, centered in the tropical East Pacific (Torrence and Webster 1999). The large-scale climate phenomenon ENSO describes an oscillation in sea level atmospheric pressure between the central Pacific and the north Australian/Indonesian region. Relatively low atmospheric pressure in the central Pacific and high pressure over Indonesia results in a negative value of the Tahiti-Darwin South Oscillation Index (SOI; based on SLP), and indicates the "warm" El Niño phase of the Southern Oscillation, while the opposite pressure regime describes the "cold" La Niña phase of the oscillation. Previous studies have shown that year with above-average precipitation during the SW monsoon season over India, are often coincident with a positive SOI, with low pressure and relatively warm temperatures over the Indonesian region and increased pressure and cool temperatures over the eastern Pacific Ocean, and vice versa in poor monsoon years (Bhatt 1989; Webster et al. 1998). In this study, the Niño 3.4 index is used as a reliable proxy for the strength of ENSO, and is based on SST (HadiSST1) anomalies in the central Pacific (Trenberth 1997; Fig. 3.6A). The field correlation in Figure 3.6B shows the weak and significant (p-value>0.0001) positive correlation between SST variability and Niño 3.4 in the interannual band. The cross-spectral analysis between gridded SST of Balhaf and Niño 3.4 reveals the typical modes of ENSO forcing in the interannual range of the SST spectrum (Fig. 3.6C). No significant coherence is found for SST and Niño 3.4 in the decadal band (HadiSST1; Fig. 3.6C).

SST exhibit a significant long-term trend since 1974 (r=0.5, p-value>0.0001 for HadiSST1). The HadiSST1 datasets indicate a SST rise of 0.55 since 1974. Available SODA SSS

data since 1974 indicate a negligible freshening trend (r=-0.23, p-value=0.18), such as the precipitation record (CRU TS3.10) since 1974 does not show a secular trend.

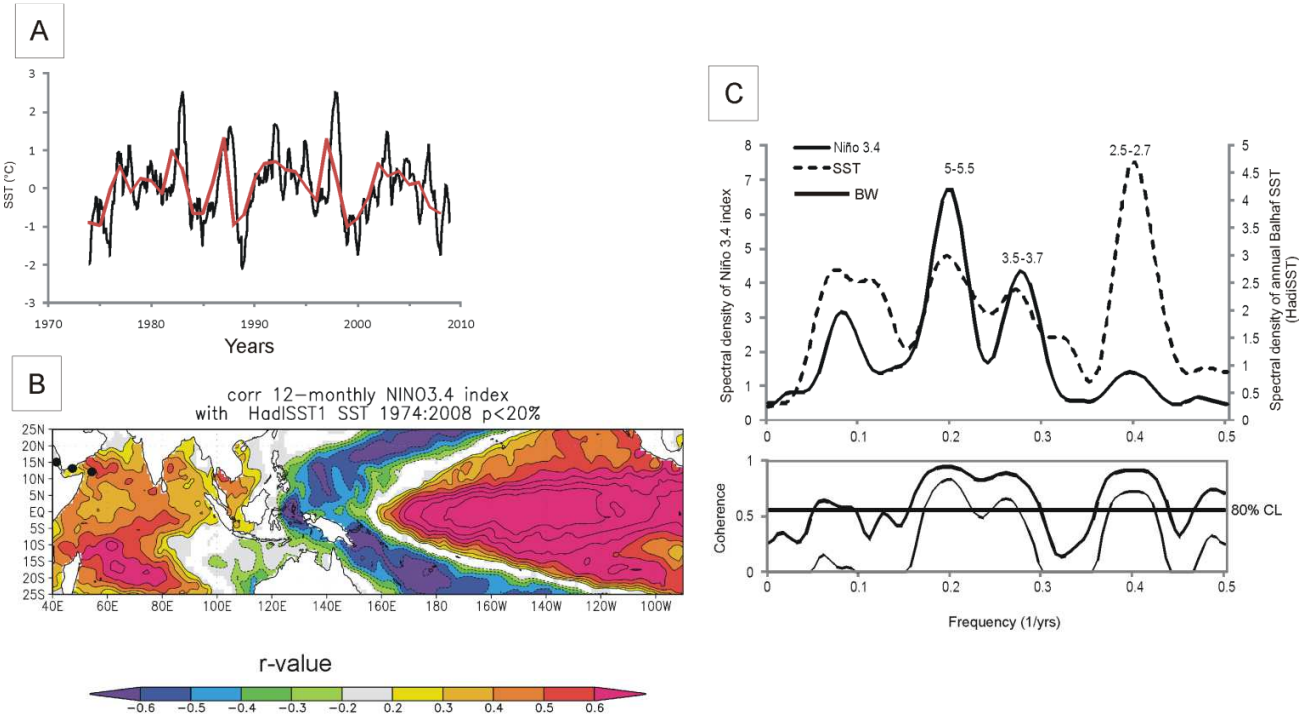

Fig. 3.6 A) Monthly and annual record of the ENSO index Niño 3.4 (based on HadiSST1). B) R-values of running correlations between the 12-months averaged high-pass filtered (year-on-year difference) record of Niño 3.4, and SST fields (based on HadiSST1) in the Indo-Pacific, based on a grid of 1°x1° for period 1974-2008. Black circles indicates the sites sampling (from left to right: Kamaran, Balhaf and Socotra). A high-pass filter (year-on-year difference) was used in order to highlight the interannual variability by removing trends or slow variations. Correlations stronger than r = +0.4 or r = -0.4 are significant at 99%, based on a two-sided student t-test. P-values < 0.2 have been masked out. Analysis was run with the KNMI climate explorer web application (van Oldenborgh and Burges, 2001; http://climexp.knmi.nl). C) Blackman-Tukey cross-spectrum between annual mean Niño 3.4 index and gridded SST (HadiSST1) from Balhaf for the period 1974 -2008. The top panel shows the variance spectra for both records, and the botton panel shows the coherence (the correlation coefficient as the function of frequency between the records). Thin line on the bottom panel indicates the one sided lower error at 90%. Coherence values > 0.8 indicate that over 64% (0.8^2) of the variance at these periods is linearly correlated. Number are given in years. The bandwidth is 0.06 (number of lags: 24). The criteria for this are that the variance peaks are aligned (in the top panel) and that the corresponding coherence exceed the 80% confidence level (CL)

3.2 Socotra (Yemen, south-west Arabian Sea)

Socotra is a Yemeni island and it is about 380 km far to the Gulf of Aden coast of Yemen, and only 100 km far to the Somali coast (Fig. 3.7A). The island stands on a broad undersea plateau, the Socotra Platform, and spanning 133 km west to east and 43 km north to south (Cheung and DeVantier 2006; Fig. 3.7B).

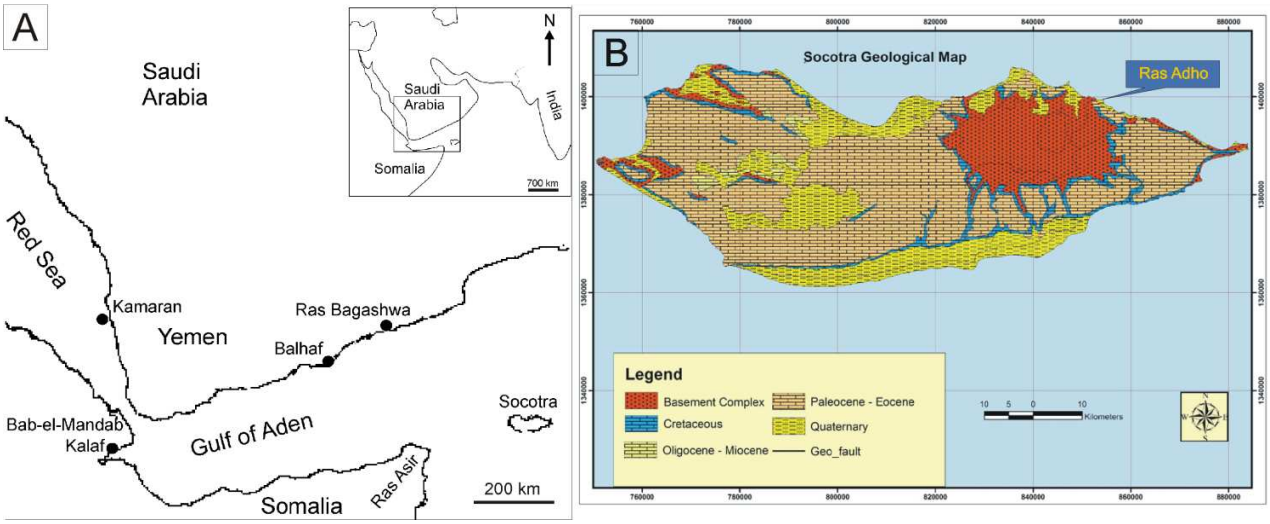

Fig. 3.7 Map of the Study area: A) location map of the South Red Sea-Gulf of Aden- South-west Arabian Sea with indication of the position of the island of Socotra; B) Geological Map of Socotra with indication of the position of the sampling site Ras Adho (from Cheung and De Vantier 2006).

Socotra is located to the southwest of the Arabian Sea, and it is bordered by the Gulf of Aden (Tudhope et al. 1996, Vecchi et al. 2004). The island is influenced by the oceanographic setting, with substantial seasonal and inter-annual variability in physical and biological oceanography. It is bathed by a variety of different water masses, including those originating to the south off East Africa, to the east by water of the central Indian Ocean, and to the north-west, north and north-east, by the Red Sea, Gulf of Aden and Arabian Sea respectively (Cheung and DeVantier 2006).

Bathymetry surrounding the islands reflects the region's tectonic history, and in several respects is comparable to the islands' landforms (Cheung and DeVantier 2006). Inshore, a relatively flat shelf generally less than 50 m deep is broken in places by narrow channels to ~80 m (Cheung and DeVantier 2006). Relict reef structures with characteristic spur and groove systems occur off sections of the north and south coasts, remnants of extensive earlier periods of reef growth (Cheung and DeVantier 2006). The site of algal sample collection is Ras Adho, in the north-east part of the island (Fig. 3.7B). Diving site in Ras Adho is about 1 km far to the coast, at 12°38.638N and 54°16.147E (GPS coordinate in WGS 84; Fig. 3.8A). It is a rocky buttresses with the base at 21 m and the top at 17 m alternate with sandy channels (Fig. 3.8B). This site is characterized by high hard and soft coral cover growing directly on the rock and by the presence of anthipatarians (unpublished report CREOCEAN). Large (up to 2 m in diameter) and flattened colonies, and *Goniastrea pectinata* are the dominant feature of this site (unpublished report CREOCEAN). Encrusting and free living corraline red algae (rhodolith) are present and abundant at first glance.

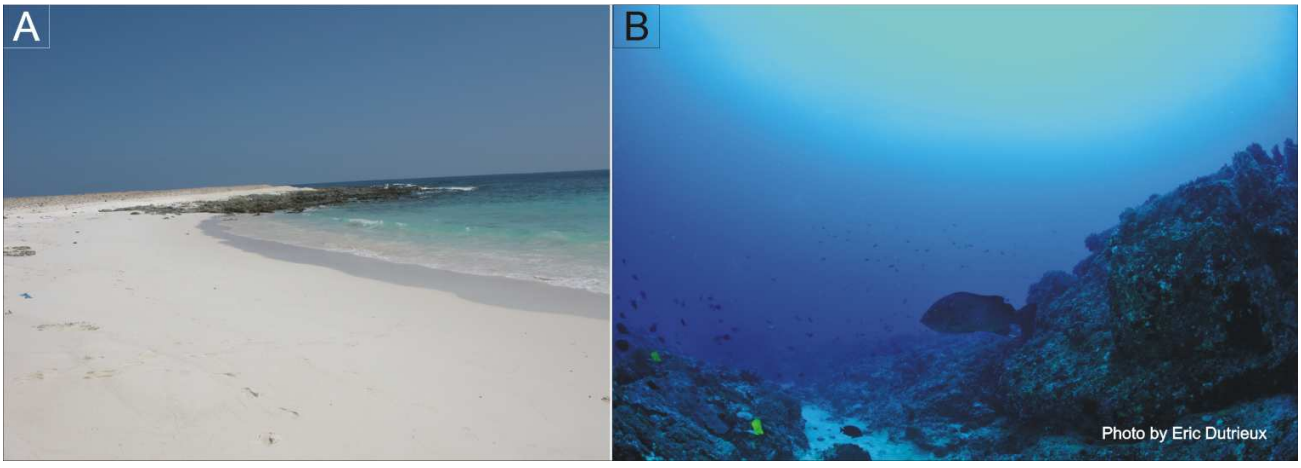

Fig. 3.8 A) photo of the north coast of Socotra to Ras Adho; B) photo of the sampling site characterized by rocky buttresses alternate with sandy channels.

The climate and surface water oceanography of the Arabian Sea region are dominated by the seasonally reversing Asian monsoon. Strong, moist SW airflow in summer (the SW monsoon) alternates with weaker, dry and more variable NE airflow in winter (the NE monsoon; Fig. 3.3). The western Arabian Sea is a region with large-scale and strong surface wind forcing during the southwest monsoon, and a vigorous dynamical ocean response that yields large SST gradients on the oceanic mesoscale, with changes in SST that can exceed 5° C over 200 Km (Vecchi et al. 2004; Fig. 3.2). The SW monsoon winds drive a strong SSC (the Somali current) across the Arabian Sea. The winds during the SW monsoon induce strong upwelling in the Arabian Sea water, that triggers spectacular phytoplankton blooms, resulting in the region being one the most productive areas of the world's oceans (Qasim, 1982; Brock et al. 1993; Fig. 3.9). The upwelling influences shallow hydrography to depths of about 250m (Brock et al. 1992).

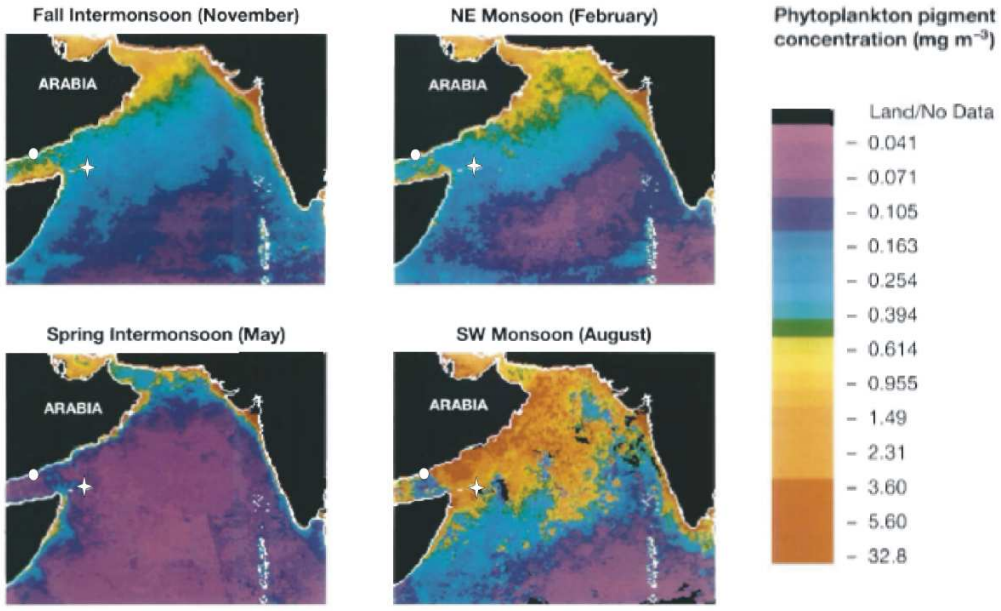

Fig. 3.9 Monthly climatologies for phytoplankton pigment concentration (mg m^{-3}) based on Coastal Zone Color Scanner data acquired during November 1978 through June 1986 (Feldman et al. 1989) and representing the four season of the annual cycle (from Brock et al. 1992). The white circles indicates Balhaf, while the white stars Socotra.

Perennial records of *in situ* records on marine climate from Socotra are not available. Therefore, have been used gridded instrumental climate records. Sources and references of all climate datasets used are given in Table 1. The wind speed record in the North-East coast of Socotra does not show a bimodal seasonal patter with the highest values in July at the onset of the wet SW monsoon (Fig. 3.10A). The seasonal reversal of the monsoon winds force the reversal of SSC at the North-East Socotra, and a local reversely current, not linked to the reversal of the monsoon winds, occurs in winter (December-March; Fig. 3.10B). Monthly zonal SSC from SODA gridded over 53-53.5°E, 12-12.5N was used in this study as an indicator of monsoon current strength in Socotra. South India precipitation from IMD dataset was used as further indicator of the strength of the summer monsoon.

Salinity fluctuates between 35.64 (November) and 36.03 (February-March) in the gridded SSS record (Fig. 3.11B). Precipitation in Socotra shows a trimodal pattern with the highest peak in October (at the onset of winter monsoon), and two lower peaks, one in May (in the end of winter monsoon), and one in January (winter; Fig. 3.11A). The combined effects of upwelling of cool subsurface water, lateral influx of cool water via the Somali current and evaporative cooling due to strong winds more than offsets solar gain, results in the lowest annual SST in August (Fig. 3.11C). During the NE monsoon, surface current flow reverses and a winter temperature minima in SST is attained in January (Fig. 3.11C). There is little upwelling associated with this weaker NE monsoon flow (Tudhope et al. 1996). Warm SST's occur in the spring (May) and autumn (October-November) transition periods between monsoon (Fig. 3.11C).

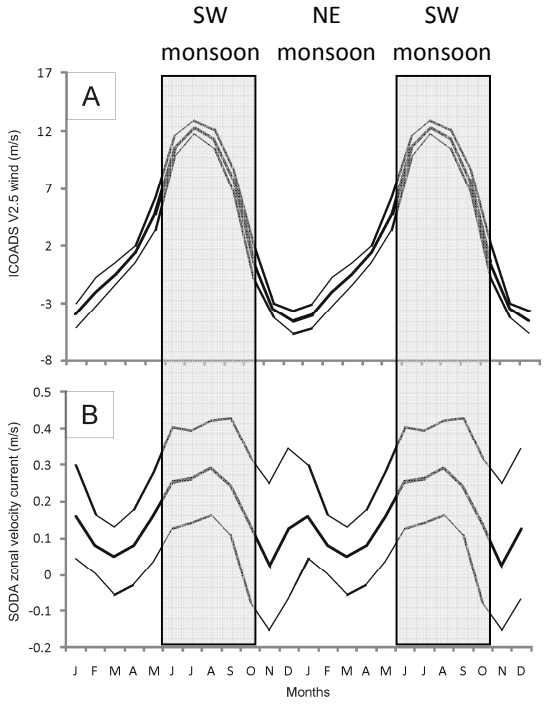

Fig. 3.10 Two mean seasonal cycles to Socotra of A) the monthly gridded ICOADS wind speed records since 1974 (Woodruff et al. 1998), B) the monthly gridded SODA zonal currents record since 1974 (graphs was run with the KNMI climate explorer web application, www.climexp.knmi.nl). Note that positive velocities correspond to zonal velocity vectors orientated towards west, predominant during SW monsoon season, while negative velocities accordingly correspond to vector oriented towards east, predominant during the NE monsoon season.

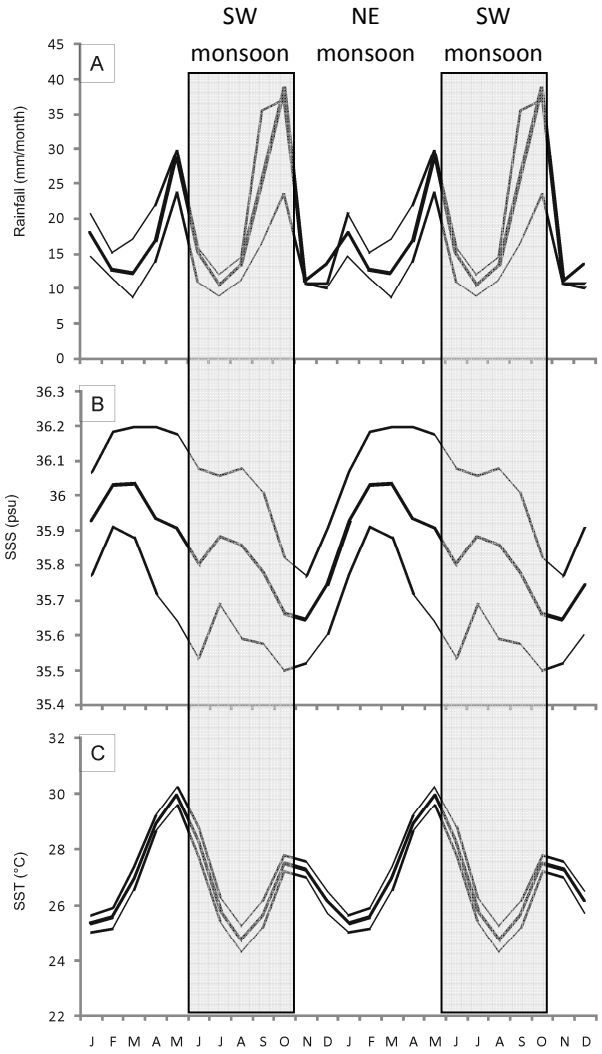

Fig. 3.11 Two mean seasonal cycles to Socotra of A) the local monthly gridded CRU precipitation records since 1974 (Mitchell and Jones 2005), B) the monthly gridded SODA SSS records since 1974 (Carton et al. 2005), C) the monthly gridded HadiSST since 1974 (Rayner et al. 2003).

Tourre and White (1995) suggested on the basis of their analysis of upper ocean temperatures for the period 1979-1991, the presence of an ENSO-style phenomenon in the Indian Ocean. They suggested that the early stages of each warm event manifested as positive SST anomalies in the Arabian Sea which then propagated equatorward and eastward through time to produce a variability similar in magnitude and timing to the Pacific ENSO. In this study, the Niño

3.4 index is used as a reliable proxy for the strength of ENSO, and is based on SST (HadiSST1) anomalies in the central Pacific (Trenberth 1997; Fig. 3.6A). The field correlation in Figure 3.6B shows a strong and significant (p-value>0.0001) positive correlation between SST variability and Niño 3.4 in the interannul band. The cross-spectral analysis between gridded SST of Socotra and Niño 3.4 reveals the typical mode of ENSO forcing in the interannul range of the SST spectrum (Fig. 3.12). No significant coherence is found for SST and Niño 3.4 in the decadal band (HadiSST1; Fig. 3.12).

SST exhibit a weakly significant long-term trend since 1973 (r=0.3, p-value=0.05 for HadiSST1). The HadiSST1 datasets indicate a SST rise of 0.3 since 1973. Available SODA SSS since 1973 does not show a secular trend.

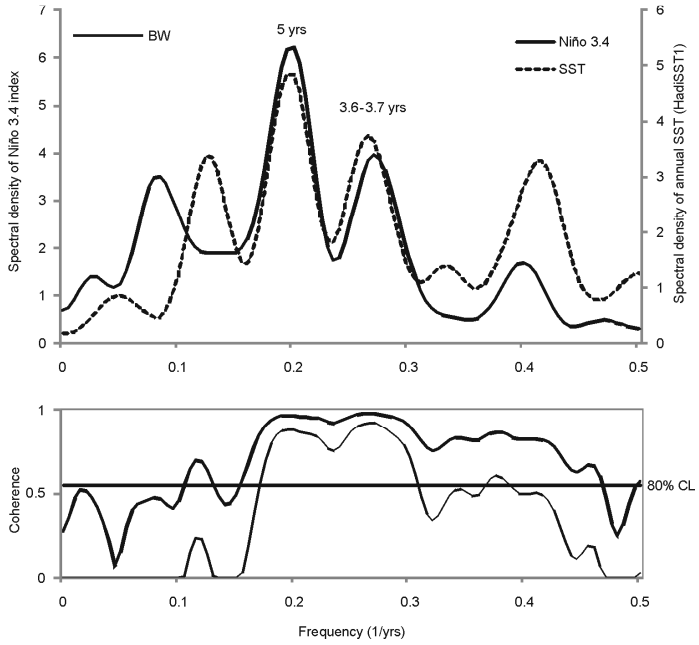

Fig. 3.12 Blackman-Tukey cross-spectrum between annual mean Niño 3.4 index and gridded SST (HadiSST1) from Socotra for the period 1974 -2008. The top panel shows the variance spectra for both records, and the bottom panel shows the coherence. Thin line on the bottom panel indicates the one sided lower error at 90%. Coherence values > 0.8 indicate that over 64% (0.8^2) of the variance at these periods is linearly correlated. Number are given in years. The bandwidth is 0.06 (number of lags: 24). The criteria for this are that the variance peaks are aligned (in the top panel) and that the corresponding coherence exceed the 80% confidence level (CL).

3.3 Kamaran (Yemen, South Red Sea)

Kamaran is a small Yemeni island about 2 km far to the Red Sea coast of Yemen (Fig. 3.1A). It is a flat arid island of about 18 Km long and 7 Km wide. It is located at the southern end of the Red Sea in the shallow water of the Arabian peninsula's continental shelf.

The diving site was close to the coast at 15°21.988N, 42°37.54E (GPS coordinate in WGS 84; Fig.3. 13A). It is a sandy substrate dominate by sponges, where several rhodoliths were observed (Fig.3. 13B).

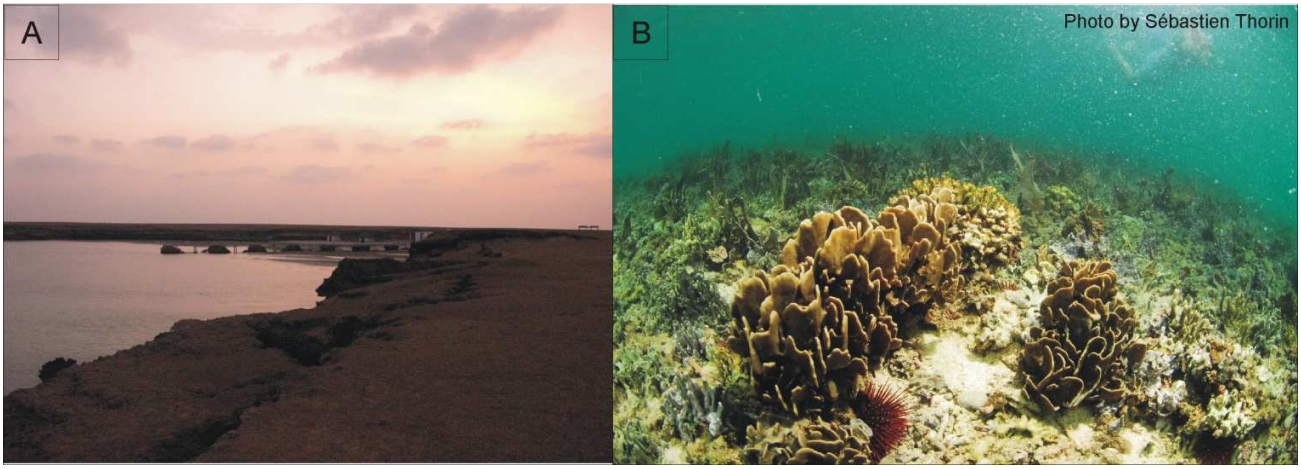

Fig. 3.13 A) photo of the sampling site to Kamaran seen from the coast; B) photo of the sampling site characterized by the presence of macro sponge.

The Red Sea is a long (~1932 km), narrow (an average of 280 km in width) body of water surrounded by the African and Eurasian continents (Head 1987). It is linked in the south to the Indian Ocean, through the Gulf of Aden, by a very shallow sill, and in the north to the Mediterranean Sea by the Suez Canal (Al Saafani and Shenoi 2004). The Hanish Sill is only 160 m deep and 5 km wide at the bottom, so that it is crucial in determining the nature of Red Sea outflow water (Aiki et al. 2006).

The climate of the Red Sea is largely controlled by the distribution of, and changes in, atmospheric pressure over a very wide area, that, with some exceptions, shows a remarkable uniformity throughout the year (Edwards 1987). Weather over the area may be divided in the year into cooler an hotter season corresponding to the conventional northern hemisphere winter and summer. The northern part of the Red Sea is subject to greater variability of weather than the south, particularly in winter when it may be influenced by disturbances in the Mediterranean, which leads typical winter rains (Edwards 1987; Felis et al. 2000). This occur in association with troughs of low pressure which move into the Red Sea from the north and are often accompanied

by changes in wind, temperature and humidity and by increased cloud (Fig. 3.14). These fronts may penetrate quite far south (to the latitude of Massawa, at ~16°N) but south of about 25°N the manifestations become much less marked and are frequently absent (Edwards 1987). In the south, variability is small and is mainly associated with seasonal wind changes (Fig. 3.14). As in the north the occasional outbreaks of rain still tend to be concentrated in the winter months (Edwards 1987). So, during winter the northern part of the Red Sea is affected by the north African wind system and northerly winds converge with the southerly winds at about 18-20°N (Edwards 1987; Fig. 3.14).

The excess evaporation over the Red Sea produces extremely salty and dense water which intermittently spills from the sill and cascades down to the intermediate depth of the Indian Ocean (Aiki et al. 2006). Passing through the Gulf of Aden, the water outflows from the Red Sea becomes a part of the intermediate circulation in the Indian Ocean, which has been observed as a mid-depth salinity maximum in the Arabian Sea and even in the southern hemisphere (Mecking and Warner 1999). The hydrography and oceanography of the Red Sea are strongly influenced by the adjacent Indian Ocean through surface and subsurface circulation regimes, governed by the south Asian monsoon system and by thermohaline circulation (Edwards 1987; Al Saafani and Shenoi 2004; Aiki et al. 2006). The thermohaline circulation in the Red Sea leads an inflow of surface water from the Gulf of Aden, and outflow of deep and dense Red Sea water in the opposite direction (Edwards 1987). During winter (November-April) the NE monsoon together with thermohaline forces, create an inflow of surface waters from the Gulf of Aden towards the southern Red Sea, while deep waters flow back out (Edwards 1987).

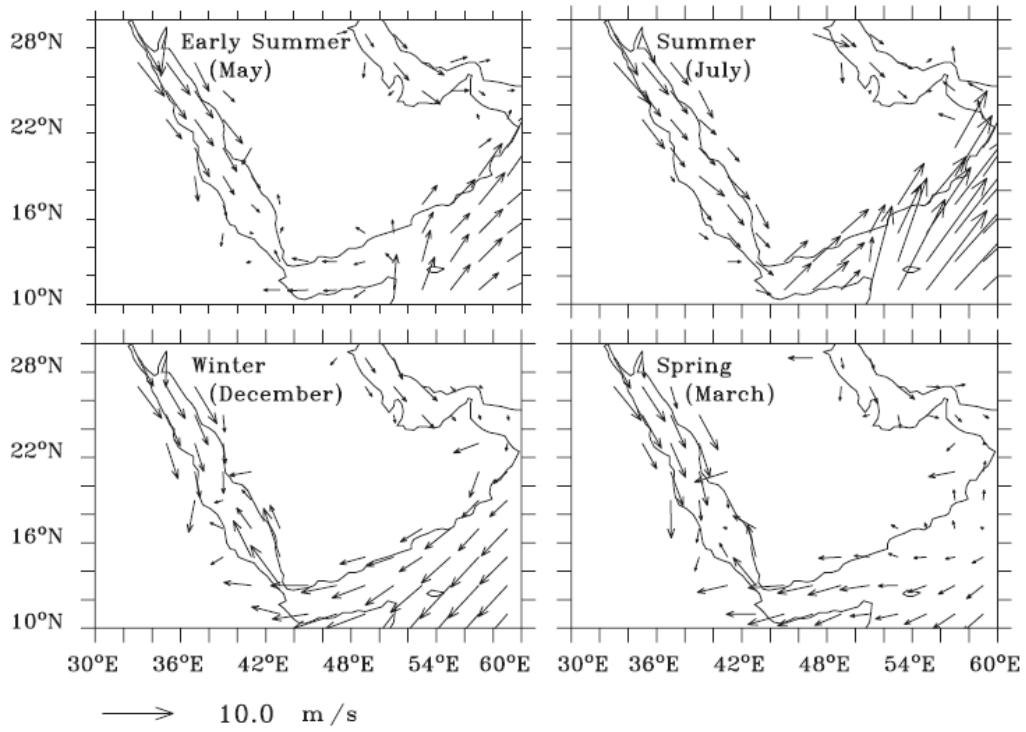

Fig. 3.14 Winds over the Red Sea during early summer, summer, winter and spring based on COADS climatology (from Al Saafani and Shenoi 2004).

During summer (May-October), the SW monsoon winds and the thermohaline forces have opposite effects, resulting in a net surface outflow towards the Gulf of Aden (Edwards 1987). The Red Sea water overflows less in summer and more in winter, due to the monsoonal winds over the Indian Ocean, that induces the summer cessation of the strait outflow (Aiki et al 2006).

Perennial records of in situ records on marine climate from Kamaran are not available. Therefore, as for other locality involved in this study, have been used gridded instrumental climate records (Tab. 1). As mentioned above weather in the Red Sea may be divided in the year into cooler an hotter season corresponding to the conventional northern hemisphere winter and summer. In fact, the wind speed record in Kamaran shows the seasonal reversal in summer and winter, resulting in positive wind speed in winter, when it blows northwards, and negative in summer, when it blows southwards (Fig. 3.15A). This is in phase with the SSC record, with a

negative value during winter, when there is an inflow of the sea surface water from the Gulf of Aden into the Red Sea, and a positive value during summer, when the Red Sea's surface water outflow into the Gulf Fig.3.15B). Both records (wind and current) are in phase with the sea level pressure (SLP) record that expectedly shows the lowest SLP in summer and the highest value in winter, when the sea surface water inflow into the Red Sea from the Gulf of Aden (Fig. 3.15C).

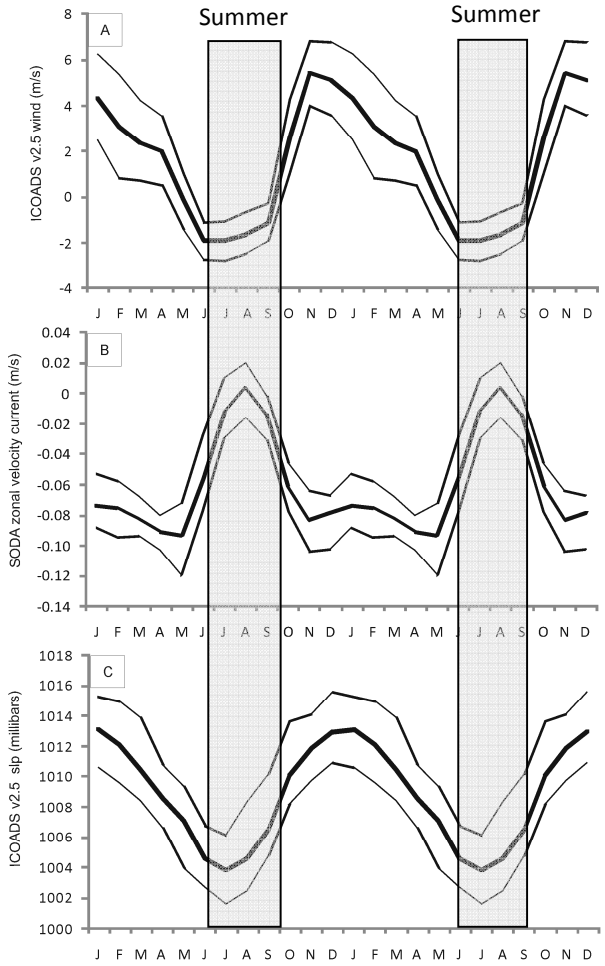

Fig. 3.15 Two mean seasonal cycles to Kamaran of A) the monthly gridded ICOADS wind speed records since 1993 (Woodruff et al. 1998), B) the monthly gridded SODA zonal currents record since 1993, C) the monthly gridded ICOAD sea level pressure (graphs was run with the KNMI climate explorer web application, www.climexp.knmi.nl).

The cross-spectral density between Alexandria precipitation record and annual SST did not reveal coherence between the two records, such as with the sea level pressure record. Instead, a cross-spectral density between the Alexandria precipitation record and the SSC revealed a coherence for the period of 5 yrs (Fig. 3.16).

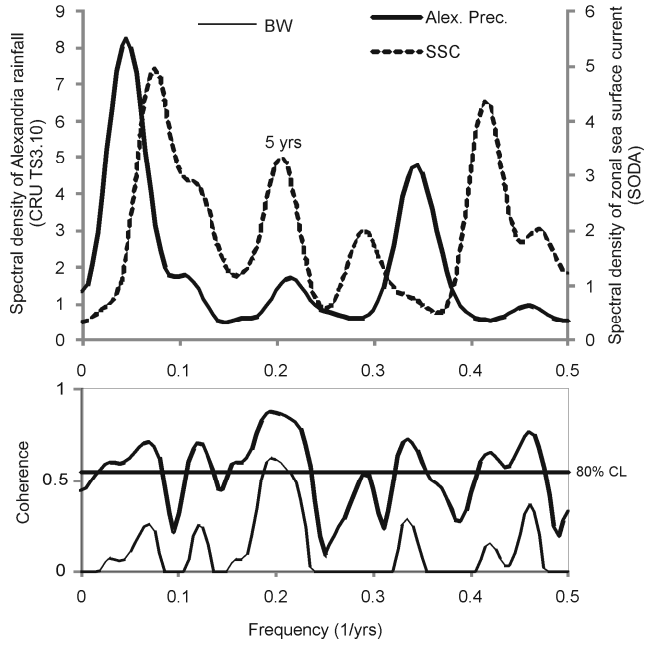

Fig. 3.16 Blackman-Tukey cross-spectrum between annual mean Alexandria rainfall and gridded zonal surface current (SODA) from Kamaran for the period 1974 -2008. The top panel shows the variance spectra for both records, and the bottom panel shows the coherence. Thin line on the bottom panel indicates the one sided lower error at 90%. Coherence values > 0.8 indicate that over 64% (0.8^2) of the variance at these periods is linearly correlated. Number are given in years. The bandwidth is 0.06 (number of lags: 24). The criteria for this are that the variance peaks are aligned (in the top panel) and that the corresponding coherence exceed the 80% confidence level (CL).

Hence, this may confirm the weak influence of the northern climate to the more south part of the Red Sea. A cross-spectral density between the SIR record and SLP record revealed a coherence for the periods of 2.8 and 2.5 yrs (Fig. 3.17), substantiating the influence of Asian monsoon system on the South Red Sea overflow.

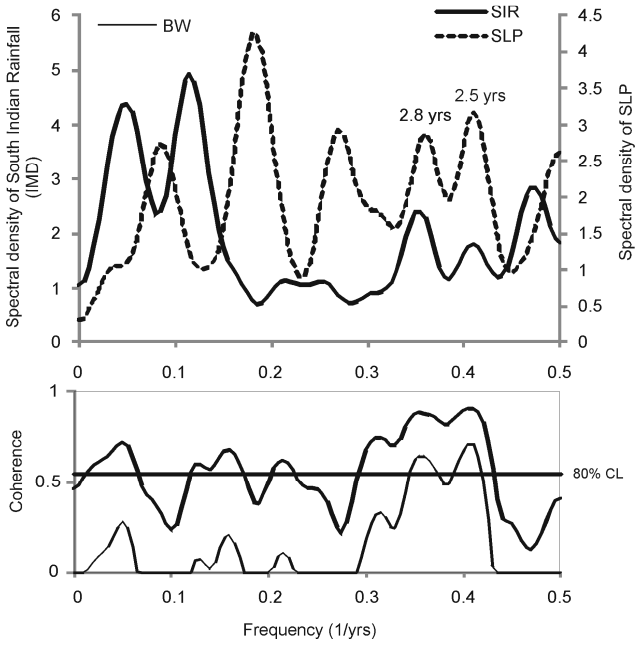

Fig. 3.17 Blackman-Tukey cross-spectrum between seasonal South India rainfall (SIR; IMD) and gridded sea surface pressure (SLP; SODA) from Kamaran for the period 1974 -2008. The top panel shows the variance spectra for both records, and the bottom panel shows the coherence. Thin line on the bottom panel indicates the one sided lower error at 90%. Coherence values > 0.8 indicate that over 64% (0.8^2) of the variance at these periods is linearly correlated. Number are given in years. The bandwidth is 0.06 (number of lags: 24). The criteria for this are that the variance peaks are aligned (in the top panel) and that the corresponding coherence exceed the 80% confidence level (CL).

The typical winter rain in the northern Red Sea is also present in Kamaran, but in this area of the southern Red Sea the highest positive peak of rainfall occur during summer (Fig. 3.18A). Salinity fluctuates between 36.5 psu (December-June) and 38.7 psu (August-September) in the gridded SSS record, and it is in phase with SSC record (Fig. 3.18B). The SST shows distinct seasonal variability in Kamaran, and it is in phase with SSS record (Fig. 3.18C). Temperature fluctuates between 25.4 °C in winter (February), and 33.2°C in the end of summer (October), and this range expectedly corresponds respectively to the lowest and highest value of SSS (Fig. 3.18B and C). HadiSST1 SST data since 1993 to 2008 do not exhibit a significant long-term trend, such as available SODA SSS data for the same period. The cross-spectral density between SST

(HadiSST1) record and SSS record revealed coherence between the two records in the periods of 5.8 yrs and 2.5 yrs, and the SSS record shares with the annual SST almost 94% of the variance in these periods (Fig. 3.19).

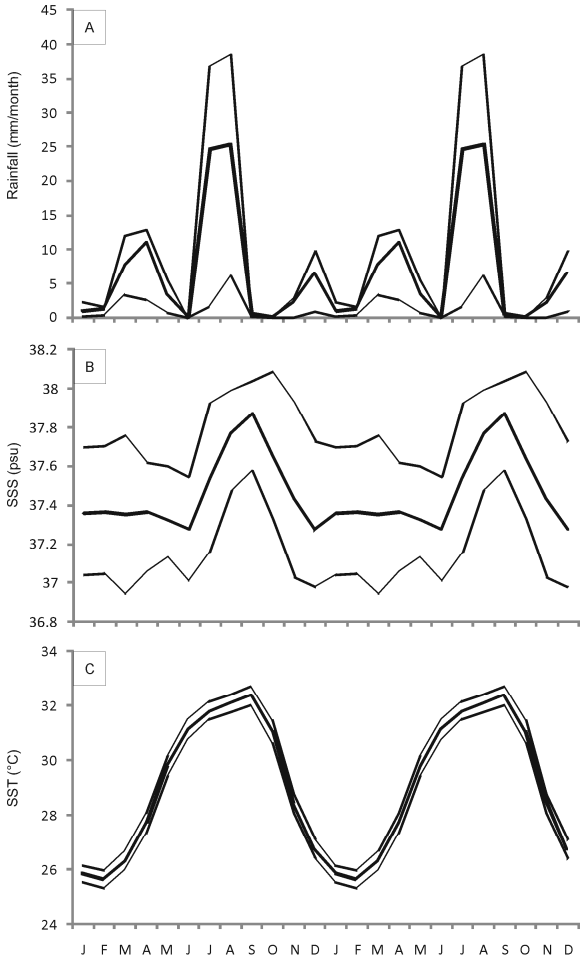

Fig. 3.18 Two mean seasonal cycles to Kamaran of A) the local monthly gridded CRU precipitation records since 1974 (Mitchell and Jones 2005), B) the monthly gridded SODA SSS records since 1974 (Carton et al. 2005), C) the monthly gridded HadiSST since 1974 (Rayner et al. 2003).

As previously said, it has long been recognized that variations in the intensity of the Asian and Africa monsoon show some degree of correlation with the Pacific ENSO (Bhatt 1989; Torrence and Webster 1999). Interdecadal variations in the coral skeleton $\delta^{18}O$ from south and

north Red Sea have been correlated with ENSO (Klein et al. 1997; Felis et al. 2000). Particularly, Klein et al. (1997) found, although weak, a significant coherence between SST and SOI, and coral skeleton $\delta^{18}O$ record and SOI for period centered at 2-2.5 yrs, in the southern Red Sea (Eritrea).

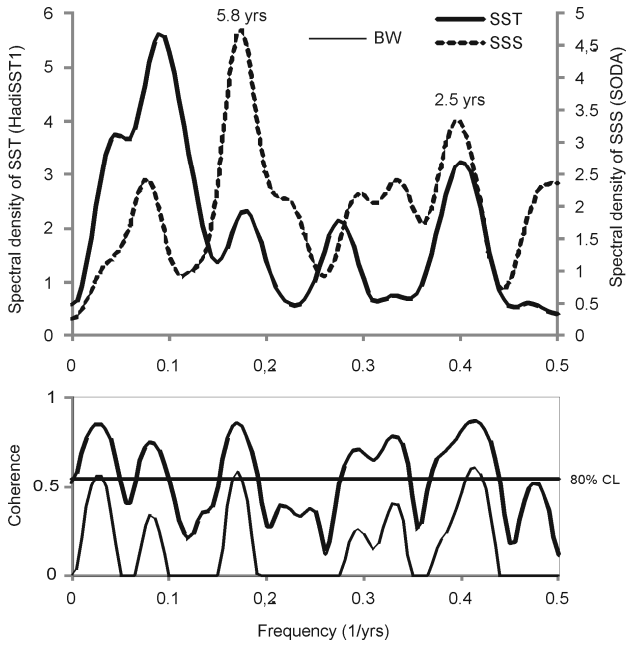

Fig. 3.19 Blackman-Tukey cross-spectrum between gridded SST (HadiSST1) and gridded SSS (SODA) from Kamaran for the period 1974 -2008. The top panel shows the variance spectra for both records, and the bottom panel shows the coherence. Thin line on the bottom panel indicates the one sided lower error at 90%. Coherence values > 0.8 indicate that over 64% (0.8^2) of the variance at these periods is linearly correlated. Number are given in years. The bandwidth is 0.06 (number of lags: 24). The criteria for this are that the variance peaks are aligned (in the top panel) and that the corresponding coherence exceed the 80% confidence level (CL).

As for the other areas of study (Balhaf and Socotra), the Niño 3.4 index is used as a reliable proxy for the strength of ENSO, which is based on SST (HadiSST1). The field correlation in Figure 3.6B shows no correlation between SST variability and Niño 3.4 in the interannual band in the southern part of the Red Sea. The cross-spectral analysis between gridded

SST of Kamaran and Niño 3.4 record reveals coherence in the typical modes of ENSO forcing in the interannual band at the periods of 3.7 and 2.5 yrs (Fig. 3.20). The latter shows the highest coherence, and the 52% of the SST variance is explained in this period. No significant coherence is found for SST and Niño 3.4 in the decadal band (Fig. 3.20).

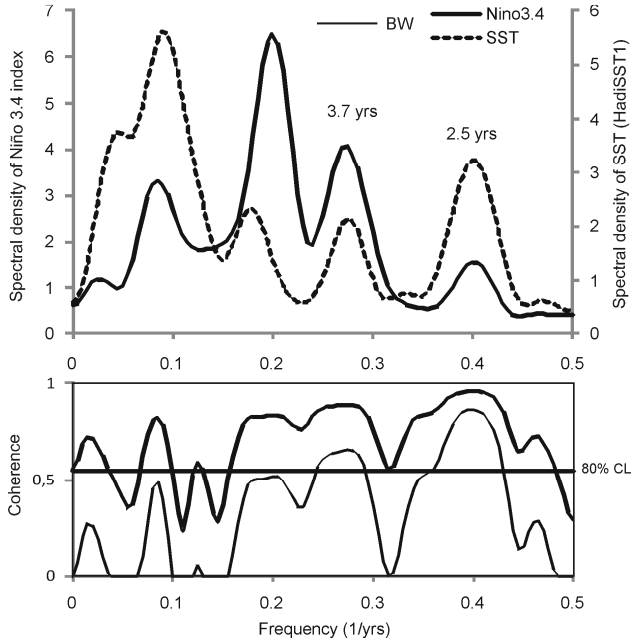

Fig. 3.20 Blackman-Tukey cross-spectrum between annual mean Niño 3.4 index and gridded SST (HadiSST1) from Kamaran for the period 1974 -2008. The top panel shows the variance spectra for both records, and the bottom panel shows the coherence. Thin line on the bottom panel indicates the one sided lower error at 90%. Coherence values > 0.8 indicate that over 64% (0.8^2) of the variance at these periods is linearly correlated. Number are given in years. The bandwidth is 0.06 (number of lags: 24). The criteria for this are that the variance peaks are aligned (in the top panel) and that the corresponding coherence exceed the 80% confidence level (CL).

4. Material and methods

4.1. Sampling and measurements

Three living rhodoliths (DB657, DB635 and DB576) and an attached specimen (DB659) were collected via SCUBA diving (Fig. 4.1). The DB657 and DB659 samples were collected at Balhaf on the coast of Yemen (13°58.5N; 48°10.5E; Fig. 3.1B) in November 2008 between 6 m and 8 m water depth (Fig. 4.1A, B). The DB635 sample was collected at Ras Adho (Socotra, Yemen; 12°38.638N, 54°16.147E) in March 2010 at 22 m depth (Fig. 4.1C). The DB576 sample was collected at Kamaran (Yemen; 15°21.988N, 42°37.54E) in September 2009 at 1.5 m depth (Fig. 4.1D).

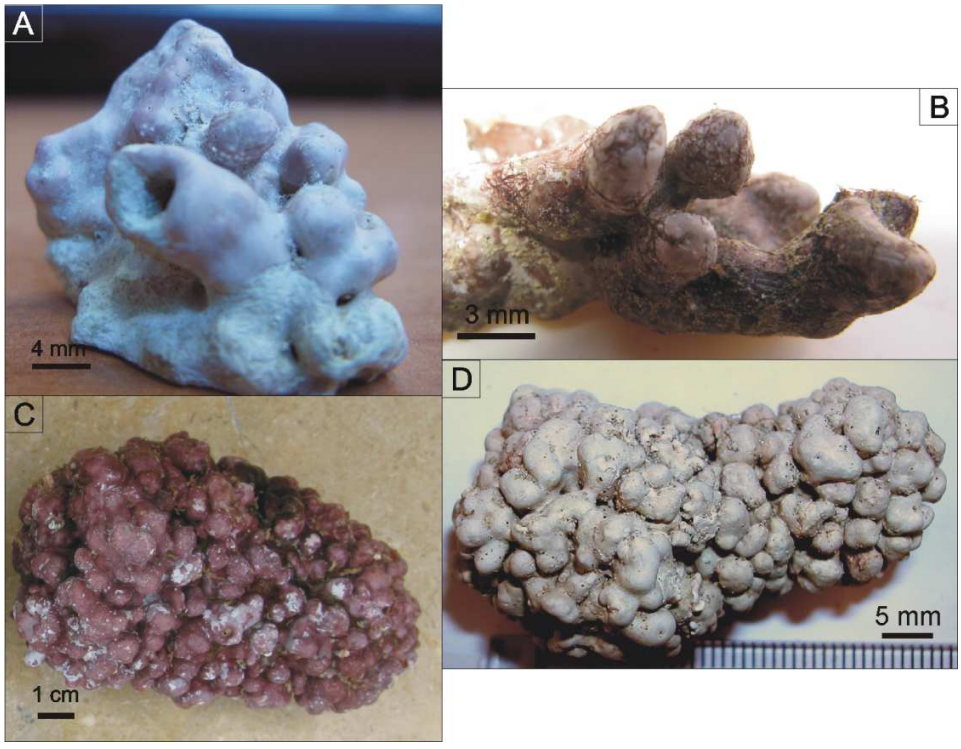

Fig. 4.1 Specimens of coralline red algae analyzed: A) rhodolith of *Lithophyllum kotschyanum* f. *affine* from Balhaf (DB657); B) attached *L. kotschyanum* f. *affine* from Balhaf (DB659), note the presence of epibionts, as the filamentous algae that grow on coralline alga; C) rhodolith of *Lithophyllum* sp. from Socotra (DB635); D) rhodolith of *L. kotschyanum* f. *affine* from Kamaran (DB576).

The air-dried coralline specimens were sectioned parallel to the direction of growth using a low speed saw with diamond blades (Fig. 4.2A, 4.3, 4.4A, 4.5 and 4.6A). The sectioned parts were polished with a 800 Grit silicon carbide paper for wet grinding, cleaned ultrasonically and organic matter was removed by immersion in a solution of diluted hydrogen peroxide (Mertz-Kraus et al. 2008).

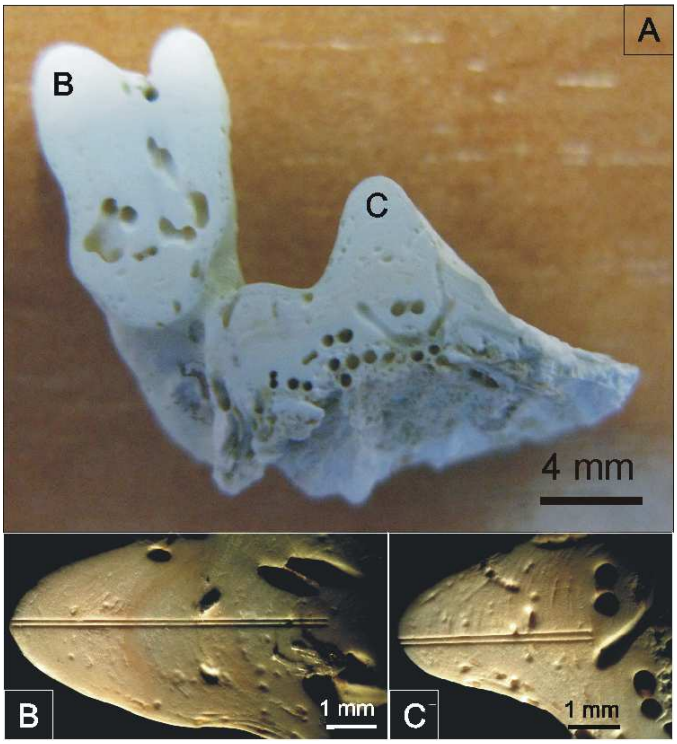

Fig. 4.2 DB659 sample: A) vertical section parallel to the direction of algal growth; B) magnification of the protuberance (B) shown in (A) and referred to in the text as DB659b; C) magnification of the protuberance (C) shown in (A), and referred to in the text as DB659a. Note in (B) and (C) the two parallel laser line transects of the LA-ICP-MS analysis. Note the high presence of infaunal.

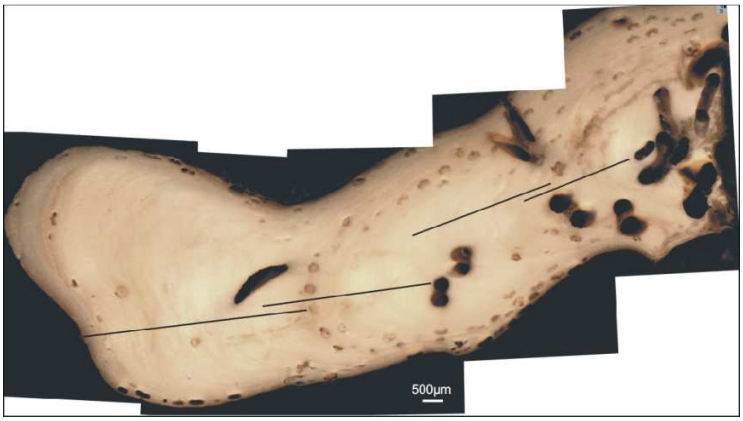

Fig. 4.3 Vertical section parallel to the direction of algal growth of the branch of DB659 sample and referred to in the text as DB659bis. The four black lines are the profile of the LA-ICP-MS transects. Note the high presence of infaunal.

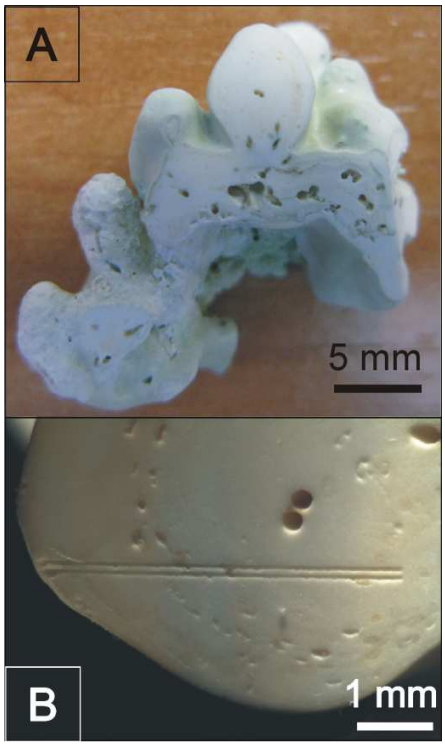

Fig. 4.4 Sample DB657 A) vertical section parallel to the direction of algal growth; B) magnification of the protuberance analyzed showing the two parallel laser line transects of the LA-ICP-MS analysis. Note the high presence of infaunal.

Fig. 4.5 Vertical section parallel to the direction of algal growth of the DB635 sample. The four black lines are the profile of the LA-ICP-MS transects. Note the high presence of infaunal.

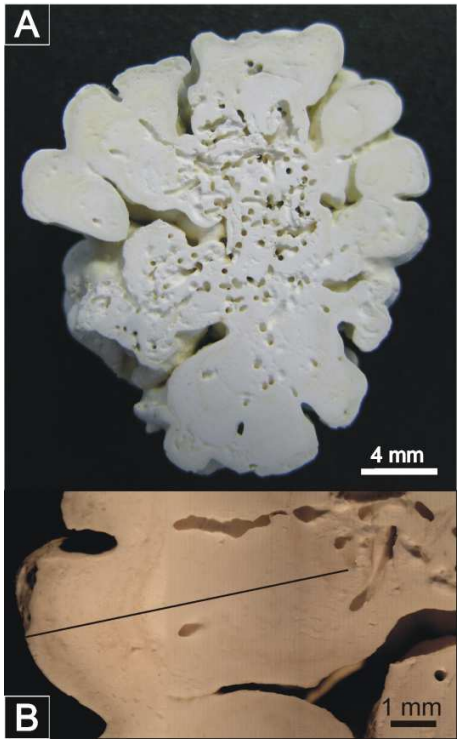

Fig. 4.6 Sample DB576 A) vertical section parallel to the direction of algal growth; B) magnification of the protuberance analyzed showing the laser line transects of the LA-ICP-MS analysis. Note the high presence of infaunal.

Elementary concentration of Li, Mg, Ca and Ba were measured at the Department of Geosciences, Johannes Gutenberg-Universität Mainz, Germany using an Agilent 7500ce

Quadrupole ICP-MS coupled to a New Wave research (NWR) UP-213 laser ablation system (213nm wavelength, Nd:YAG Laser) for DB659a and b, DB657specimens and to a NWR 193 (193nm wavelength, Nd:YAG Laser) for DB659bis, DB635 and DB576 specimens. Measurements were carried out with laser energy densities of 2.76 J/cm^2 and helium as carrier gas. Transects parallel to the direction of growth were analyzed with a scan speed of 10 μm/s, and 10 Hz pulse rate. The transects' width were of 65 μm for DB659a and b, DB657 specimens, and of 50 μm for DB659bis, DB635 and DB576 specimens. On sample DB659, two parallel transect on two algal protuberances (DB659a and b) were analyzed, each couple of transects were of 6.5 mm and 3.5 mm long (Fig. 4.2B and C). Additionally, at DB659 four consecutive transects, to follow the changes of the direction of growth, were analyzed, and they were combined to get a single transect of 12.2 mm length (Fig. 4.3). At DB657, two parallel transect of 4.8 mm long on an algal protuberance were analyzed (Fig. 4.4B). At DB635 four consecutive transects, to follow the changes of the direction of growth, were analyzed to get a single transect of 8.5 mm length (Fig. 4.5). At DB576 a transect of 7.2 mm long on an algal protuberance was analyzed (Fig. 4.6B). ^{43}Ca was used as internal standard, and glass reference material NIST (US National Institute of Standard and Technology Standard Reference Material) SRM 610 as external standard. Data reduction was carried out with the commercial software GLITTER 4.4.2 (Macquarie University, Sydney). Values for NIST SRM 610 reported in the GeoReM database were used as the "true" concentrations in this reference glasses (Jochum et al. 2006). Detection limits (99% confidence) were: ^{7}Li=0.038ppm, ^{24}Mg=0.02ppm, ^{43}Ca=9.26ppm, ^{137}Ba=0.027ppm; the relative standard deviation (RSD) from repeated analysis for NIST SRM 610 is equal or less than 5%: ^{7}Li/^{43}Ca=3%, ^{24}Mg/^{43}Ca=5%, ^{137}Ba/^{43}Ca=1%. The two parallel transects in DB659a,b and DB657 of Mg/Ca, Li/Ca and Ba/Ca were averaged and a single transect for each ratio was considered for further analysis.

Values of Mg, Li and Ba in the carbonate lattice of algal thallus were received by mean of LA-ICP-MS measures and they have been converted from ppm to mmol mol^{-1} and in the end to mol % by the following equations:

$$A\ (mol\ mol^{-1}) = B / C \qquad (1)$$

$$Y\ (mmol\ mol^{-1}) = (D/A)*1000 \qquad (2)$$

$$mol\ \%\ element = Y * 100 / (1000 + Y) \qquad (3)$$

Conversion factor (A) for each element used in this study has been calculated dividing the standard-atomic weight of the element (B) for the standard-atomic weight of calcium (C). Afterward, conversion from $\mu g\ g^{-1}$ to mol mol^{-1} for each element value measured (Y) has been calculated dividing each element ratio measured (D) for conversion factor and multiply for 1000. In the end to calculate the mol% for each element the fast version equation was used (3).

The age models were established based on the seasonal cycles in algal Mg/Ca time series (Fig. 4.7). Mg/Ca values were mainly tied to January for samples from Balhaf (Fig. 4.7A), to August and January for sample from Socotra (Fig. 4.7B), and to February for sample from Kamaran (Fig. 4.7C; HadlSST1 dataset minimum). Moreover, in samples from Balhaf (DB659 and DB657), where little decreases of Mg/Ca, between two adjacent minimum ratio values were recognized, corresponding to summer monsoon, maximum Mg/Ca values were tied to June and September (pre and post monsoon month). The chronology was thus tied two anchor points within each year (Fig. 4.7A). In Socotra sample maximum Mg/Ca values were tied to May (maximum SST month from HadiSST1; Fig. 4.7B). Conversely, in Kamaran sample maximum Mg/Ca values were tied to September-October (maximum SST month from HadiSST1; Fig. 4.7C). Since the distance from each Mg/Ca measurement from the living surface of the algae was known, two adjacent annual Mg/Ca minima were used to estimate annual growth rate by subtracting distance of these minima from the living surface .

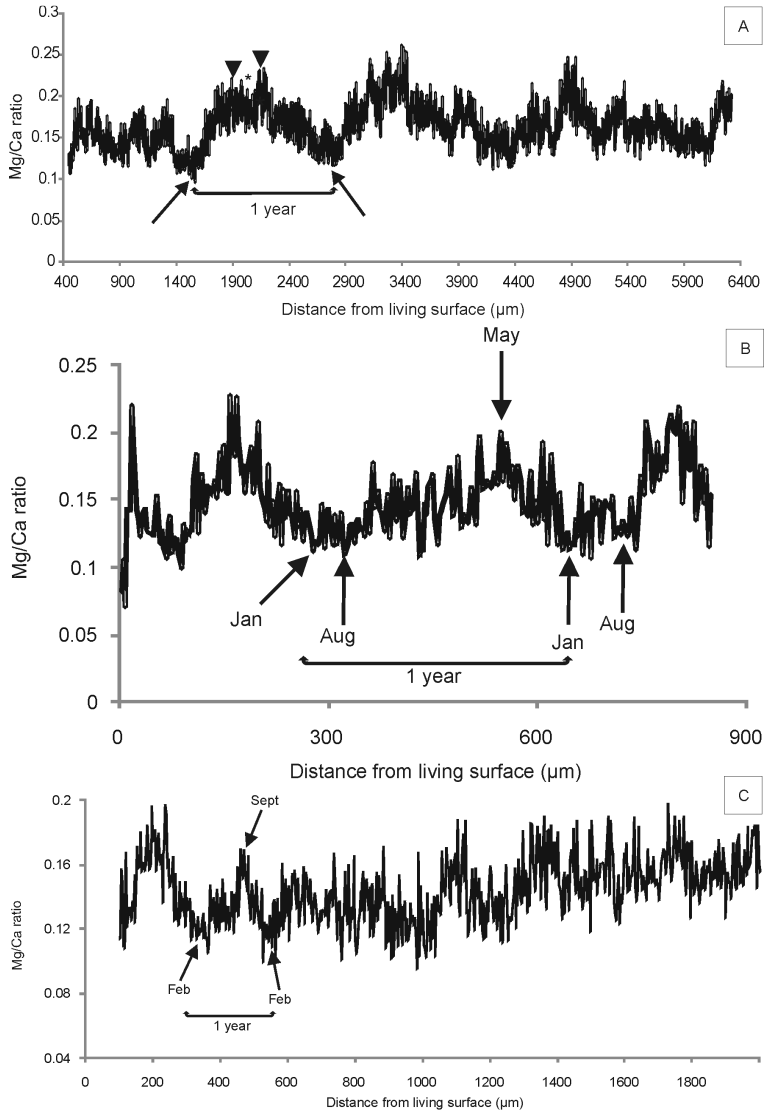

Fig. 4.7 LA-ICP-MS measured of Mg/Ca cycles used for calculating annual growth-increment widths in: A) *L. kotschyanum* f. *affine* from Balhaf, example of the DB659b specimen where arrows indicate the lowest value of Mg/Ca corresponding to the lowest value of SST in January, the arrowheads the highest values of Mg/Ca corresponding to the highest value of SST (pre and post monsoon) and the star the summer monsoon in the month of August; B) *Lithophyllum* sp. from Socotra, the lowest values of Mg/Ca correspond to the month of August; C) *L. kotschyanum* f. *affine* from Kamaran, the lowest values of Mg/Ca correspond to the month of February.

Monthly and annual time series were calculated by averaging of values within each chronological series. They were compared to gridded SST (HadiSST1).

The samples were decalcified with Tellyeniczkyi's solution for 3-5 days (Bressan 1974) for algal identification and observations on algal biometry. Once decalcified, the samples were washed in distilled water for 10-20 min. They were then dehydrated through a graded ethanol series and embedded in methacrylate resin (Technovit 7100; Heraeus Kulzer, Wehrheim, Germany). Specimens were serially sectioned with a rotary microtome (Leica, Wetzlar, Germany) and stained with 1% toluidine blue "O" in sodium tetraborate (O'Brien and McCully 1981). Serial sections were mounted in Eukitt (O. Kindler GmbH & Co; Freiburg, Germany), and permanent slides were examined and photographed with a LEICA DM-RD microscope.

On DB659a-b and DB657 cell size variations were measured and compared with variation in cell wall thickness by scanning electron microscopy (SEM). After geochemical analysis, the samples were prepared and mounted on stubs with silver glue and were gold scatter-coated and imaged with a Vega Tescan TS5136XM.

Anatomical terminology for coralline algae follows Johansen (1981).

4.2. Statistical treatment

Standard correlative statistics were used to estimate the similarity between each proxy record along the same transect, in coral spot analysis and between these proxy records and gridded SST. For DB659a,b and DB657 specimens, A t-test was performed between the 2-parallel transects with the package Statistica 6.0 (StatSoft 2001). When the t-test revealed no significant difference, the two transects were merged into one and only the average between them was used.

For the spectral analyses of the algae and instrumental climate data the software Analyseries 2.0.4.2 was used. Prior to spectral analyses, the individual time-series were detrended

by removing the linear trend and normalizing to unit variance. The Blackman Tukey method was used (Blackman and Tukey, 1958), which is the classical method for spectral analyses, and widely used in coral spectral analysis. The algorithm computes first the autocovariance of the data, and then applies a window (Barlett), and finally Foutier-trasforms the covariance functions to compute a power spectrum (Paillard et al. 1996). The chosen window should not considerably affect the results for typical short and noisy time series. A further advantage of this method is the possibility to apply cross spectra for two time series. This method provides the statistical tool to detect correlations between two time series in the spectral range.

5. Results

5.1. Balhaf

5.1.1. DB657 and DB659a-b

To date, the coralline flora of the study area is very poorly known. The encrusting plant lived on a reefal limestone and the rhodolith was growing over a serpulid empty tube. Both specimens are darkish pink, fruticose in growth form, with protuberances up to about 10 mm in length. Histological sections reveal cells of adjacent filaments joined by secondary pit connections, absence of cell fusions, uniporate tetrasporangial conceptacles in DB659 (diameter 300 µm, height130 µm, length of the pore canal 50.5 µm; Fig 5.1A), and carposporangial conceptacles in DB657 (Fig. 5.1B). Based on these attributes, the coralline algae involved in this study were identified as *Lithophyllum kotschyanum* f. *affine*.

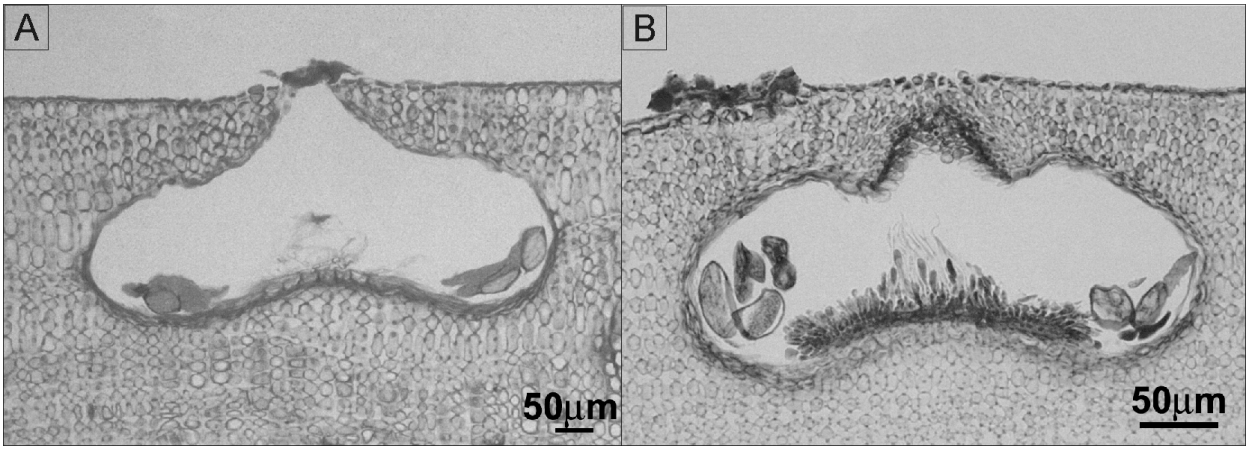

Fig. 5.1 Histological section of *L. kotschyanum* f. *affine* from Balhaf A) tetrasporangial conceptacles in DB659 sample; B) carposporangial conceptacles in DB657 sample.

Histological sections showed a variability in cell elongation of the same cell filament along

the main growth axis (Fig. 5.2A, B).

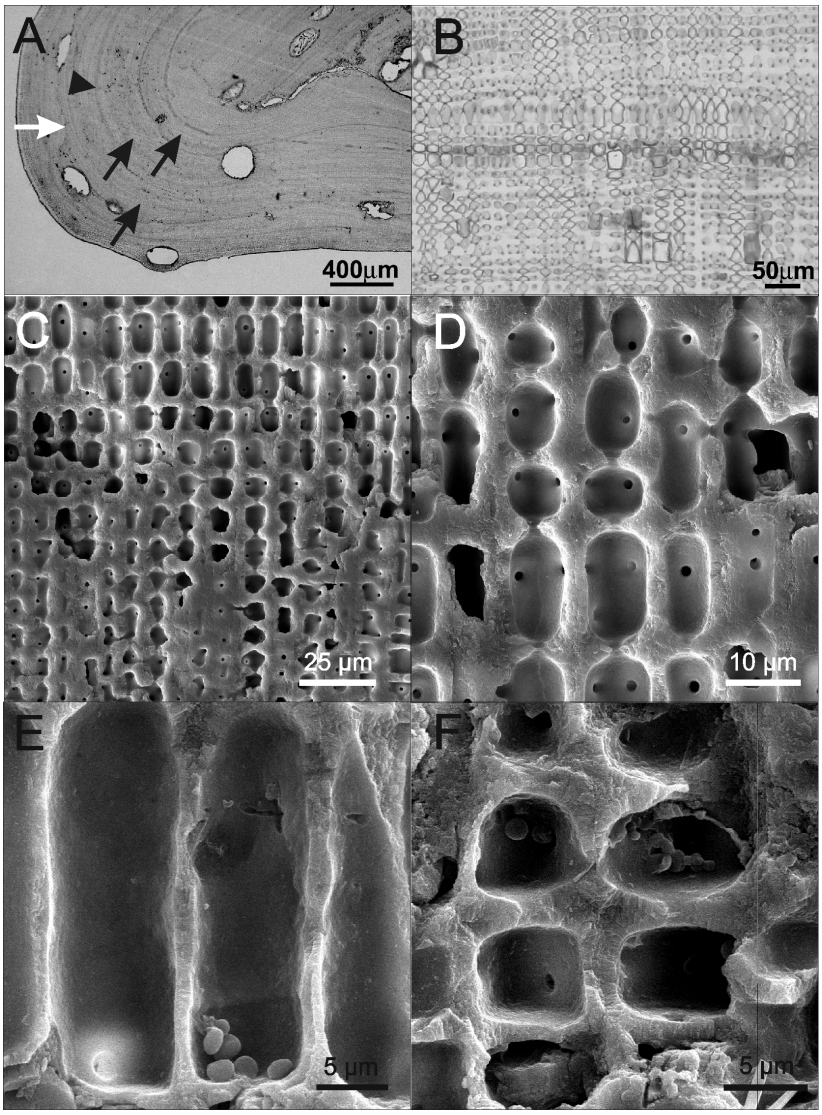

Fig. 5.2 Histological section of DB657 thallus: A) longitudinal section of a protuberance showing band periodicity (arrowhead), three growth stages (arrows), and thallus discontinuity (white arrow); B) magnification of A showing different cell elongations along the same filament. SEM picture of DB657 section: C) longitudinal section of calcite thallus showing different cell dimension along filaments; D) magnification of C showing presence of longer/smaller cell along filaments; E) magnification of longer cells showing thin wall cell; F) magnification of smaller cells showing thick wall cell.

Investigations by SEM have also shown this variability in cell size (Fig. 5.2C, D). Thus, both methods of observations pointed out an alternation of small/large cells from surface inward. Moreover, SEM pictures show that the shortest cells yield a thicker wall then the longest ones (Fig. 5.2E, F).

During the SEM observations it was not possible to measure the cell lumen in calcified samples, since they were obliterated after polishing. Hence, only histological measures of cells elongation from the meristematic cell inward along the same perithallial cell filament were plotted to show cycling features (Fig. 5.3), since the diameter of cells along the same filament was constant.

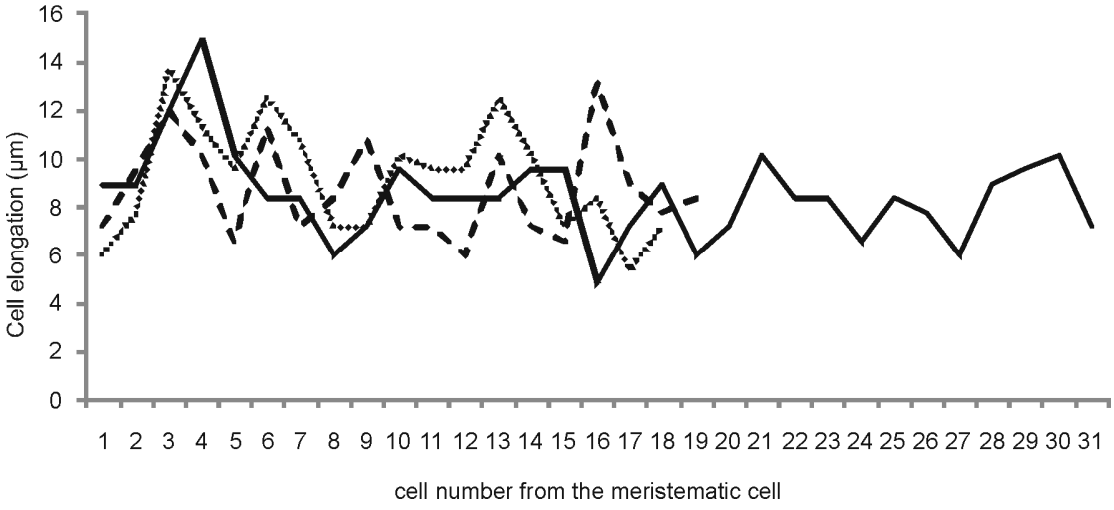

Fig. 5.3 Graph of the cell elongation measured from the meristematic cell inward of three different filaments in the histological section of the DB657 sample.

The two parallel transects of each analyzed protuberance in sample DB659 are not significantly different (t-test) in the Mg/Ca, Li/Ca and Ba/Ca time series, while in sample DB657 the time series of Mg/Ca and Li/Ca bear significant differences (Tab.2). The curves of Mg/Ca ratio measured in DB657 along the two transects showed several peaks, possibly due to the

measurement of secondary calcite, deposited inside the conceptacles (Fig. 5.4). Microscopical observations of sectioned samples provide evidence that the highest peak corresponds to a conceptacle, while the other minor spikes correspond to conceptacles buried under a thin layer of calcite. Observations of Mg/Ca time series in DB657 show that the production of carposporangial conceptacles in *L. kotschyanum* f. *affine* occurs at the end of winter, when SST is rising (Fig. 5.4). For these reasons, the elements average of the two transects in specimen DB657 was not retained for the correlation with the SST record. Hence, the relationship between elements and SST was investigated only in the two transects of specimen DB659.

Table 2 Statistical analysis (T-test) between elements/Ca ratios measured along the two parallel transects in each protuberance (DB659a, DB659b and DB657) and between the two protuberances of sample DB659 (DB659a-b).

Samples	T-value			p-value			df		
	Mg/Ca	Li/Ca	Ba/Ca	Mg/Ca	Li/Ca	Ba/Ca	Mg/Ca	Li/Ca	Ba/Ca
DB659a	1.82	1.04	-0.48	0.07	0.3	0.63	1600	1402	1402
DB659b	2.6	0.26	-1.34	0.01	0.79	0.18	3901	3902	3902
DB659a-b	-3.7	-0.8	5.4	<0.001	0.4	<0.001	86	86	86
DB657	3.03	6.4	0.77	0.002	<0.001	0.44	2458	2398	2460

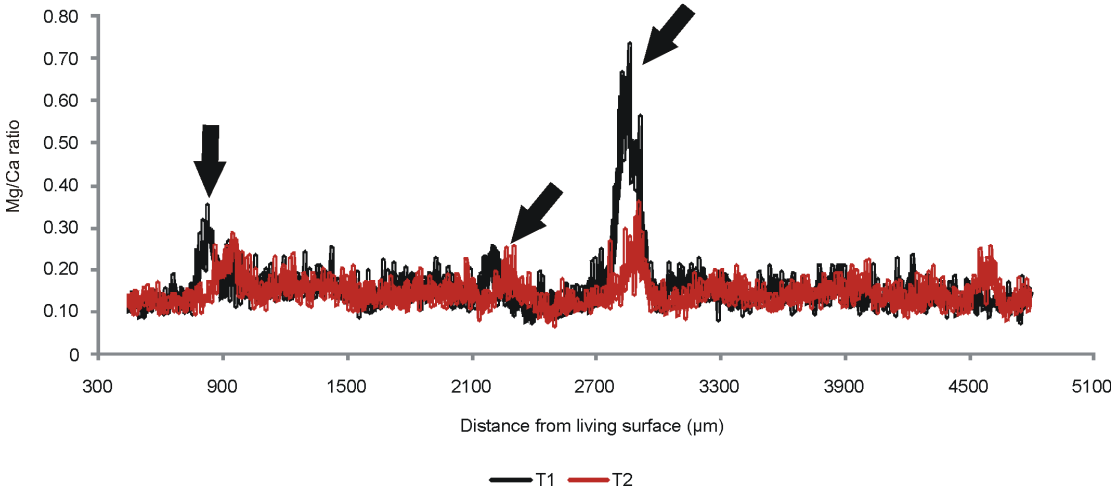

Fig. 5.4 LA-ICP-MS measured Mg/Ca cycles of the two parallel transects of the DB657 specimen showing the peaks of high Mg/Ca value measured into the conceptacles found along the transects (arrows).

T-tests between the mean elementary ratios of the two protuberances of sample DB659 (DB659a and DB659b) show significant differences in monthly Mg/Ca and Ba/Ca time series, while these differences does not occur for monthly Li/Ca (Tab.2).

All time series from both specimens show fluctuations of the analyzed elemental ratios from living surface inward (Fig. 5.5). Values of Mg, Li and Ba in the carbonate lattice of algae thallus are shown in Table 3. The samples contained an average of 20 mol % $MgCO_3$ (1 SE), 8 µmol % $LiCO_3$ (0.7 SE) and 0.5 µmol % $BaCO_3$ (0.03 SE).

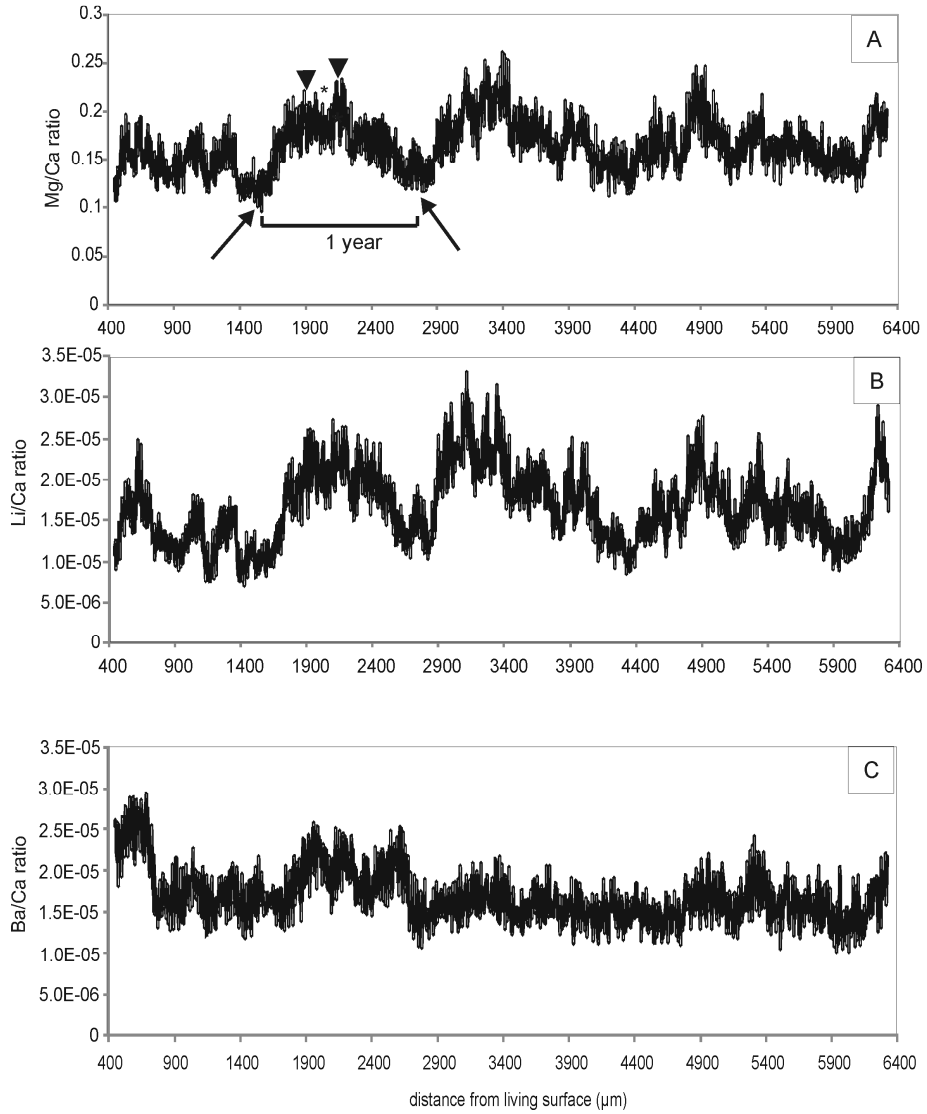

Fig. 5.5 LA-ICP-MS measured on DB659b of the two parallel transects of: A) Mg/Ca cycles used for calculating annual extension rates, showing two consecutive lower Mg/Ca values (arrows) corresponding to a year, and showing monsoon Mg/Ca value (star) between the two Mg/Ca peaks of the pre and post monsoon (arrowheads); B) Li/Ca cycles; C) Ba/Ca cycles.

Table 3 Annual extension rates of all samples. Values were obtained by mean of annual extension rates of samples gotten from Mg/Ca age model. For each sample were indicated the elements values mediated from time series measured by LA-ICP-MS.

Sample	Location	extension rate (µm)	$MgCO_3$ mol%	$LiCO_3$ µmol%	$BaCO_3$ µmol%
DB657	Balhaf	1182.9 (SD 422.2)	19.3 (SD 4.0)	7.3 (SD 2.0)	0.5 (SD 0.2)
DB659a	Balhaf	727.5 (SD 151.4)	19.6 (SD 4.6)	8.4 (SD 3.4)	0.5 (SD 0.1)
DB659b	Balhaf	1541.9 (SD 321.7)	21.2 (SD 4.2)	8.7 (SD 2.5)	0.5 (SD 0.1)
DB659bis	Balhaf	337.75 (SD 124.08)	20.2 (SD 4.3)	8.8 (SD 2.8)	0.5 (SD 0.2)
DB635	Socotra	208.2 (SD 86.78)	20.1 (SD 4.9)	6.9 (SD 2.5)	0.4 (SD 0.1)
DB576	Kamaran	446.4 (SD 216)	19.9 (SD 3.5)	6 (SD 1.6)	0.4 (SD 0.1)

The annual mean extension rate has been measured from Mg/Ca age model for all samples (Tab. 3). Extension rate was found to be highly variable between the years and in different parts of the same specimen (Fig. 5.6). The annual extension rate was on average 1134.75 µm (SD 484) in the encrusting specimen (DB659) and 1182.9 µm (SD 422.25) in the rhodolith (DB657) (Tab.3).

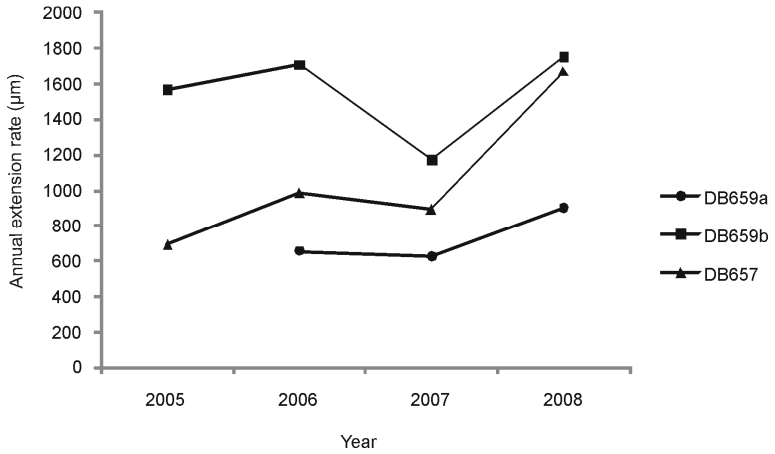

Fig. 5.6 Annual extension rates measured by Mg/Ca cycles in three specimens from Balhaf.

The monthly Mg/Ca mean ratio coincides with seasonal variations in SST (Fig. 5.7A). Linear regressions between monthly mean Mg/Ca and Li/Ca show a significant correlation

(r=0.85-0.9, p<0.0001) in both samples. Monthly Mg/Ca and Li/Ca time series reveal a temporal coherence (Fig. 5.7B). Linear regressions between the elementary ratios and reconstructed SST (HadiSST) were calculated using monthly values, and a positive relationship is observed for DB659a-b (r=0.6-0.7, p<0.0001; Fig. 5.8, Tab. 4). The regression between monthly algal Mg/Ca with SSTs revealed an alga Mg/Ca to SST relationship of 0.0065 ratio $°C^{-1}$, thus 1.06 mol % of $MgCO_3$ $°C^{-1}$ (DB659a) and 0.0078 ratio $°C^{-1}$, thus 2.06 mol % of $MgCO_3$ $°C^{-1}$ (DB659b) (Fig. 5.8). The regression of Li/Ca ratio with SSTs revealed an algae Li/Ca-SST relationship of 10^{-6} ratio $°C^{-1}$, thus 0.57 µmol % of $LiCO_3$ $°C^{-1}$ (Fig. 5.8).

Table 4 Statistical analysis (linear correlation) for algal samples between monthly elements/Ca ratio and SST (HadiSST1), and for *Lithothaminion glaciale* and *Phymatolithon calcareum* with *in situ* SST by Kamenos et al. (2008), and *Clathromorphum compactum* and *Clathromorphum nerostratum* with ERSST record by Hetzinger et al. (2010).

Samples	Species	Element	r-correlation	p-value
DB659a	*L. kotschyanum* f. *affine*	Mg/Ca ratio	0.6	<0.0001
		Li/Ca ratio	0.7	<0.0001
		Ba /Ca ratio	No statistically significant correlation	
DB659b	*L. kotschyanum* f. *affine*	Mg/Ca ratio	0.7	<0.0001
		Li/Ca ratio	0.6	<0.0001
		Ba/Ca ratio	0.4	0.002
DB659bis	*L. kotschyanum* f. *affine*	Mg/Ca ratio	0.36	<0.0001
		Li/Ca ratio	0.37	<0.0001
		Ba/Ca ratio	No statistically significant correlation	
DB635	*Lithophyllum* sp.	Mg/Ca ratio	0.46	<0.0001
		Li/Ca ratio	0.38	<0.0001
		Ba/Ca ratio	No statistically significant correlation	
DB576	*L. kotschyanum* f. *affine*	Mg/Ca ratio	0.48	<0.0001
		Li/Ca ratio	0.42	<0.0001
		Ba/Ca ratio	No statistically significant correlation	
Kamenos et al (2008)	*Lithothamnion glaciale*	Mg/Ca ratio	0.97	<0.0001
	Phymatolithon calcareum	Mg/Ca ratio	0.89	<0.0001
Hetzinger et al. (2010)	*Clathromorphum compactum*	Mg/Ca ratio	0.77	<0.001
		Ba/Ca ratio	-0.37	<0.01
	Clathromorphum nerostratum	Mg/Ca ratio	0.54	<0.001
		Ba/Ca ratio	No statistically significant correlation	

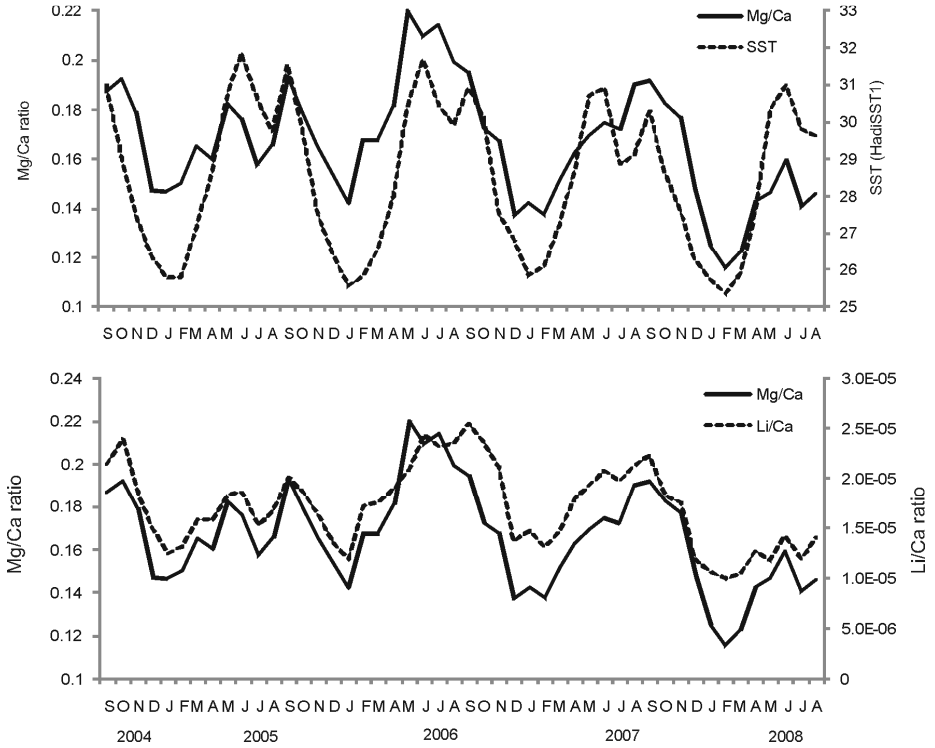

Fig. 5.7 Monthly mean comparison in DB659b specimen between: A) Mg/Ca ratio and SST (HadiSST1); B) Mg/Ca ratio and Li/Ca ratio.

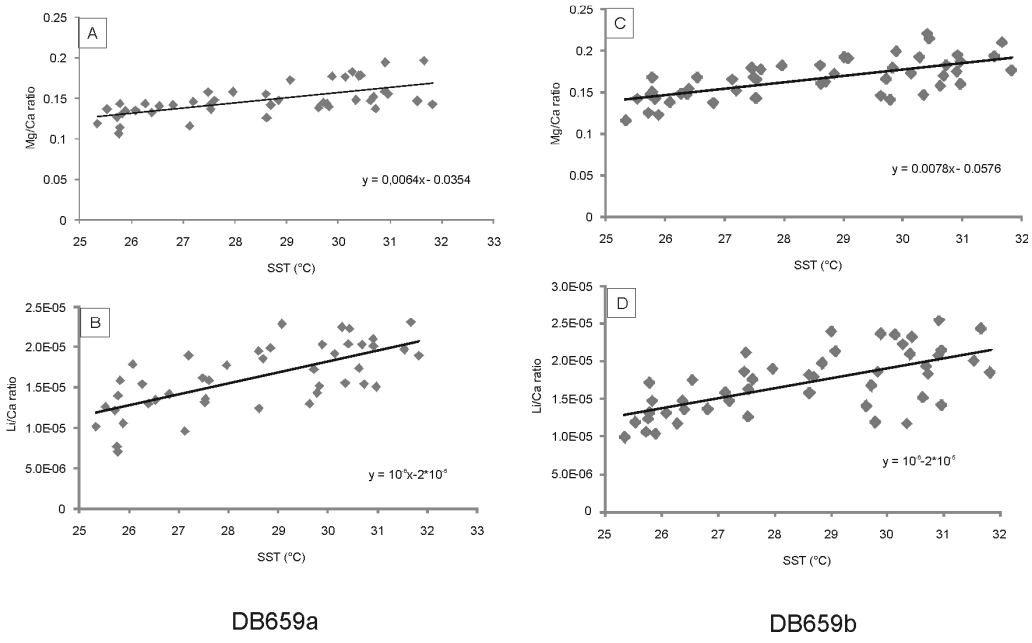

Fig. 5.8 Correlation between mean monthly Mg/Ca ratio and SST (HadiSST1) in : A) DB659a specimen; B) DB659b specimen. Correlation between mean monthly Li/Ca ratio and SST in: C) DB659a specimen; D) DB659b specimen.

The increase and decrease of Mg/Ca in the monthly averaged time series coincide with the increase of Ba/Ca (Fig. 5.9A), however, no significant correlation was found between the two ratios. Correlation between monthly Ba/Ca and SST was not significant in DB659a, and significant but weak in DB659b (r=0.4, p=0.002) (Tab.4). The highest Ba/Ca peak coincides with spring-summer 2007, but it did not coincide with the highest Mg/Ca peak (Fig. 5.9A). This peak in Ba/Ca was found in both protuberances of sample DB659, but not in DB657 (Fig. 5.9B).

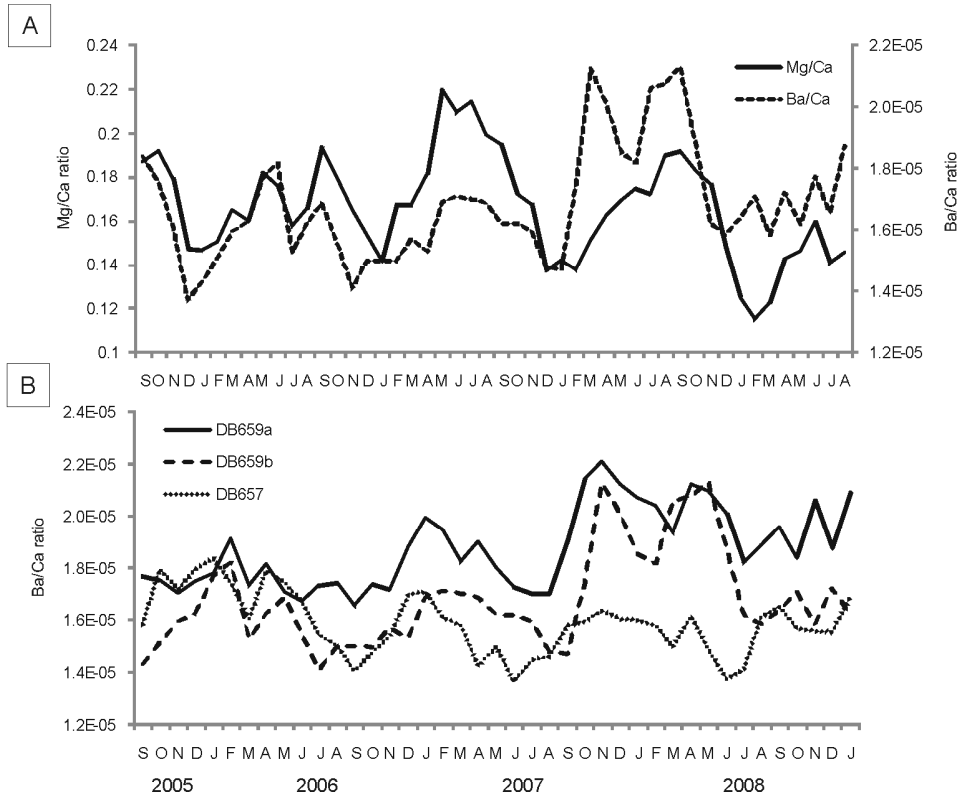

Fig. 5.9 Monthly mean of: A) the Mg/Ca ratio compering with Ba/Ca ratio in DB659b specimen; B) Ba/Ca ratio measured on thallus of the two protuberance of DB659 sample and DB657 sample.

5.1.2. DB659bis

This is the longest protuberance of DB659 sample, where an age model of 33 yrs has been reconstructed. All time series show fluctuations of the analyzed elemental ratios from living surface to inward, and both Mg/Ca and Li/Ca time series displayed a similar trend (Fig. 5.10). Values of Mg, Li and Ba in the carbonate lattice of algae thallus are shown in Table 3. The specimen contained an average of 20.2 mol % $MgCO_3$ (4.3 SD), 8.8 µmol % $LiCO_3$ (2.8 SD) and 0.5 µmol % $BaCO_3$ (0.2 SD), values that are similar to what has been found in the others specimens of Balhaf (Tab. 3).

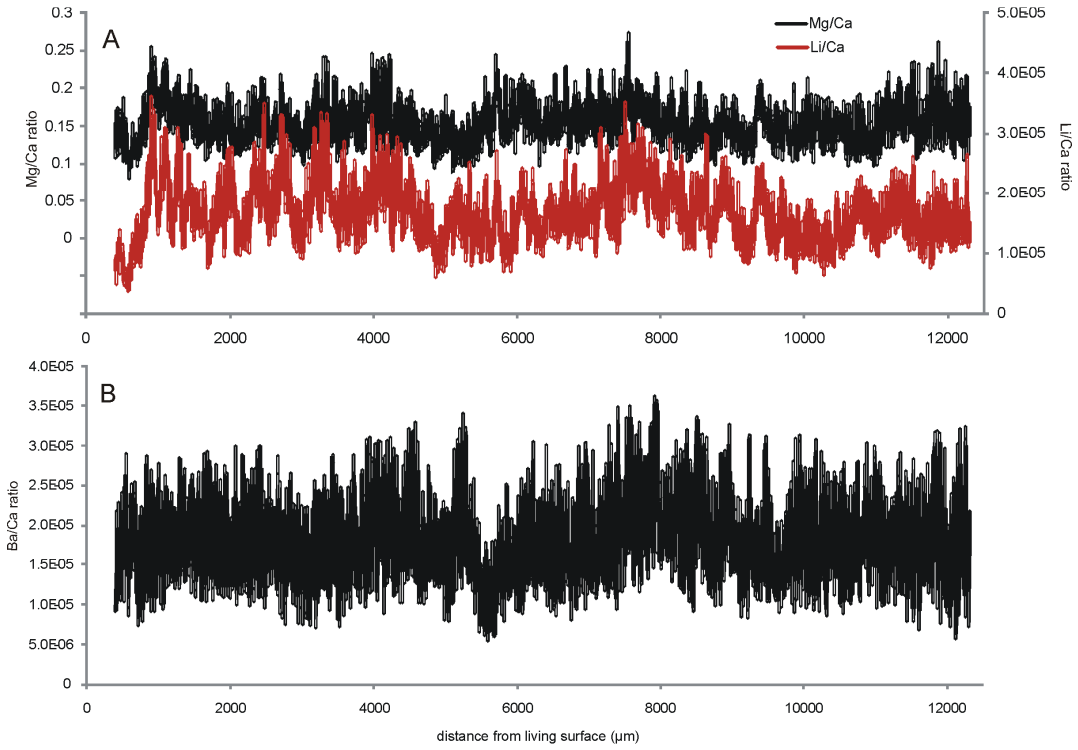

Fig. 5.10 LA-ICP-MS measured on DB659bis specimen of: A) Mg/Ca and Li/Ca cycles; B) Ba/Ca ratio cycles

The annual mean extension rate has been measured from Mg/Ca age model (Tab. 3). Extension rate was found to be highly variable between the years (Fig. 5.11). The annual extension

rate was on average 337.75 µm (SD 124.08) and it range between a minimum of 185.5 µm and a maximum of 592.9 µm. No significant correlations is found between extension rates and gridded SST (HadiSST1). Linear regression between extension rate and gridded SSS (SODA v2.2.4) revealed a weak correlation (r=0.3, p-value=0.07).

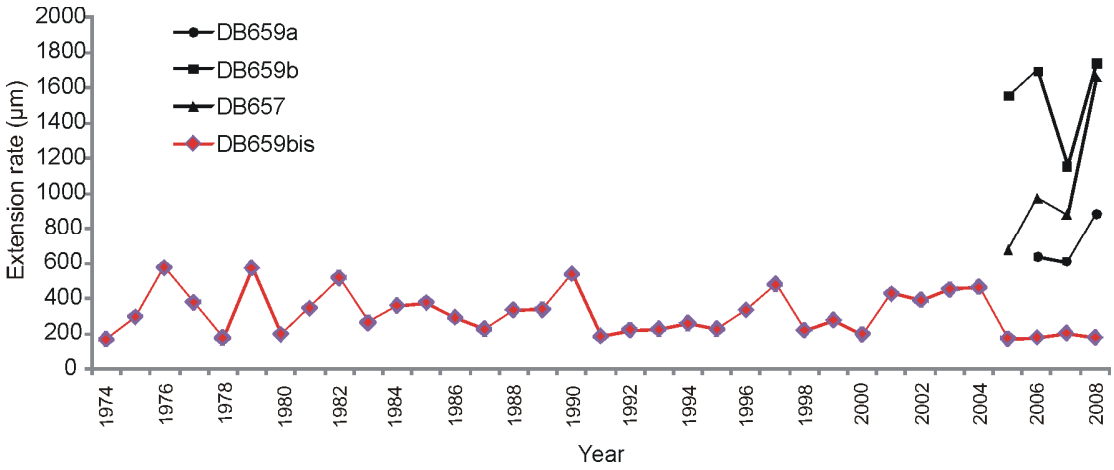

Fig. 5.11 Annual extension rates measured by Mg/Ca cycles in all specimens from Balhaf.

The monthly Mg/Ca mean ratio coincides with seasonal variations in SST (Fig. 5.12). Linear regressions between monthly mean Mg/Ca and Li/Ca showed a strong positive and significant correlation (r=0.67, p-value < 0.001). Monthly Mg/Ca and Li/Ca time series reveal a temporal coherence except since 1978 to 1980 (Fig. 5.13). Linear regressions between the elementary ratios and reconstructed SST (HadiSST1) were calculated using monthly values, and a positive weak, but significant is observed (Tab. 4). The regressions between monthly algal Mg/Ca with SSTs revealed an alga Mg/Ca to SST relationship of 0.0038 ratio $°C^{-1}$, thus 0.62 mol % of $MgCO_3$ $°C^{-1}$ (Fig. 5.14A). The regression of Li/Ca ratio with SSTs revealed an algal Li/Ca-SST relationship of $8*10^{-7}$ ratio $°C^{-1}$, thus 0.46 µmol % of $LiCO_3$ $°C^{-1}$ (Fig. 5.14B). The increase and decrease of Mg/Ca in the monthly averaged time series coincide with the increase of Ba/Ca, except in 1992 and since 1974 to 1982 (Fig. 5.15). However, no significant correlation was found between

the two ratios. Correlation between monthly Ba/Ca and gridded SST was not significant.

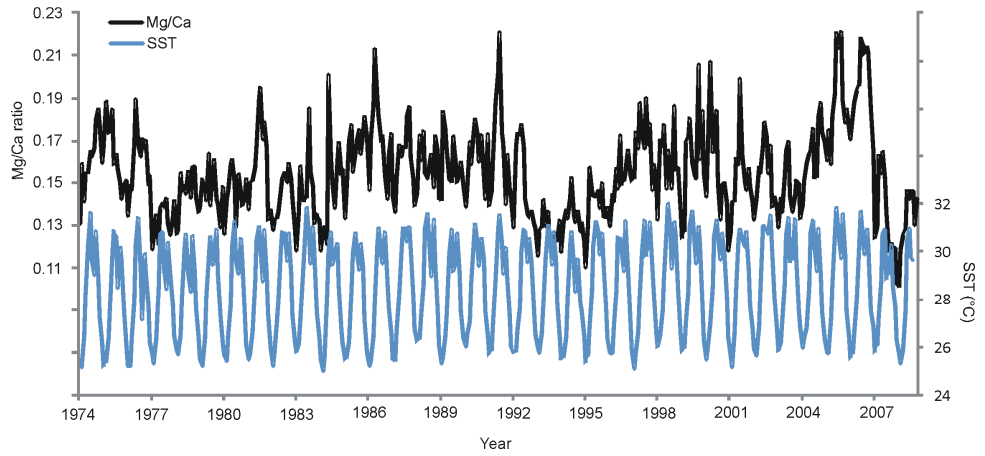

Fig. 5.12 Monthly mean of Mg/Ca ratio measured on thallus of DB659bis specimen, comparing with monthly mean of gridded SST (HadiSST1).

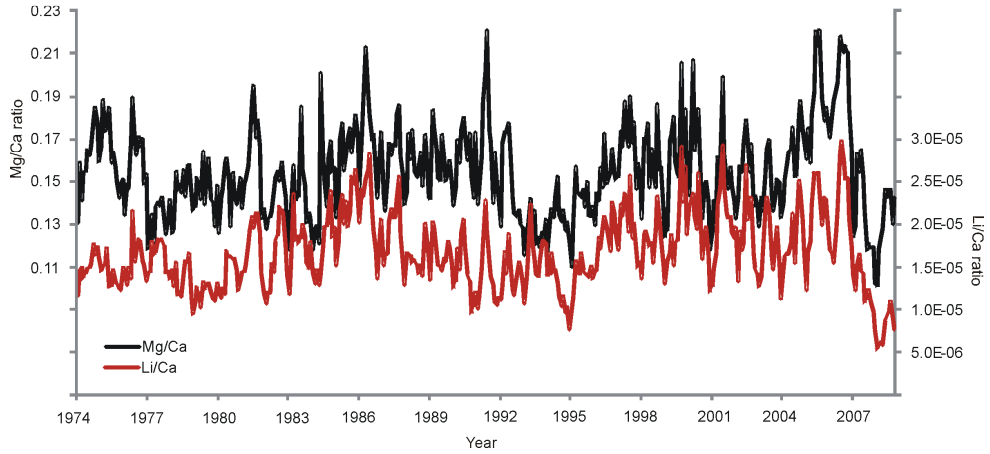

Fig. 5.13 Monthly mean of Mg/Ca ratio and Li/Ca ratio measured on thallus of DB659bis specimen.

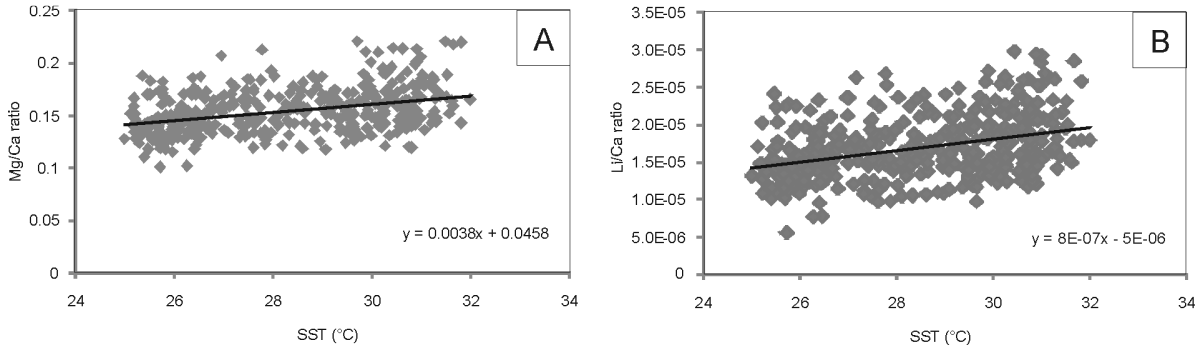

Fig. 5.14 DB659bis specimen, correlation between: A) mean monthly Mg/Ca ratio and SST (HadiSST1); B) mean monthly Li/Ca ratio and SST.

The annual Mg/Ca coincides with annual variations in SST except since 1982 to 1984, that showed an inverse relationship between the two time series (Fig. 5.16A). Annual Mg/Ca and Li/Ca time series revealed a temporal coherence except in 1979 and 1992 (Fig. 5.16B). Linear regressions between elementary ratios and reconstructed SST were calculated using annual values, and a positive weak relationship was observed for Li/Ca ($r=0.42$, p-value=0.01), but no correlation was found for Mg/Ca ($r=0.26$, p-value=0.1). Linear regressions between annual mean Mg/Ca and annual SST since 1976 to 2007 (avoided the years since 1974 to 1976) showed an increase of statistical relationship, thus a weak correlation was found ($r=0.34$, p-value=0.06). The increase and decrease of annual mean Ba/Ca coincides with the increase of annual Mg/Ca. However, no significant correlation was observed between the two time series (Fig. 5.16C).

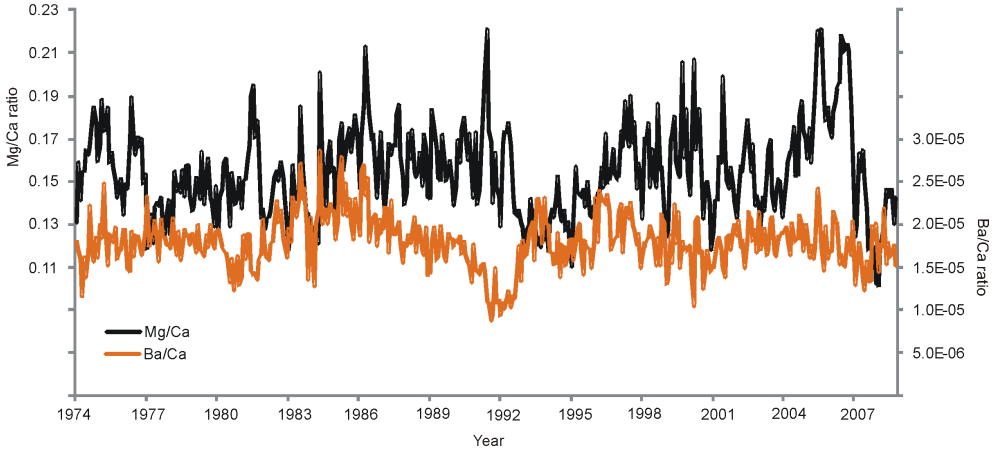

Fig. 5.15 Monthly mean of Mg/Ca ratio and Ba/Ca ratio measured on thallus of DB659bis specimen.

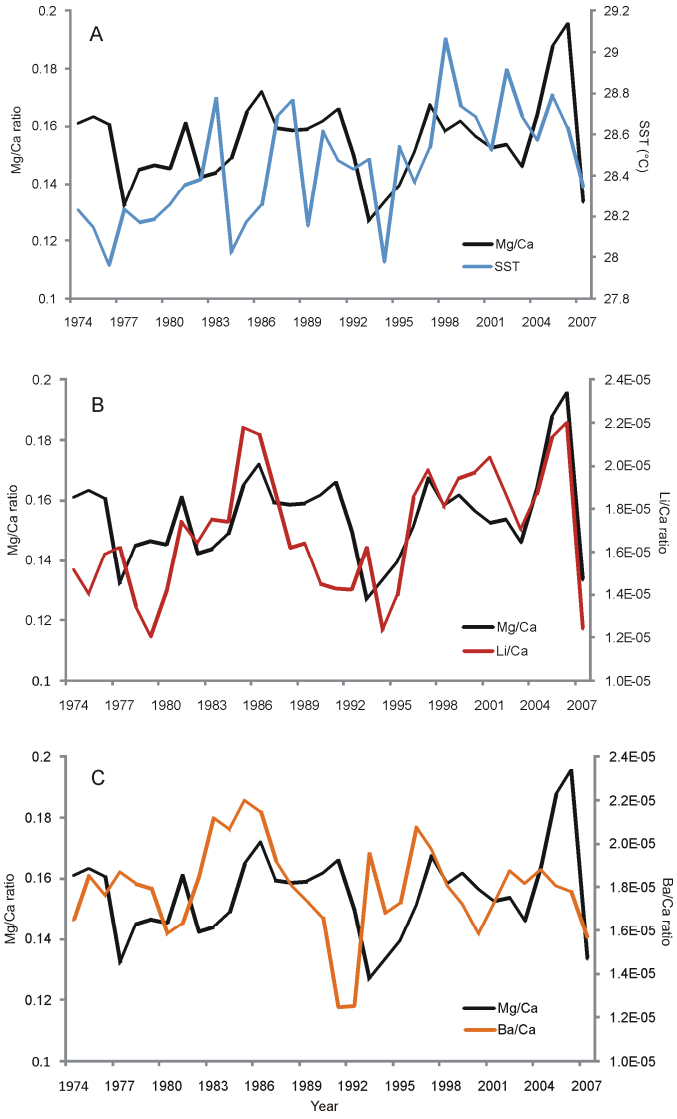

Fig. 5.16 DB659bis, annual mean of: A) Mg/Ca ratio and gridded SST (HadiSST1); B) Mg/Ca and Li/Ca ratio; C) Mg/Ca and Ba/Ca ratio.

5.2. Socotra

To date, the coralline flora of Socotra is very poorly known. This is an area with several endemism, mainly found in studies of terrestrial flora and fauna, while marine environment is little studied. Histological section of DB635 specimen revealed cells of adjacent filaments joined by secondary pit connection, absence of cell fusions, uniporate tetrasporangial conceptacles (diameter 240 µm, height 115 µm, length of the pore canal 553 µm; Fig. 5.17). Based on these attributes, the coralline algae involved in this study was identified as *Lithophyllum* sp. Morpho-genetic analysis (studying in progress) showed that this sample not correspond to any species described in literature.

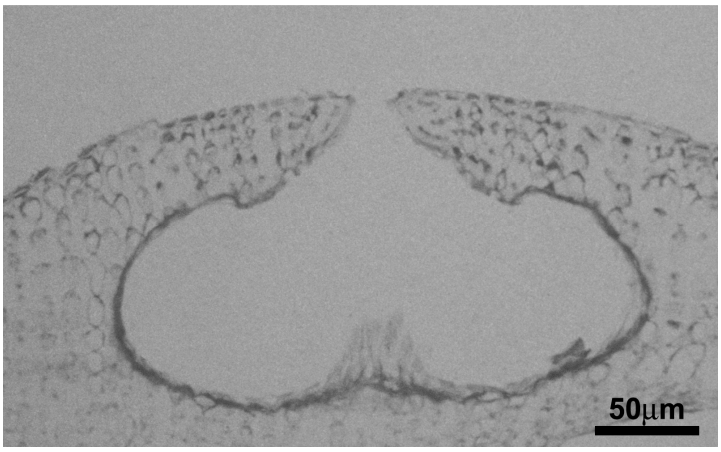

Fig. 5.17 Histological section of *Lithophyllum* sp. from Socotra showing a tetrasporangial conceptacle.

All time series showed fluctuations of the analyzed elemental ratios from living surface inward (Fig. 5.18), and an age model of 35 yrs has been reconstructed (since August 1972 to December 2009). The Mg/Ca and Li/Ca ratio displayed a similar trend (Fig. 5.18A, B). Values of Mg, Li and Ba in the carbonate lattice of alga thallus are shown in Table 3. The sample contained an average of 20.1 mol % $MgCO_3$ (SD 4.9), 6.9 mol % $LiCO_3$ (SD 2.5) and 0.4 mol % $BaCO_3$ (SD

0.1).

The annual mean extension rate has been measured from Mg/Ca age model (Tab. 3). Extension rate was found to be highly variable between the years (Fig. 5.19). The annual extension rate was on average 208.2 µm (SD 86.78), and it range between a minimum of 67.38 µm and a maximum of 410.43 µm. No significant correlations was found between extension rates and gridded SST (HadiSST1). Linear regression between extension rate and gridded SSS (SODA v2.2.4) revealed a strong correlation (r=0.5, p-value=0.002).

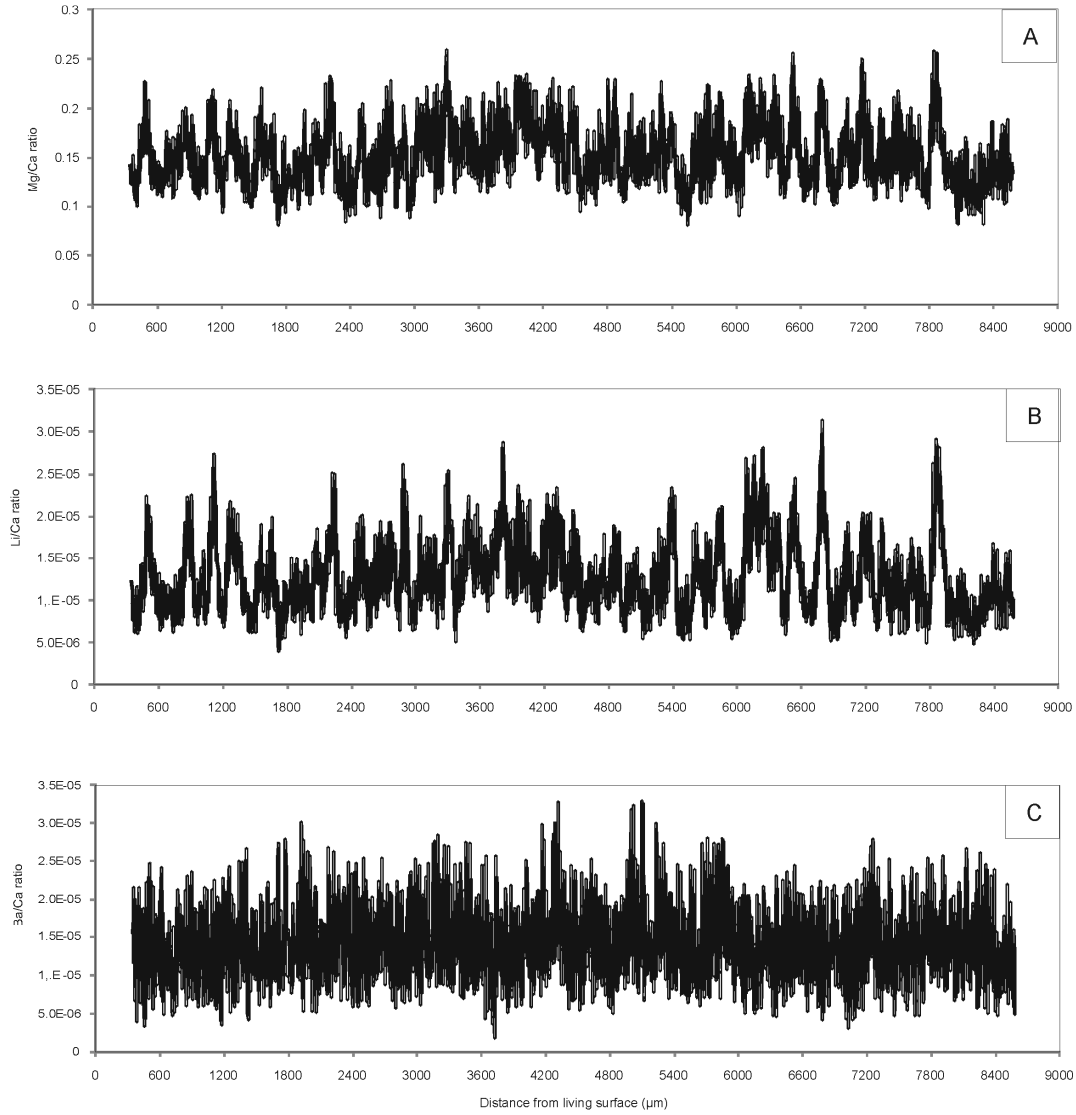

Fig. 5.18 LA-ICP-MS measured on *Lithophyllum* sp. from Socotra of: A) Mg/Ca cycles; B) Li/Ca cycles; C) Ba/Ca cycles.

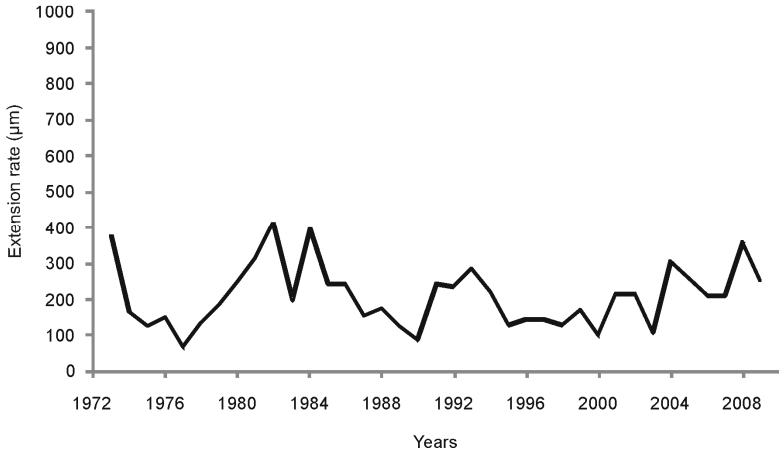

Fig. 5.19 Annual extension rates of *Lithophyllum* sp. from Socotra.

The monthly Mg/Ca mean ratio coincides with seasonal variations in SST (Fig. 5.20A). Linear regressions between monthly mean Mg/Ca and Li/Ca ratio showed a strong positive and significant correlation ($r=0.67$, p-value < 0.0001). Monthly Mg/Ca and Li/Ca time series revealed a temporal coherence from 1972 to 2009 (Fig. 5.20B).

Linear regressions between the elementary ratios and reconstructed SST (HadiSST1) were calculated using monthly values, and a positive weak, but significant is observed (Tab. 4). The regressions between monthly algal Mg/Ca with SSTs revealed an alga Mg/Ca to SST relationship of 0.0075 ratio $°C^{-1}$, thus 1.22 mol % $MgCO_3$ $°C^{-1}$ (Fig. 5.21A). The regression of Li/Ca ratio with SSTs revealed an algal Li/Ca-SST relationship of $9*10^{-7}$ ratio $°C^{-1}$, thus 0.52 µmol % of $LiCO_3$ $°C^{-1}$ (Fig. 5.21B).

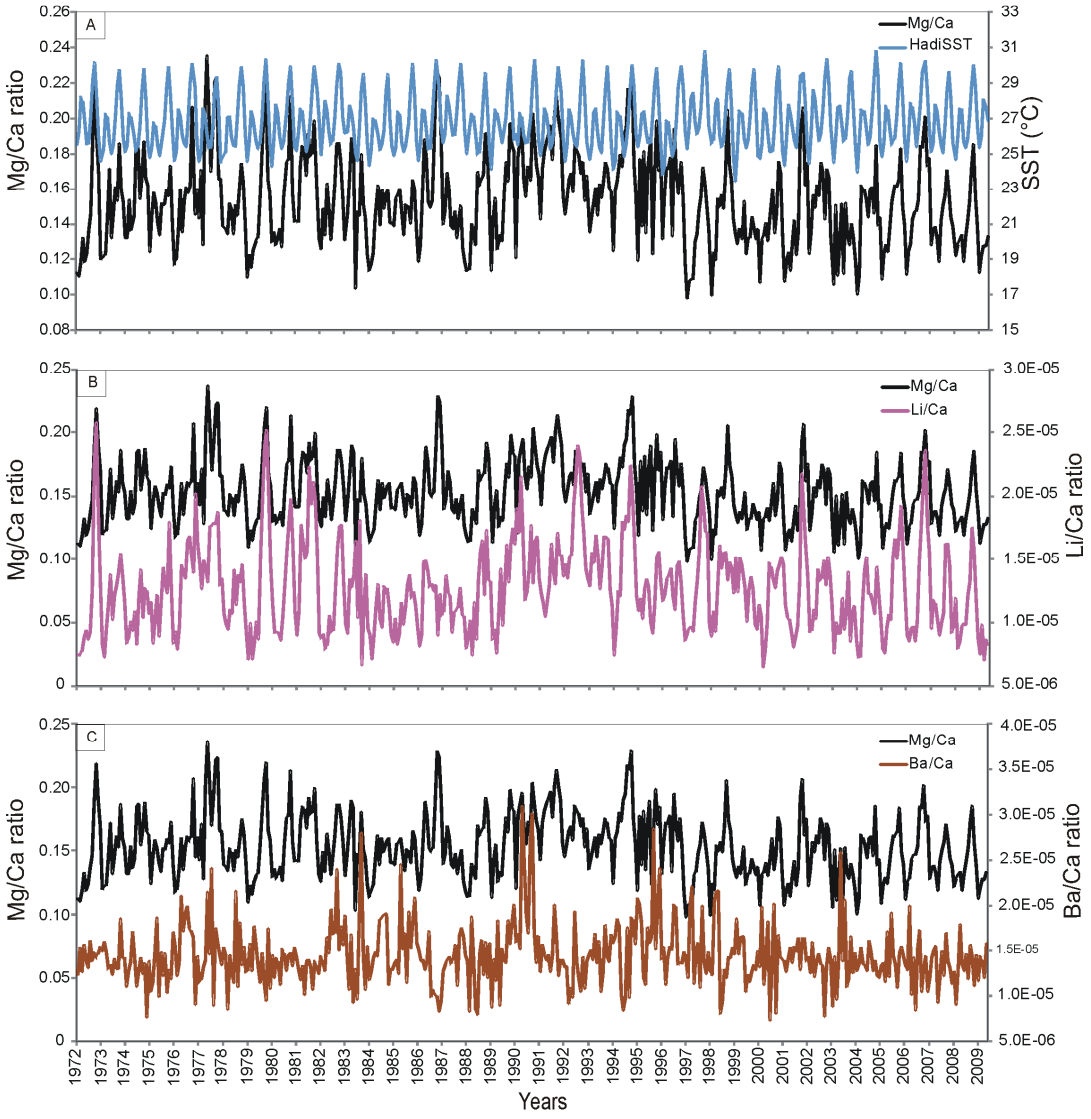

Fig. 5.20 *Lithophyllum* sp. from Socotra, monthly mean of: A) Mg/Ca ratio and gridded SST (HadiSST1); B) Mg/Ca and Li/Ca ratio; C) Mg/Ca and Ba/Ca ratio.

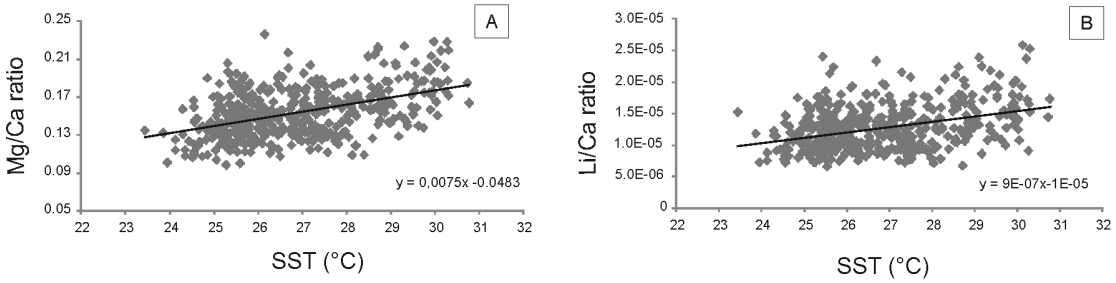

Fig. 5.21 *Lithophyllum* sp. from Socotra, correlation between: A) mean monthly Mg/Ca ratio and SST (HadiSST1); B) mean monthly Li/Ca ratio and SST.

The increase and decrease of Mg/Ca in the monthly averaged time series coincide with the increase of Ba/Ca (Fig. 5.20C). However, no significant correlations was found between the ratios. Correlation between monthly Ba/Ca and gridded SST was not significant.

The increase and decrease of annual mean Mg/Ca ratio coincides with the increase and decrease of annual mean SST except since 1972 to 1976, and since 1997 to 2000, that showed an inverse relationship between the two time series (Fig. 5.22A). The annual Mg/Ca and Li/Ca time series revealed a temporal coherence except since 1972 to 1976 (Fig. 5.22B). Linear regressions between elementary ratios and reconstructed SST were calculated using annual values, and no relationship is observed between both time series. The increase and decrease of annual Ba/Ca did not coincide with increase and decrease of annual Mg/Ca, except since 1988 to 1996 (Fig. 5.22C).

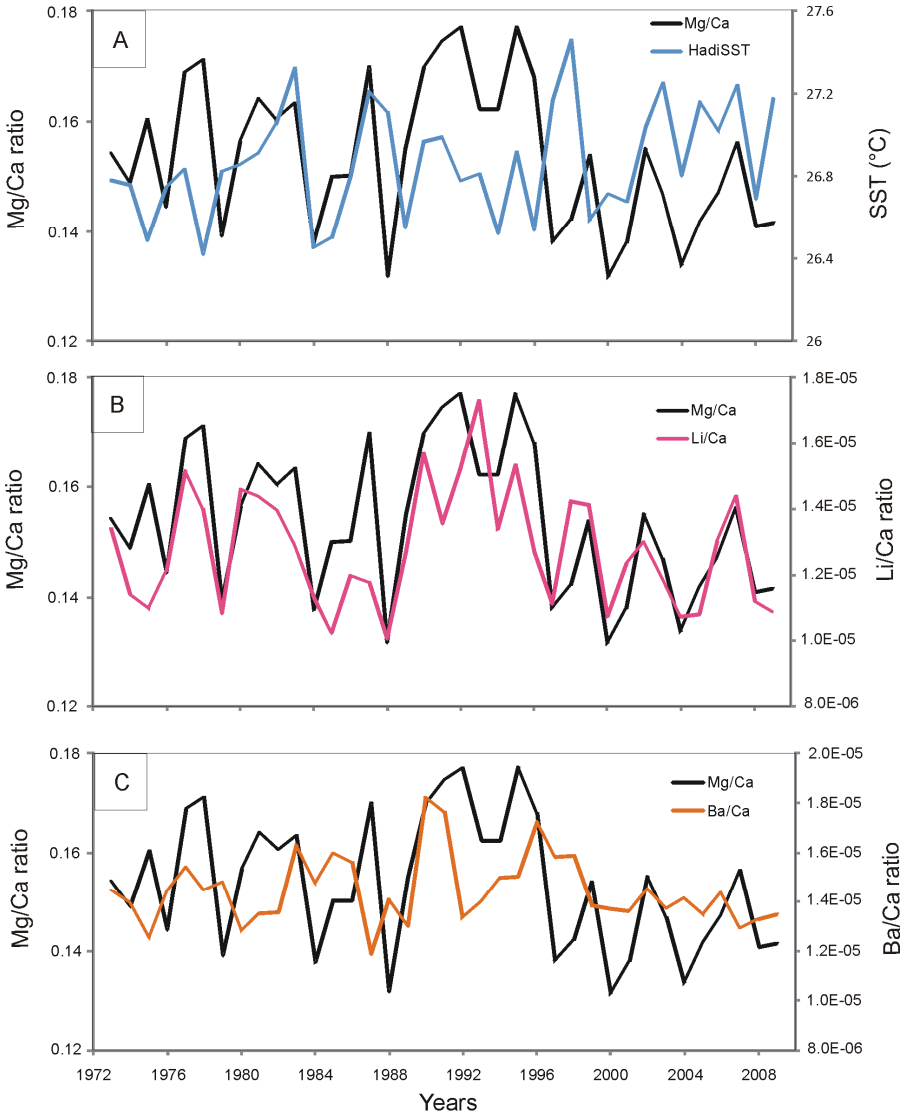

Fig. 5.22 *Lithophyllum* sp. from Socotra, annual mean of: A) Mg/Ca ratio and gridded SST (HadiSST1); B) Mg/Ca and Li/Ca ratio; C) Mg/Ca and Ba/Ca ratio.

5.3. Kamaran

Histological section of DB576 sample revealed cells of adjacent filaments joined by secondary pit connection, absence of cell fusions, uniporate tetrasporangial conceptacles (diameter 268 µm, height 153 µm, length of the pore canal 568 µm; Fig. 5.23). Based on these attributes, the coralline algae involved in this study was identified as *L. kotschyanum* f. *affine*.

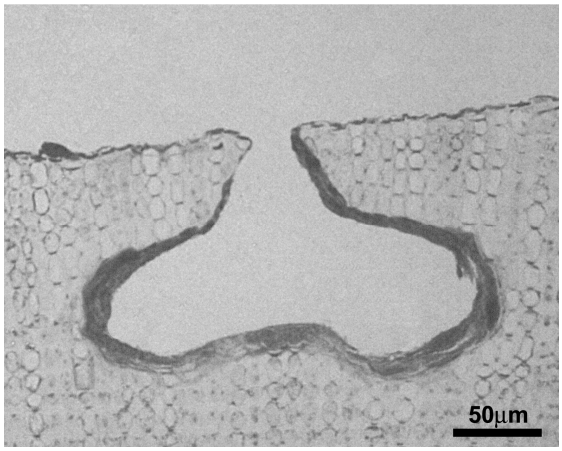

Fig. 5.23 Histological section of *Lithophyllum kotschyanum* f. *affine* from Kamaran showing a tetrasporangial conceptacle.

All time series showed fluctuations of the analyzed elemental ratios from living surface inward (Fig. 5.24), and an age model of 15 yrs has been reconstructed (since January 1994 to December 2008). The Mg/Ca and Li/Ca ratio displayed a similar trend (Fig. 5.24A and B). Values of Mg, Li and Ba in the carbonate lattice of alga thallus are shown in Table 3. The sample contained an average of 19.9 mol % $MgCO_3$ (SD 3.5), 6 mol % $LiCO_3$ (SD 1.6) and 0.4 mol % $BaCO_3$ (SD 0.1).

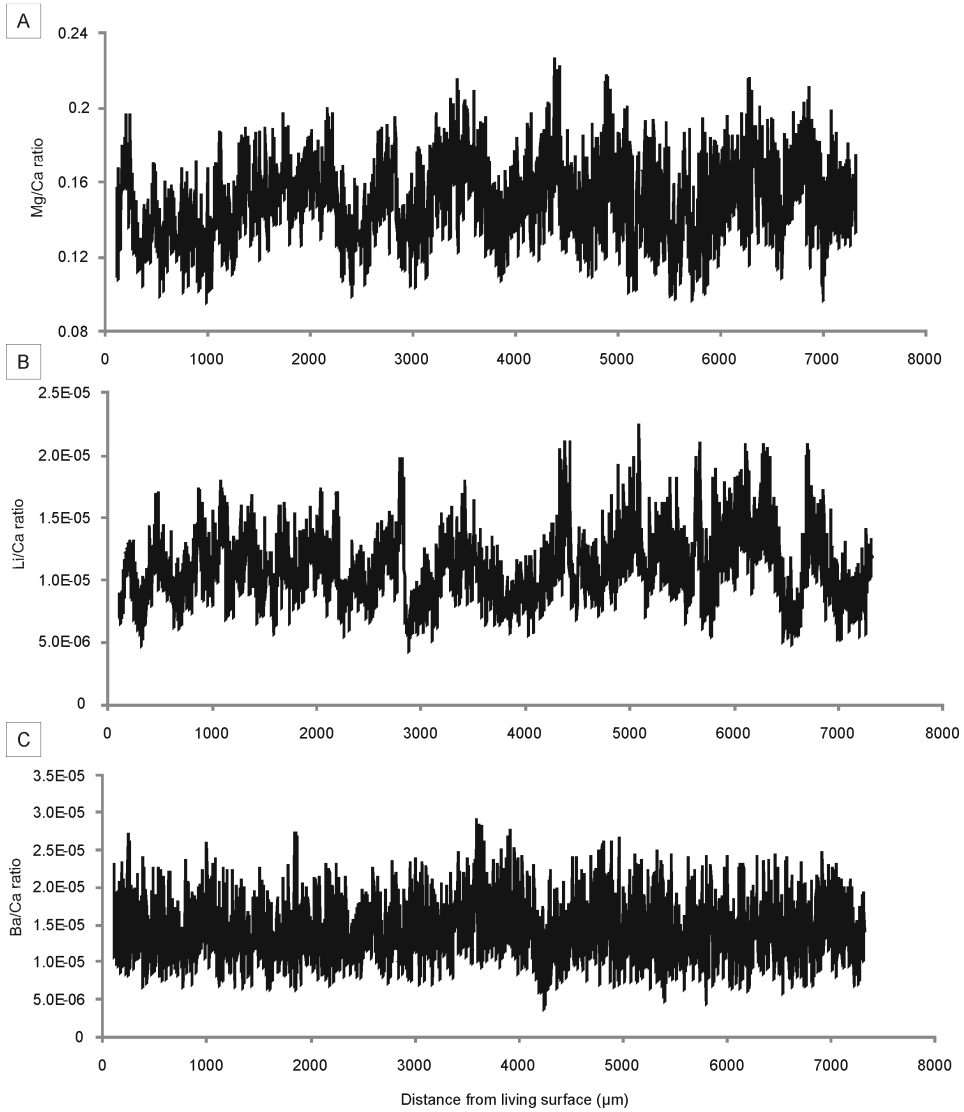

Fig. 5.24 LA-ICP-MS measured on *L. kotschyanum* f. *affine* from Kamaran of: A) Mg/Ca cycles; B) Li/Ca cycles; C) Ba/Ca cycles.

The annual mean extension rate has been measured from Mg/Ca age model (Tab. 3). Extension rate was found to be highly variable between the years (Fig. 5.25). The annual extension rte was on average 446.4 µm (SD 216), and it range between a minimum of 218.91 µm and a maximum of 915.15 µm. No significant correlations was found between extension rates and gridded SST (HadiSST1). Linear regression between extension rate and gridded SSS (SODAv2.2.4) did not show significant correlation.

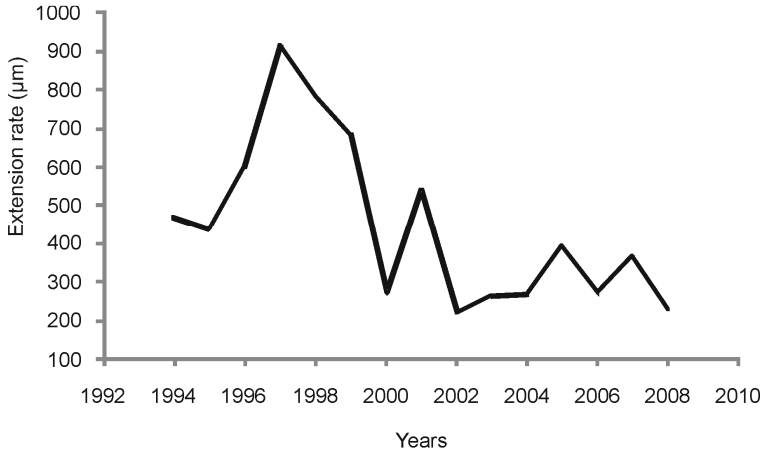

Fig. 5.25 Annual extension rates of *L. kotschyanum* f. *affine* from Kamaran.

The monthly Mg/Ca mean ratio coincides with seasonal variations in SST (Fig. 5.26A). Linear regression between monthly mean Mg/Ca and Li/Ca ratio showed a positive and significant correlation (r=0.5, p-value <0.00001). Monthly Mg/Ca and Li/Ca time series revealed a temporal coherence since 1994 to 2008 (Fig. 5.26B). Linear regressions between the elementary ratios and gridded SST were calculated using monthly values, and a positive weak, but significant is observed (Tab. 4). The regression between monthly algal Mg/Ca with SSTs revealed an alga Mg/Ca to SST relationship of 0.0086 ratio $°C^{-1}$, thus 1.4 mol % $MgCO_3$ $°C^{-1}$ (Fig. 5.27A). The regression of Li/Ca ratio with SSTs revealed an alga Li/Ca-SST relationship of $1*10^{-6}$ ratio $°C^{-1}$, thus 0.57 µmol % of $LiCO_3$ $°C^{-1}$ (Fig. 5.27B).

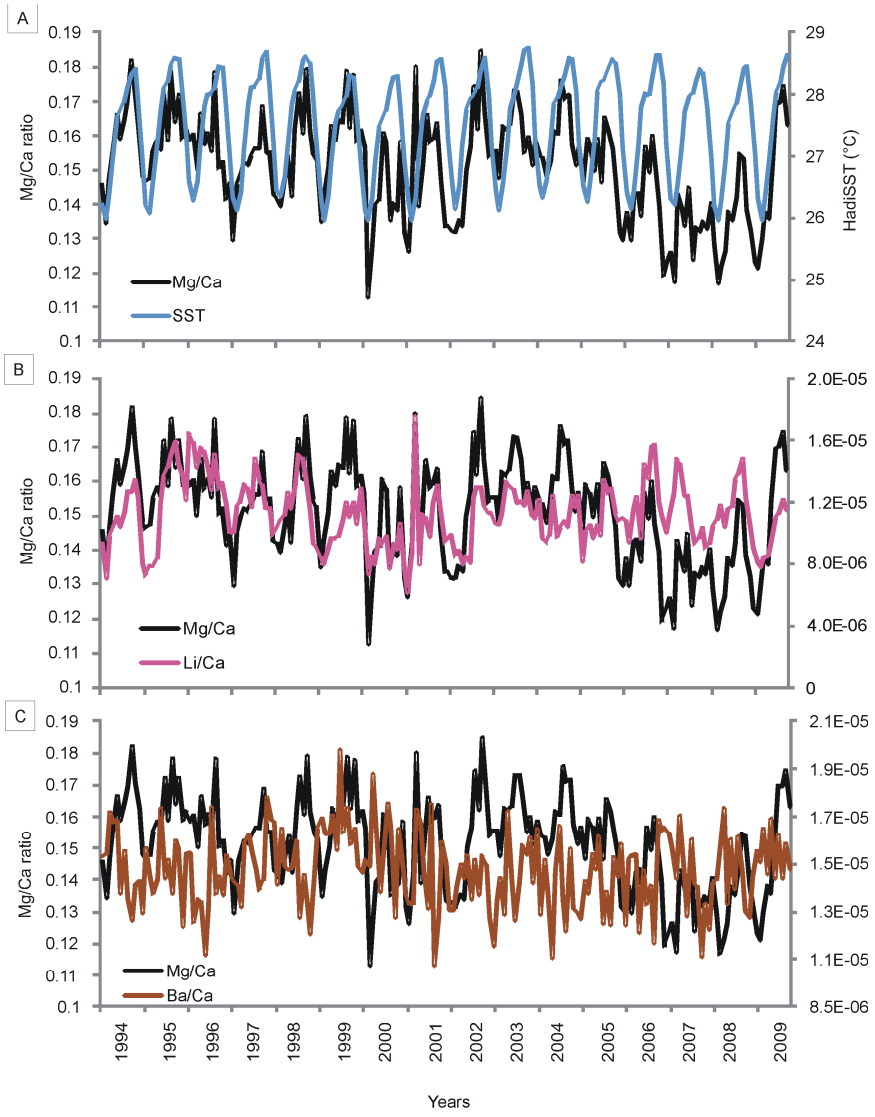

Fig. 5.26 *L. kotschyanum* f. *affine* from Kamaran, monthly mean of: A) Mg/Ca ratio and gridded SST (HadiSST1); B) Mg/Ca and Li/Ca ratio; C) Mg/Ca and Ba/Ca ratio.

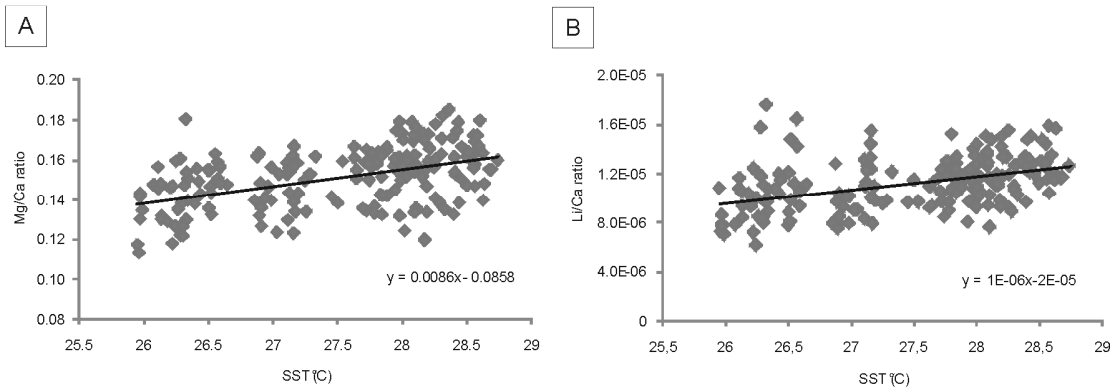

Fig. 5.27 *L. kotschyanum* f. *affine* from Kamaran, correlation between: A) mean monthly Mg/Ca ratio and SST (HadiSST1); B) mean monthly Li/Ca ratio and SST.

The increase and decrease of Mg/Ca in the monthly averaged time series coincide with the increase of Ba/Ca (Fig. 5.26C). However, no significant correlations was found between the ratios. Correlation between monthly Ba/Ca and gridded SST was not significant.

The increase and decrease of annual mean Mg/Ca ratio coincides with the increase of annual mean SST except for year 2004, that showed an inverse relationship between the two series, and the annual record peak of the year 1999, that it lags the SST by 1 yr (Fig. 5.28A). The annual Mg/Ca and Li/Ca time series revealed a temporal coherence except since 2005 to 2008 (Fig. 5.28B). Linear regession between elementary ratios and reconstructed SST were calculated using annual values, and no relationship is observed between both time series. the increase and decrease of annual Ba/Ca did not coincide with increase of annual Mg/Ca, except since 1994 to 1996, and since 1998 to 2000 (Fig. 5.28C).

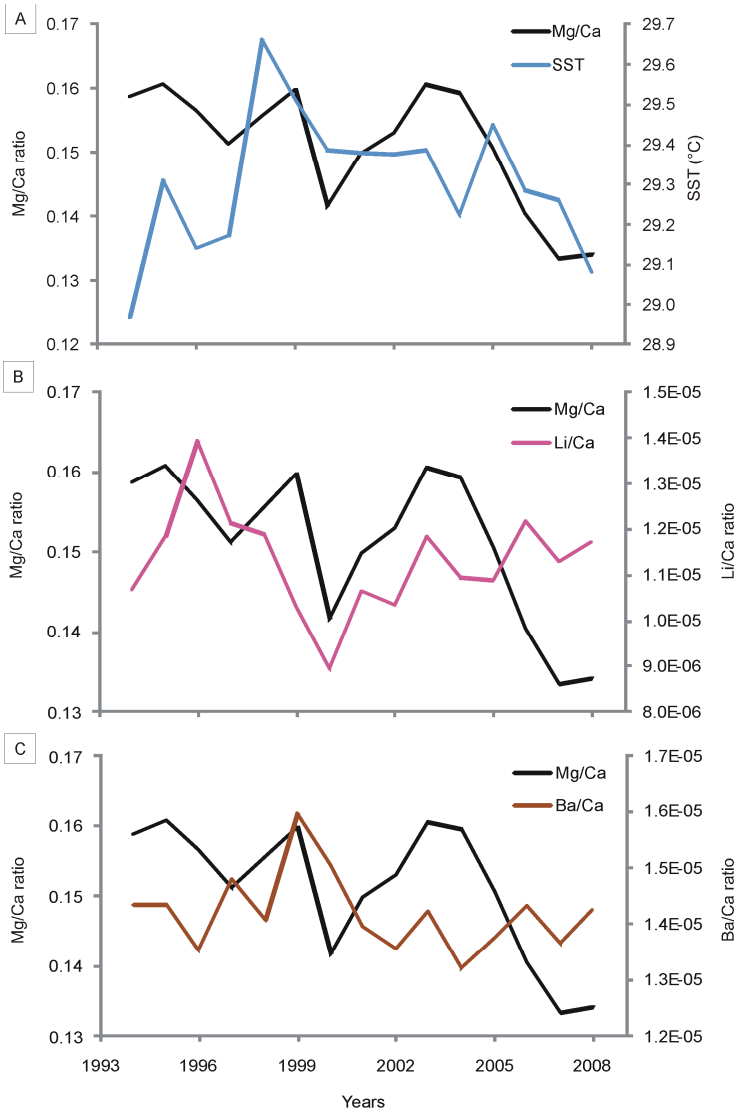

Fig. 5.28 *L. kotschyanum* f. *affine* from Kamaran, annual mean of: A) Mg/Ca ratio and gridded SST (HadiSST1); B) Mg/Ca and Li/Ca ratio; C) Mg/Ca and Ba/Ca ratio.

6. Discussion

6.1. Biological features and algal banding

Based on morphological features, the coralline algae analyzed in this study were identified as belonging to the species of *L. kotschyanum* f. *affine* (Foslie) Foslie (1909) for the samples DB659, DB657 and DB576, and to the species of *Lithophyllum* sp. Philippi (1837) for sample DB635.

Banding in longitudinal sections of coralline red algae thalli has been well described in species from high and medium latitudes (Cabioch 1966; Adey and McKibbin 1970; Agegian 1981; Freiwald and Henrich 1994; Basso 1994; Basso et al. 1997; Halfar et al. 2000; Blake and Maggs 2003). Although the genus *Lithothamnion* has been the most frequently used to date in studies of band periodicity, the present study shows the occurrence of annual banding also in the genus *Lithophyllum*. Banding in *Lithothamnion* is caused by different growth rates of alternating thick-walled short cells versus thin-walled long cells (Basso 1994; Basso et al. 1997). This different rate of calcite deposition on cell wall corresponds also to a different cell size as showed by histological sections of *L. kotschyanum* f. *affine* (Fig. 5.2 and 5.3). Adey and McKibbin (1966) argued that difference in cell size found in histological sections could be an artifact of sample preparation, i.e. the use of the blade. This hypothesis can be excluded here, because differences in length of cells revealed in the histological sections were found also in the SEM pictures. To date the reasons for different growth rate are poorly understood, and more samples of this species from wider geographical areas and a control of growth pattern over longer periods will be needed to unravel the origin of banding in *L. kotschyanum* f. *affine*. The origin of banding in coralline algae is not fully understood. Cabioch (1966) argued that banding was due to growth cessation in rhodoliths by burial events. Recent studies have revealed that the growth interruption by burial is

frequently accompanied by surface abrasion resulting in a clear thallus discontinuity, which is a detectable taphonomic feature (Basso et al. 2009; Fig. 5.2A). Adey and McKibbin (1970) and Basso (1994) explain band formation by annual winter and summer growth rhythms. Freiwald and Henrich (1994) address banding patterns to monthly/lunar rhythms superimposed on annual cycle, and winter organic matter enrichment. Halfar et al. (2000) found second-order cycles of unknown nature, five to seven of which occur within an annual cycle.

Although conceptacles presence was not evident, during LA-ICP-MS analysis along DB657 transects several conceptacles were found. Their presence can be recognized by peaks in the values of Mg and Li, because conceptacles were filled with secondary calcite. They were probably hidden by a thin layer of calcified cells which became evident by the laser ablation. Although this drawback has made the geochemical data of this sample unsuitable for comparison with climate data, this provided information about ecology of this algae along the Yemeni coast. It is suggested that the conceptacles in *L. kotschyanum* f. *affine* are produced in late winter shortly before the rise of SST in spring. In non-geniculated coralline algae, conceptacles are located on the surface of crusts or on protuberances. They originate when groups of perithallial meristematic cells differentiate into conceptacle primordia (Johansen 1981; Woelkerling 1988), and it is assumed that one layer of conceptacles is produced in *Lithophyllum incrustans* each year in the British Isles (Irvine and Chamberlain 1994). Carposporophytes are formed when the post-fertilization development with diploid cells occurs within female conceptacles (Johansen 1981). Conceptacle formation is probably seasonal in most species in temperate areas, and sexual and asexual reproduction occurs in different time of the year (Johansen 1981). Species of *Lithophyllum* from Pacific coast of Japan produce reproductive organs at the warmest time of the year, with the onset of the summer until fall (Johansen 1981). In *L. incrustans* from British Isles, all reproductive types occur predominantly from October to April (Irvine and Chamberlain 1994). Timing of

reproduction of the species investigated in this study correspond to those described for *Lithophyllum* from the British Isles and *Clathromorphum* spp. from the Gulf of Main (Adey 1965), but not to those for *Lithophyllum* spp. of the Pacific coast of temperate Japan.

6.2. Annual extension rates

6.2.1. Balhaf

The annual extension rate of *L. kotschyanum* f. *affine* from Balhaf for the period 1974 to 2008 was variable with a mean of 470.96 µm y^{-1}, and a minimum of 185.46 µm y^{-1} and a maximum of 1.7 mm y^{-1}. Average vertical growth rates of coralline algae were reported to be highly variable, such as for *C. compactum* from the Gulf of Maine (Halfar et al. 2011). Several factors act on coralline algae growth. Growth rate is generally affected by 1) light intensity, only few species tolerate bright light (Johansen 1981), although growth is positively correlated with light at higher temperatures (Adey and McKibbin 1970); 2) sedimentation rate: fine sedimentation threatens corallines survival by smothering, since they are slow-growing plants (Dethier and Steneck 2001; Foster 2001); 3) hydrodynamics: a moderate water movement is required to keep the coralline surface clean and prevent poisoning by water stagnation (Steneck and Adey 1976); 4) intensity and type of herbivory: a moderate herbivory is vital to corallines since herbivores keep encrusting algae free from excessive shading by fast-growing soft algae (Steneck 1983). This is one of the pioneering studies on coralline algae that live along the Yemeni coast, with that of Benzoni et al (2011). Still, growth rate data of *L. kotschyanum* f. *affine* are missing in literature. The extension rate of the investigated coralline algae is lower than reported by other authors. For instance, extension rates of up to 8 mm y^{-1} were found for *Lithophyllum congestum* from a Caribbean algal ridge (Steneck, Adey 1976). Adey and Vassar (1975) found an average accretion rate of 1-5.2 mm

y^{-1} in tropical algae, including *L. congestum*. They report that in most reef environments with considerable grazing pressure the accretion rate was considerably decreased to 0.5-2 mm y^{-1}. The observed growth rate of our specimens falls within this latter range. Both specimens are affected by endobionts, and as observed by Halfar et al. (2011) the different position of the analytical transects along the main axis of the protuberances might have reduced the accuracy of the extension rate measurement. Light incidence on algal surface is likely to decrease during the monsoon season, owing to increased cloud cover and decrease water transparency by upwelling. Irradiation might be inhomogeneous in the different surfaces of the alga. As show in figure 4.1B, epibionts, as the filamentous algae, often grow on coralline algae likely affecting the incidence of light on the thallus surface. Observations at the sampling site show that shading by macroalgal cover did not occur, as well as fine sedimentations and hydrodynamics of the study area did not cause water stagnation events. Hence, out of several factors affecting the coralline growth, it is speculated that mainly light and grazing by fishes might influence the observed annual extension of *L. kotschyanum* f. *affine* in Balhaf. Moreover in DB659bis, the protuberance of DB659 sample with the lowest annual mean extension rates, in addition to endobionts it showed dichotomization of branch resulting in changes in the direction of the main axis of growth that leaded to an irregular internal structure, that could explain the intra-specimen variability in the extension rates observed in DB659 sample. Additionally, for the irregular internal structure observed in DB659bis, it was not possible to analyze the alga in this protuberance along a single transect, but it has been needed to divide it in four transects for following the direction of the main axis of growth.

6.2.1.1. Extension rates *vs.* SST

The annual extension rates were poorly used as climate proxy (Tiwari and Rao 2004;

Kamenos and Law 2010; Halfar et al. 2011; Storz and Gischler 2011a, b). In particular the use of coralline algal extension rates as archives of past climate has only recently been investigated (Kamenos and Law 2010; Halfar et al. 2011). Although Kamenos and Law (2010) did not find a relationship between temperature and extension rates in aquaculture experiment of *L. glaciale*, Halfar et al. (2011) were able to detect in the North Atlantic Ocean, multidecadal AMO (monthly Atlantic Multidecadal Oscillation) teleconnection with a record of extension rates in *C. compactum* from the Gulf of Main.

Investigations on coralline red algae proxy of the study area have never been conducted. Contributions to the understanding of Indian Ocean climate variability only resulted from coral proxy studies of the NW and W Indian Ocean (Tudhope et al. 1996; Charles et al. 1997; Cole et al. 2000; Pfeiffer et al. 2004a; Pfeiffer et al. 2004b; Zinke et al. 2004 Pfeiffer and Dullo 2006; Crueger et al. 2009; Storz and Gischler 2011 a, b). Since the samples of DB657 and DB659a-b resulted unsuitable for paleoclimate reconstruction because their short life span and thus their too much limited temporal resolution, the DB659bis specimen, with its age model of 33 years, was the only specimen used in this study to investigate the suitability of *L. kotschyanum* f. *affine* in the reconstruction of climate variability in the Gulf of Aden. Hence, the following discussion regarding to the use of *L. kotschyanum* f. *affine* extension rate as proxy of the climate variability along the Yemen coast, it is only referred to the DB659bis specimen.

Although *C. compactum* from Gulf of Main revealed a poorly but significant correlation between extension rates and gridded ERSST, *L. kotschyanum* f. *affine* from Balhaf did not show relationship with gridded SST (HadiSST1). Kamenos and Law (2010) in *L. glaciale* did not find consistent relationship between algal band width and *in situ* temperature. Halfar et al. (2011) suggested that branched growth morphologies, which is the typical shape of *L. glaciale*, are more susceptible to damage or breakage than the massive algae (*C. compactum*), leading to an irregular

internal structure and an interrupted environmental record. Albeit the branches in *L. kotschyanum* f. *affine* are more robust than in *L. glaciale,* the dichotomization of the branches and the endobionts presence observed in DB659bis, yielded an irregular internal structure, and a possible interrupted environmental record, which could explain the lack of relationship found in *L. kotschyanum* f. *affine* between extension rate and SST. Despite the limitation of gridded datasets used in this study and the several already mentioned factors affecting coralline growth, the SST is not likely the dominant factor, but light and grazing by fishes are the mainly factors that influence the observed annual extension of *L. kotschyanum* f. *affine* in Balhaf.

6.2.1.2. Interannual and decadal climate variability

The Gulf of Aden connects the Red Sea with the NW Indian Ocean. Studies on coral proxy from Seychelles (Charles et al. 1997), Kenya (Cole et al. 2000), la Réunion (Pfeiffer et al. 2004b), the Chagos Archipelago (Pfeiffer et al. 2004a), and Maldives (Storz and Gischler 2011a) have demonstrated ENSO-driven interannual and decadal climate variability. The Indian Ocean SSTs are externally forced by the ENSO, centered in the central Pacific (Webster et al. 1998). El Niño events in the Pacific lead to a turnaround in the large-scale Walker circulation. The result is the reversal of zonal wind stress, and therefore in zonal SSTs. Hence, strong El Niño years cause higher than normal SSTs in the western equatorial Indian Ocean (Webster et al. 1999). As already mentioned in chapter 3.2., the area of Balhaf revealed a significant but weak relationship with ENSO (Fig. 3.6B). Moreover, since between the annual extension-rates and SST variations is not found a significant relationship, one could expect also no evidence for ENSO signature in this record. A cross-spectral analysis revealed several spectral peaks from sub-decadal to interannual range centered at ~6.7 yrs, ~3.6 yrs, ~2.9 and ~2.3 yrs, and expectedly these peaks are not link with

SST (Fig. 6.1).

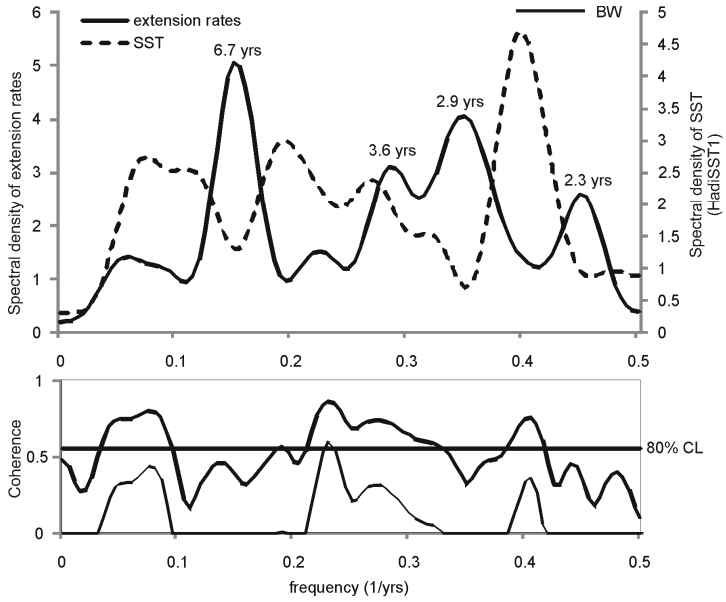

Fig. 6.1 The results of Blackman-Tukey cross-spectral analysis between DB659bis annual extension rates and SST (HadiSST1) for 1974-2008. Bandwidth = 0.06, number of lags = 24. See Figure 3.6C for legend.

Although the periods of 3.6, 2.9 yrs and 2.3 yrs are some of the typical modes of the ENSO-driven interannual variability (Charles et al. 1997; Conversi and Hammed 1998; Pfeiffer et al. 2004; Tawari and Rao 2004; Zinke et al. 2004; Storz and Gischler 2011), and significant coherence was found for the periods 3.5-3.7 yrs and 2.5-2.7 yrs in the cross-spectral analysis between field SST and Niño 3.4 index (Fig. 3.6C), these peaks in spectral density of algal extension rate are not link with ENSO. Indeed, the cross-spectral analysis between extension rates and Niño 3.4 index showed significant coherence for 3.6 yrs period, but cross-phase analysis revealed that the Niño3.4 index lags the extension-rate record for this period by 1 yr, which disproves causality (Fig. 6.2).

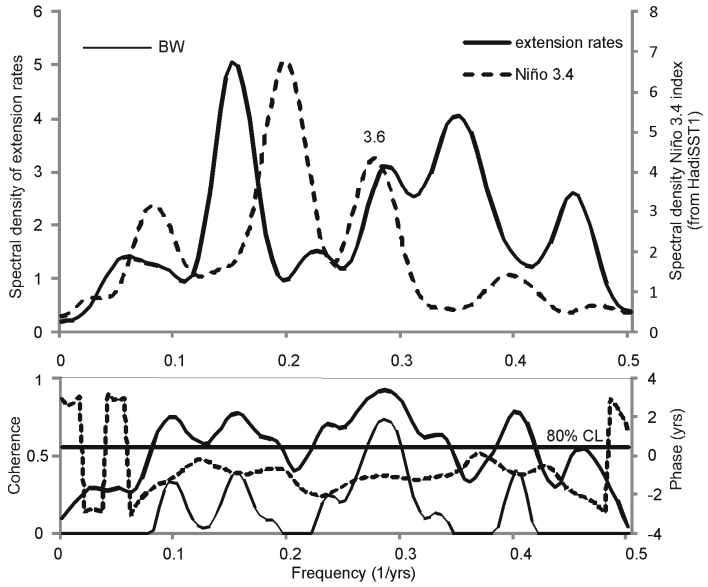

Fig. 6.2 Cross-spectral analysis of DB659bis extension rates versus Niño3.4 index (from HadiSST1) for 1974-2008. Note that it reveals strong coherence for period centered at 3.6, but cross-phase analysis (dashed line in the bottom panel) shows that extension rates record lags the Niño3.4 index by 1 yr, which disprove causality. Bandwidth = 0.06, number of lags = 24. See Figure 3.6C for legend.

All this endorses the idea that the temperature is not the main factor that influences the coralline growth in Balhaf. Before it was speculated that mainly light and grazing by fishes might influence the observed extension rate of *L. kotschyanum* f. *affine* in Balhaf. However, the cross-spectral analysis between extension rates and gridded cloud cover record showed two aligned and coherent peaks for periods 2.9 yrs and 2.2-2.3 yrs, but cross-phase analysis revealed that algal growth lags cloud cover, which disproves causality (Fig. 6.3). The lack of relationship between coralline annual extension rate and cloud cover does not invalidate the hypothesis that mainly light influences the algal growth in Balhaf because, as already mentioned, despite the limitation of gridded datasets used in this study, availability of light is affected by other factors of which are not available dataset (e.g. decrease in water transparency by upwelling).

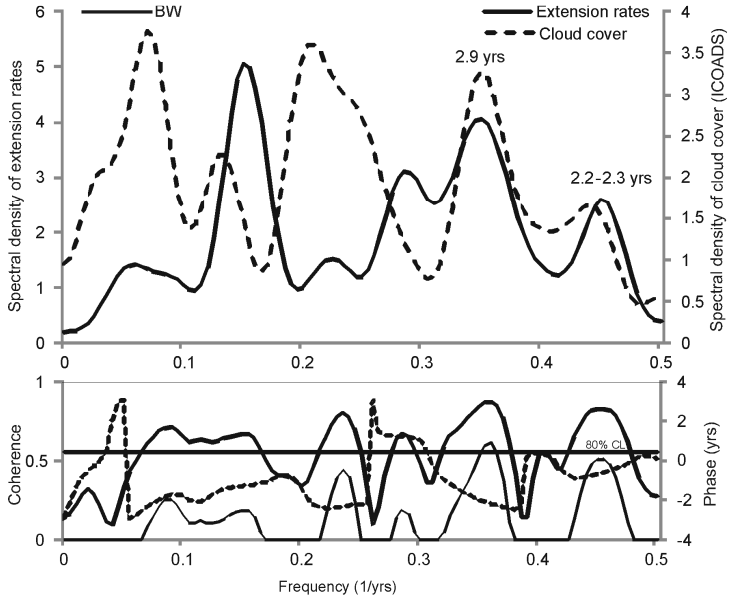

Fig. 6.3 Cross-spectral analysis of DB659bis extension rates versus cloud cover (ICOADS) for 1974-2008. Note that it reveals coherence between the two time series for period centered at ~2.9 and ~2.2 yrs, but cross-phase analysis (dashed line in the bottom panel) shows that there is not causality for these periods. Bandwidth = 0.06, number of lags = 24. See Figure 3.6C for legend.

6.2.1.3 Extension rates *vs.* Asian monsoon system

Since NW Indian Ocean, and the Gulf of Aden are strongly affected by Asian monsoon system, variability in monsoon strength could be recorded in the algal extension rates. To date, only Storz and Gischler (2011b) have provided successful studies in reconstructing temporal variability of the Indian monsoon system in the NW Indian Ocean by coral extension rates from Maldives. Although the seasonal reversion of currents for the NE and SW monsoon in Gulf of Aden including Balhaf was observed (Fig. 3.4B), coralline annual extension measured from 1974 to 2007 did not show link with gridded zonal currents record (not shown). Hence, the annual extension rate seems not to be affected by variations in hydraulic energy due to Asian monsoon system at Balhaf.

Decadal variations in the strength of the Indian monsoon system are forced by endemic Indian Ocean SST variations, rather than by ENSO (Kucharski et al. 2006). The basic principle of the Asian monsoon system are that, during summer, as a result of the differential sensible heating between land and ocean, there is formation of low atmospheric pressure over the Tibetan Plateau, and high atmospheric pressure above the relatively cold Indian Ocean at about 30°S. This results in a strong surface southwest airflow across the northern Indian Ocean. When the moist air from the ocean moves inland over the Indian subcontinent it cause heavy rain, known as the summer SW monsoon rainfall (Webster et al. 1999). Therefore, in addition to the monsoon current a further parameter trigger by the strength of the monsoon system is the summer South India monsoon rainfall (SIR). The CCCR provided the record of SIR for 1974-2007, and it has been used as a SW monsoon strength index (Sontakke et al. 2008). A cross spectral analysis between algal extension rates and CCCR record revealed coherence between the records in the period of ~18 yrs, and weak coherence in the period of 2.9 yrs (Fig. 6.4). Cross-phase analysis showed that annual extension rates lags the SIR by 2.5 yrs in the period of ~18 yrs (Fig. 6.4).

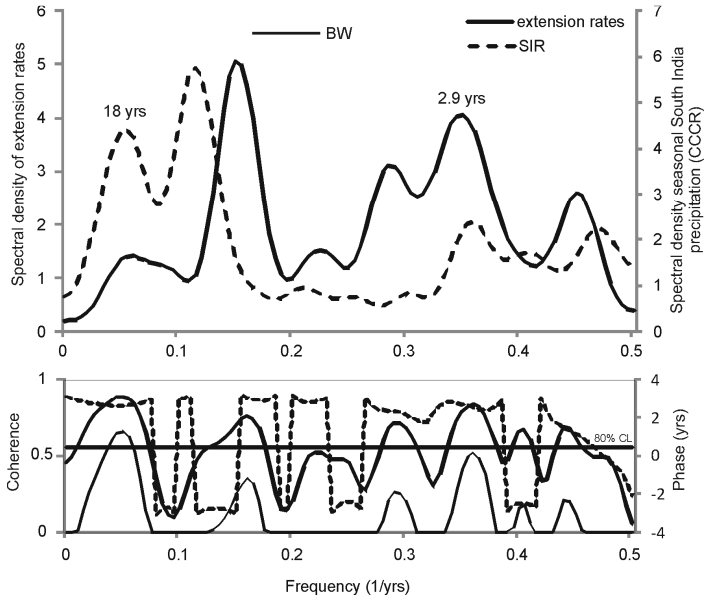

Fig. 6.4 Cross-spectral analysis of DB659bis extension rates versus the seasonal South India rainfall record (IMD) for 1974-2008. Note that it reveals coherence between the two time series for period centered at ~18 yrs and a weak coherence for period centered at ~2.9 yrs. Bandwidth = 0.06, number of lags = 24. See Figure 3.6C for legend.

Storz and Gischler (2011b) found link between coral extension rates from Maldives and SIR for the same period (18-19 yrs), and coral extension rate lags SIR by 2 yrs, similar to extension rate record of *L. kotschyanum* f. *affine* from Balhaf. Almost 92% of coral extension rate variance is explained in this period comparing with the only 22% of coralline. That might be due to: 1) longer time series used by authors: 89 yrs of coral (since 1917 to 2006) comparing with the only 33 yrs of coralline (since 1974 to 2007); 2) different gridded SIR used: 3°x2° by authors comparing with 0.5°x0.5° used in this study; 3) different strength of the monsoon affecting the study areas (Maldives *vs*. Balhaf). Periodicity in the range of 18-19 yrs has not been found in the annual mean coral $\delta^{18}O$ records of the NW Indian Ocean reported by Charles et al. (1997), Cole et al. (2000), and Pfeiffer and Dullo (2006). Storz and Gischler (2011b) suggested that this is likely due to the fact that variations in monsoon strength are not accompanied by measurable SST and salinity changes in the areas of these studies.

A weak negative, but poorly significant correlation was found between annual extension rates and SIR (r = -0.31, p-value = 0.07). Storz and Gischler (2011a) found in coral extension rates from Maldives a negative correlation with precipitation over India. They suggested that periods of stronger Indian monsoons that generate stronger monsoon rainfall over India, and enhanced SW monsoon current velocities in the NW Indian Ocean, these led elevated hydrodynamic energy in center of Maldives explaining reduced coral extension rates during such periods. Despite correlation between algal extension rates and SIR was poorly significant, it is suggested that the negative correlation found in *L. kotschyanum* f. *affine* extension rate is likely due to an increase of hydrodynamic energy in Balhaf during periods of stronger Indian monsoon, that it led to an decrease water transparency by upwelling and thus to an decrease of algal growth.

6.2.1.4. Red Sea teleconnections

About 37% of the total volume of water mass in Gulf of Aden is the Red Sea water, one of the most saline water masses in the world oceans (Al Safani and Shenoi 2004; Al Saafani 2008). Although weakly correlated, a relationship was found between annual extension rates and annual gridded SSS. Klein et al. (1997) found in coral $\delta^{18}O$ from South of Red Sea signals of the Asian monsoon. Interannual variations in coral $\delta^{18}O$ showed a weak correlation with the southern Red Sea SST, but were strongly correlated with the Indian Ocean SST, especially on the decadal time-scale. Hence, since several climate and environmental factors act on coralline algae growth, and already mentioned above (chapter 6.2.1.), one could expect evidence for Asian monsoon, as well as for Red Sea climate in the extension rate record. Cross spectral analysis between extension rates and gridded SSS revealed coherence for periods of 3.6 yrs and 2.9 yrs (Fig. 6.5A). The surface water in the Gulf of Aden reach a salinity maxima near the surface, and it forms as a mixture of

local water and water from western Arabian Sea during winter, and Red Sea surface water during summer (Al Saafani and Shenoi 2007; Al Saafani 2008). Moreover, during summer monsoon, upwelling of deeper water occur in the Gulf, and this bottom water is a mixture of Red Sea water and water of southern origin (Al Saafani and Shenoi 2007). Since cross spectral analysis between Balhaf SSS and Arabian Sea SSS did not reveal alignments (not shown), it is suggested that zonal SSS variability is mainly affected by influx of seawater from Red Sea into the Gulf of Aden. Hence, the SSS variability was used in this study as a index of the Red Sea climate influence in Balhaf. In order to demonstrate that coralline extension rate is affected by Red Sea SSS, cross correlations were applied for the annual record with (1) the mean summer (May-September) SSS (SSSS) of Balhaf (2) the difference between winter and summer SSS (ASSSG) of Balhaf, as an intra-annual gradient (3) the SSS of South Red Sea. This analysis led to:

1) *Link between summer SSS of Balhaf and extension rate*. Expectedly, the spectrum between the time series of summer SSS and extension rate record reveals both spectral alignment and significant coherence for the periods 3.6 yrs and 2.9 yrs (Fig. 6.5C). At these periods, almost 70% of the variance is linearly correlated between these time series. No temporal lag between both time series is found (Fig. 6.5C). Although weakly coherent a correspondence is still found for period centered at ~18 yrs. Cross-phase analysis revealed that extension rate lags the zonal SSS record for this period by 1.5 yrs (Fig. 6.5C). Since link between extension rates and SIR is found for the same period, it suggested an influence of the summer monsoon strength to the surface water influx from Red Sea to the Gulf of Aden.

2)*No link between Winter-Summer SSS difference and extension rates*. The generated time series of seasonal differences between summer and winter SSS shows stronger spectral coherence for periods centered at ~3.6 yrs and ~2.9 yrs. Cross-phase analysis showed that the SSS record lag the extension rate for these periods by respectively 0.4 y and 0.8 y, which disproves causality (Fig.

6.5D).

3) *Link between SSS of South Red Sea and extension rates.* The spectrum of the annual mean SSS record showed coherence with the extension rates for period 3.6 yrs (Fig. 6.6). Cross-phase analysis showed that the extension rate lags the SSS record for this period by 0.5 y, as found in cross-spectral analysis between extension rates and zonal SSS for the same period (Fig. 6.5A and 6.6).

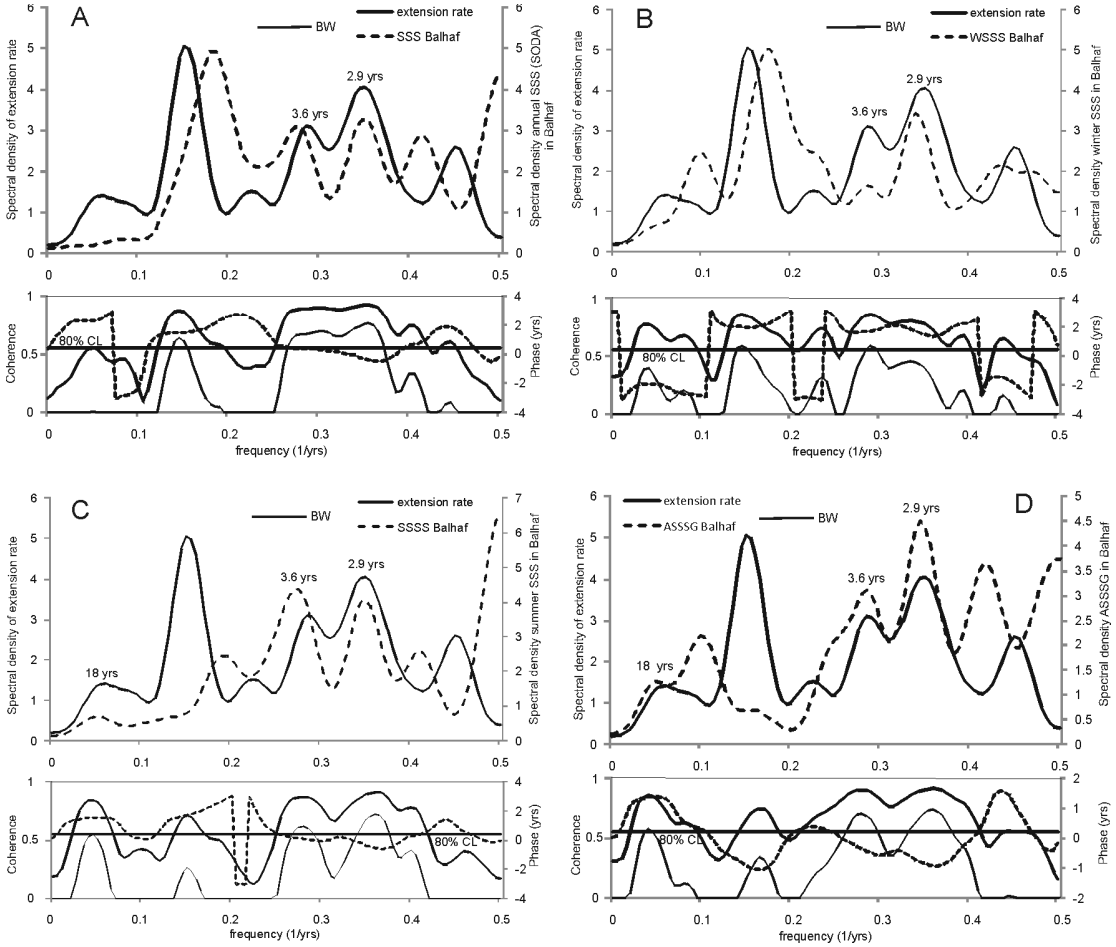

Fig. 6.5 A) cross-spectral analysis of DB659bis extension rates versus local SSS (SODA) for 1974-2008; B) corresponding analysis for extension rates versus mean winter monsoon SSS (extracted from SODA); C) corresponding analysis for extension rates versus mean summer monsoon SSS (extracted from SODA); D) Cross-spectral analysis of annual algal extension rates versus annual SSS gradient record (ASSSG, difference between mean summer and winter monsoon SSS, extracted from SODA) for 1974-2008. Bandwidth = 0.06, number of lags = 24. See Figure 3.6C for legend.

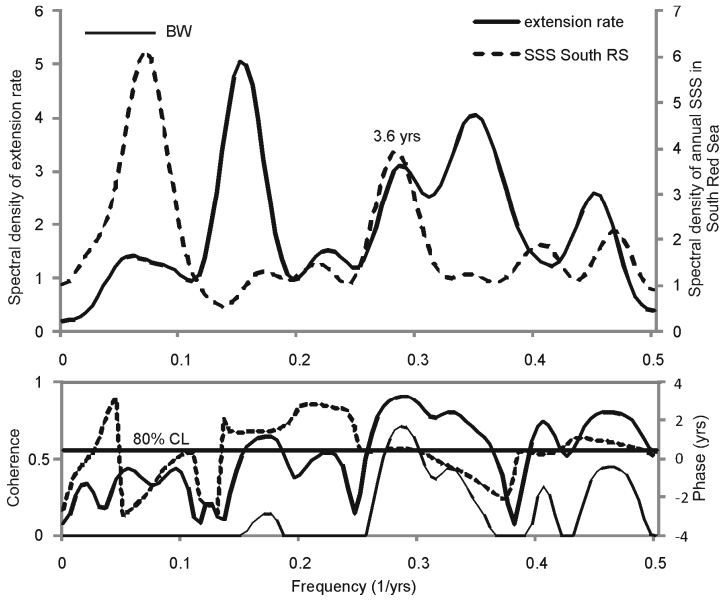

Fig. 6.6 Cross spectral analysis of DB659bis extension rates versus annual SSS in South Red Sea (SODA) for 1974-2008. Note strong coherence for period centered at ~3.6 yrs. Bandwidth = 0.06, number of lags = 24. See Figure 3.6C for legend.

Years of higher extension rate are matched to higher annual SSS values. The cross spectral analysis between gridded SSS of Balhaf and SIR revealed coherence for period 2.9 yrs (Fig. 6.7A). That suggested that SSS variability recorded in the coralline extension rate for this period is of bottom water origin, that reaches the surface during summer monsoon for the upwelling events, that occur in this season. While, cross spectral analysis between gridded SSS of Balhaf and gridded SSS of South Red Sea showed coherence for period 3.6 yrs (Fig. 6.7B). Hence, SSS variability recorded in the coralline extension rate for this period is likely linked to the sea surface water mass outflow from Red Sea during summer monsoon.

Therefore, *L. kotschyanum* f. *affine* from Balhaf recorded the Asian monsoon system and the Red Sea teleconnections in the extension rates record by SSS variability. Since SSS variability has never been described as a factor to act the coralline growth, it is assumed that the SSS variability observed in Balhaf is likely link to variation in nutrient content in sea water mass, and it

is an index of the intensity of the Red Sea surface water outflow into the Gulf of Aden and of the upwelling intensity during the summer monsoon.

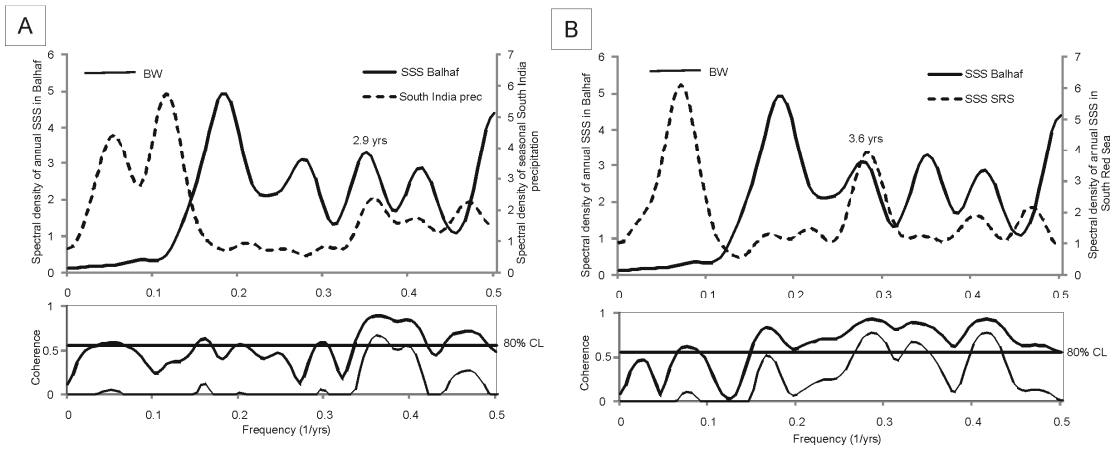

Fig. 6.7 Cross-spectral analysis for 1974-2008 of annual SSS (SODA) in Balhaf versus: A) seasonal South India rainfall; B) annual SSS (SODA) in South Red Sea. Bandwidth = 0.06, number of lags = 24. See Figure 3.6C for legend.

Cross-spectral analysis between algal extension rates and annual South Red Sea current revealed a weak coherence for periods of 2.7-2.8 yrs, and 2.3 yrs (Fig. 6.8A). In summer the Red Sea water mass outflow into the Gulf of Aden. Cross spectral analysis between extension rates and summer South Red Sea current variability showed an aligned peak with a weak coherence at 5.5-6.7 yrs, and cross-phase analysis showed that extension rate lags the summer South Red Sea current by 1.2 yrs (Fig. 6.8C). Storz and Gischler (2011b) found in coral extension rates from Maldives for the same period of 6.7, as well as of 18-19 yrs, coherence with seasonal South India precipitation, thus signal in the coral extension rate of the Asian monsoon system. It is suggested that the variation of hydrographic energy in the South Red Sea in this period could be influence by Asian monsoon system, thus the relationship found between coralline extension and current variability in the South Red Sea for period of 5.5-6.7 might be indirectly a signal of the Asian monsoon variability. In the end analysis between algal growth rates and the gradient of current

reconstructed in the South Red Sea (difference between summer and winter mean current) reveals significant coherence for period 2.3 yrs. Cross-phase analysis showed that the extension rates record lags the gradient of current record by 1.5 yrs for this period (Fig. 6.8D). Since of the weak coherences found between algal extension rate record and the annual South Red Sea current, it is highly recommended further studies to investigate the useful of algal extension rate as proxy of the Red Sea hydrographic energy in the Gulf of Aden.

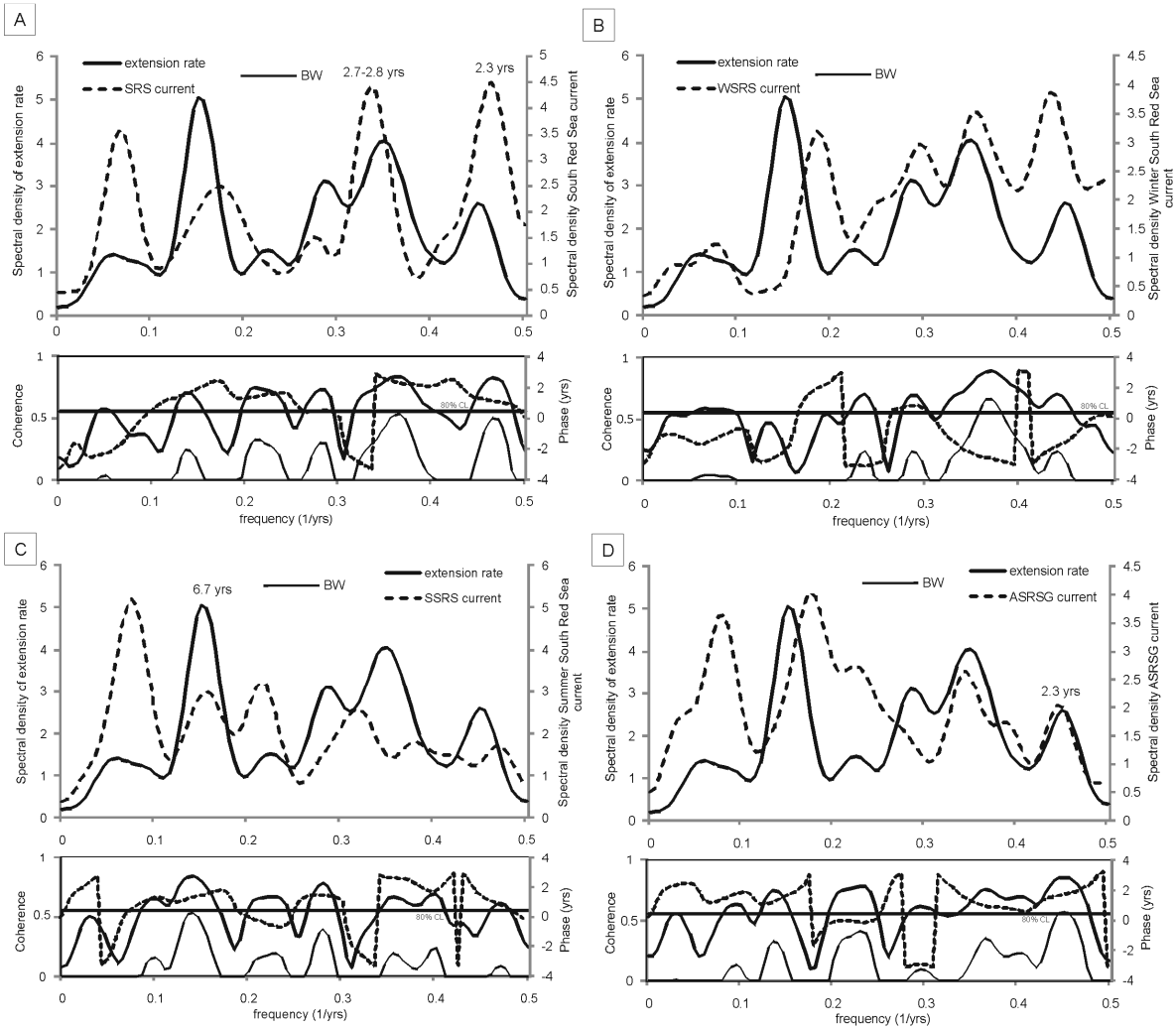

Fig. 6.8 A) cross-spectral analysis of DB659bis extension rates versus zonal current velocities in the South Red Sea (SODA) for 1974-2008; B) corresponding analysis for extension rates versus mean winter monsoon zonal current velocities in the South Red Sea (extracted from SODA); C) corresponding analysis for extension rates versus mean summer monsoon zonal current velocities in the South Red Sea (extracted from SODA); D) Cross-spectral analysis of annual algal extension rates versus annual zonal current velocities gradient record in the South Red Sea (ASRSG current, difference between mean summer and winter monsoon zonal current velocities in the South Red Sea, extracted from SODA) for 1974-2008. Bandwidth = 0.06, number of lags = 24. See Figure 3.6C for legend.

Climate of the South Red Sea is partially affected by North Red Sea climate (Eshel et al. 1994). The negligible winter rains that reach the northern Red Sea are part of the Mediterranean

climate regime to the north (Eshel et al. 1994). Felis et al. (2000) found in coral $\delta^{18}O$ from Ras Umm Sid signal of the Alexandria precipitation, as index of the Mediterranean climate influence to the northern Red Sea regime. In this study it is investigated the presence of northern Red Sea climate signals on coralline thallus using the Alexandria precipitations variability as index of the northern Red Sea climate. Cross spectral density between algal extension rates and Alexandria rainfall revealed a strong coherence at period 2.9 yrs, but the cross-phase analysis showed that the Alexandria precipitation record lags the extension rates record for this period by 1 y, which disproves causality (Fig. 6.9). Hence, coralline growth rate did not record the northern Red Sea climate variability.

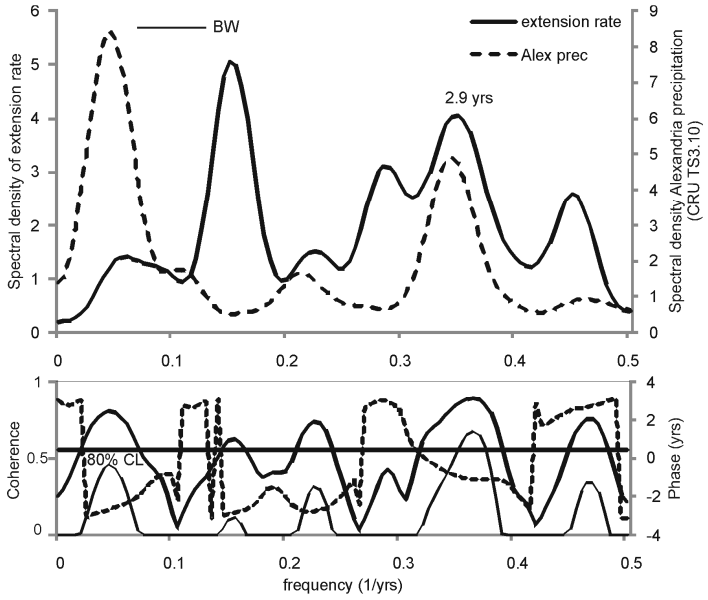

Fig. 6.9 Cross spectral analysis of DB659bis extension rates versus annual Alexandria precipitation (CRU TS3.10) for 1974-2008. Note coherence for period centered at ~2.9 yrs, but cross-phase analysis (dashed line in the bottom panel) shows that there is not causality for this period. Bandwidth = 0.06, number of lags = 24. See Figure 3.6C for legend.

6.2.2. Socotra

Based on morphological features, the coralline alga collected to Socotra and involved in this study (DB657), was identified as the genera of *Lithophyllum* Philippi (1837). Since these morphological features not correspond to any species described in the literature, as well as molecular analysis revealed that this sample is genetically different from other species of *Lithophyllum* (studying in progress), the sample from Socotra is generally considered in this study as a *Lithophyllum* sp.

The annual extension rate of *Lithophyllum* sp. of Socotra for period 1972 to 2009 was variable with a mean of 208.2 µm y^{-1}, and a minimum of 67.38 µm y^{-1} and a maximum of 410.43 µm y^{-1}. As already mentioned above (chapter 6.2.1.), average vertical growth rates of coralline algae were reported to be highly variable, and several factors act on coralline algae growth. Adey and McKibbin (1970) assumed that coralline growth is positively correlated with light at higher temperature. This is one of the pioneering study on coralline algae that live along Socotra Island coast. The extension rate of the investigated rhodolith is lower than reported by the other authors for coralline algae from subtropic (Adey and Vassar 1975). In the sample has been observed the presence of endobionts that resulting in changes in the direction of the main axis of growth, and thus it leaded to an irregular internal structure. Hence, it was not possible to analyze the alga along a single transect, but it has been needed to divide it in four transects for following the direction of the main axis of growth. Halfar et al. (2011) observed that the different position of the analytical transects along the main axis of coralline thallus might reduced the accuracy of the extension rate measurement. Moreover, although light penetration will be less if water is turbid, in the very clear water of the open ocean less than 25% of the surface light reaches a depth of 10 m (Davis 1991). *Lithophyllum* sp. of Socotra was collected at 22m depth, at a greater depth than the *L. kotschyanum*

f. *affine* of Balhaf and Kamaran (respectively 6-8 m and 1.5m depth). Moreover, light incidence on algal surface is likely to decrease during the monsoon season, owing to increase cloud cover and decrease water transparency by upwelling. Additionally, in agreement with Cabioch (1966) and Halfar et al. (2011) growth cessation can occur in *Lithophyllum* sp. from Socotra by burial. Hence, out of several factors affecting the coralline growth, it is speculated that mainly light and temporal burial might influence the observed annual extension of *Lithophyllum* sp. of Socotra.

6.2.2.1. Extension rates *vs*. SST

Investigations on coralline red algae proxy of the study area have never been conducted. As for *L. kotschyanum* f. *affine* from Balhaf, *Lithophyllum* sp. from Socotra did not show relationship with gridded SST (HadiSST1), in agreement with Kamenos and Law (2010). Despite the limitation of gridded datasets used in this study, temporal burial of rhodolith from Socotra may have led to growth cessation, thus to an interrupted environmental record (Cabioch 1966, Halfar et al. 2011). Halfar et al. (2011) found on *C. compactum* from Gulf of Main a poorly but significant relationship between extension rates and SST (ERSST). At the same time the authors suggested the more suitable of attached living (*C. compactum*) than free living algae (rhodoliths) for partial and temporal burial affecting the rhodoliths leading growth cessation. Moreover, Adey and McKibbin (1970) assumed that coralline growth is positively correlated with light at higher temperature, thus the SST is not likely the dominant factor, but light is the mainly factor that influence the observed annual extension of *Lithophyllum* sp. in Socotra, as well as of *L. kotschyanum* f. *affine* in Balhaf (see chapters 6.2.1.1. and 6.2.2.).

6.2.2.2. Interannual and decadal climate variability

Socotra island is located to the southwest of the Arabian Sea, and is bordered by the Gulf of Aden. It is bathed by a variety of different water masses, including those originating to the south off East Africa, to the east by water of the central Indian Ocean, and to the north-west, north and north-east, by the Red Sea, Gulf of Aden and Arabian Sea respectively (Cheung and DeVantier 2006). Studies on coral proxy distributed in the Indian Ocean have demonstrated ENSO-driven interannual and decadal climate variability (Charles et al. 1997, Cole et al. 2000, Pfeiffer et al. 2004b, Pfeiffer et al. 2004a, Storz and Gischler 2011a). The extension rate record of *L. kotschyanum* f. *affine* from Balhaf has not demonstrated ENSO-driven climate variability (chapter 6.2.1.2). Comparing to Gulf of Aden the Socotra area showed a stronger positive and significant relationship between field SST variability and ENSO in the interannual band (Fig. 3.6B and Fig. 3.12). Since no relationship was observed between coralline extension rates and gridded SST, one could expect also no evidence for ENSO signature in this record. The cross-spectral analysis revealed several peaks from decadal to interannual range centered at ~25, ~11 yrs and ~2.2 yrs (Fig. 6.10).

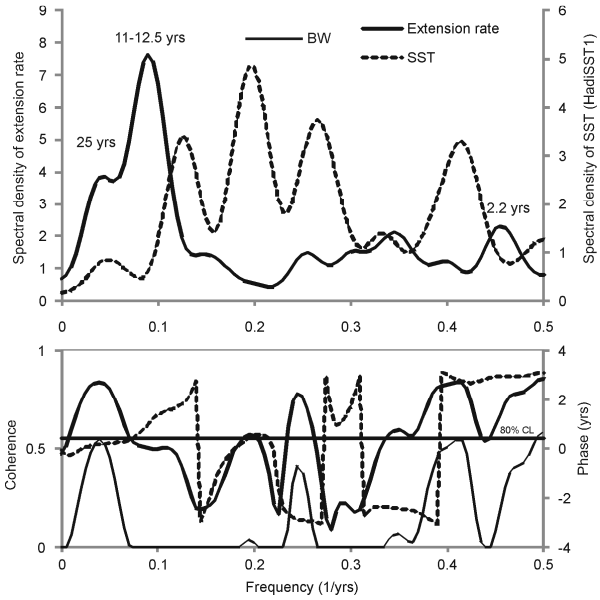

Fig. 6.10 Cross-spectral analysis of Socotra sample (DB635) extension rates versus annual SST (HadiSST1) for 1972-2009. Note that it does not show any aligned peaks between the spectral density of both time series. Bandwidth = 0.06, number of lags = 24. See Figure 3.6C for legend.

Expectedly, these peaks are not link with gridded SST. The period of ~2.3 yrs in the Blackman Tukey spectrum is the typical mode of the Quasi-biennial oscillation (QBO), a phenomenon that was originally observed between westerly and easterly equatorial stratospheric winds (Baldwin et al. 2001). The QBO significantly influences the Indo-Pacific realm and is found in a variety of meteorological records of precipitation, wind-speed and SST (Conversi and Hammed 1998). Although Tawari and Rao (2004) found the QBO in the extension rates record of coral from the northern Arabian Sea, cross-spectral analysis between *Lithophyllum* sp. extension rate and Niño3.4 index did not show aligned peaks for this period (Fig. 6.11), as well as cross-spectral analysis between Niño3.4 index and gridded SST did not revealed coherence for this period (Fig. 3.12). However, this cross-spectral analysis revealed coherence for period at 10-12 yrs, and cross-phase analysis showed that extension rate lags the Niño3.4 index by 1 yr (Fig. 6.11). Although studies on coral proxy observed mainly an interannual climate variability link to

ENSO-force, Cole et al. (2000) found in coral proxy from Kenya a decadal link.

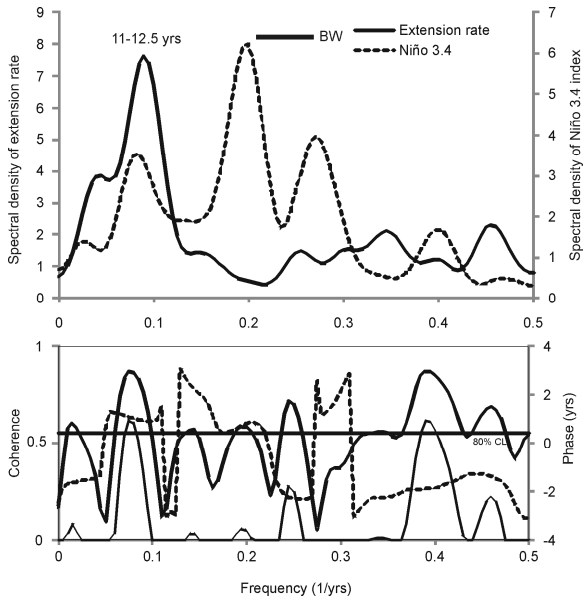

Fig. 6.11 Cross-spectral analysis of Socotra sample (DB635) extension rates versus Niño3.4 index (from HadiSST1) for 1972-2009. Note that it shows coherence for period centered at ~12 yrs. Bandwidth = 0.06, number of lags = 24. See Figure 3.6C for legend.

Since it has been assumed that mainly light might influence the observed extension rate of *Lithophyllum* sp. in Socotra, the relationship between coralline extension and cloud cover was investigated. The cross-spectral analysis between the both records revealed no aligned peaks (not shown), in agreement with extension rate record of *L. kotschyanum* f. *affine* from Balhaf. The lack of relationship between coralline annual extension rate and cloud cover does not invalidate the hypothesis that mainly light influences the algal growth in Socotra, as well as in Balhaf because, as already mentioned, despite the limitation of gridded datasets used in this study, availability of light is affected by other factors of which are not available dataset (e.g. decrease in water transparency by upwelling).

6.2.2.3. Extension rates *vs*. Asian monsoon system

Since NW Indian Ocean is strongly affected by Asian monsoon system, variability in monsoon strength could be recorded in the algal extension rates. Although the seasonal reversion of currents for the NE and SW monsoon in Socotra was observed (Fig. 3.10B), cross-spectral analysis between *Lithophyllum* sp. extension rate and zonal current did not show link between the records (not shown), as also observed in extension rate record of *L. kotschyanum* f. *affine* from Balhaf. The current dataset used in this study (SODA) provide data of surface current velocity , thus of the first 5 m depth. Since rhodolith of Socotra lived at 20 m depth, it is reasonable to assume that at this depth, the coralline alga has not recorded the surface current variability caused by wind monsoon.

In addition to the monsoon current a further parameter trigger by the strength of the monsoon system is the summer SIR. Thus seasonal South India rainfall is used as index of the Asian monsoon intensity. Cross-spectral analysis between extension rate record of *Lithophyllum* sp. from Socotra and SIR did not showed aligned peaks (Fig. 6.12). Thus rhodolith from Socotra did not record the Asian monsoon system in the extension rates record. Halfar et al. (2011) suggested the more suitable of attached living (*L. kotschyanum* f. *affine* from Balhaf) than free living algae (*Lithophyllum* sp. from Socotra) for partial and temporal burial affecting rhodoliths leading growth cessation, and therefore to an interrupted environmental record. Since annual extension of *L. kotschyanum* f. *affine* from Balhaf resulted a proxy of Asian monsoon variability by SIR, it is assumed that Socotra rhodolith has likely been affected to temporal burials which led to a growth cessation, and therefore to an interrupted environmental record, as well as at 20 m deep the oceanographic environment is likely to be more stable than at 6-8 m of the sample from Balhaf and thus less influenced by climatic and oceanographic changes related to the monsoonal system.

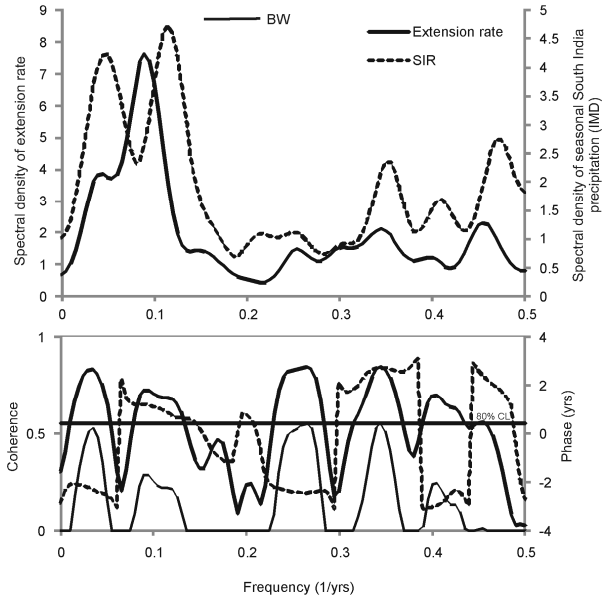

Fig. 6.12 Cross-spectral analysis of Socotra sample (DB635) extension rates versus seasonal South India precipitation (IMD). Bandwidth = 0.06, number of lags = 24. See Figure 3.6C for legend.

6.2.2.4. Red Sea teleconnections

Socotra is bathed by a variety of different water masses, including those originating to the north-west by the Red Sea. Passing through the Gulf of Aden, the water outflows from the Red Sea becomes a part of the intermediate circulation in the Indian Ocean, which has been observed as a mid-depth salinity maximum in the Arabian Sea and even in the southern hemisphere (Mecking and Warner 1999). *L. kotschyanum* f. *affine* from Balhaf revealed Red Sea teleconnections by SSS variability. Moreover, as already mentioned above, several climate and environmental factors act on coralline algae growth (see chapter 6.2.1.). From these observation, one could expect evidence for Red Sea climate signals in the extension rate record of *Lithophyllum* sp. from Socotra. Cross-spectral analysis between extension rate and gridded SSS revealed a strong coherence for period of 25 yrs (Fig. 6.13A). Coherence value for this period is higher than 0.8 indicating that over

64% of the variance at this period is linearly correlated. Thus coralline growth rate increase with increase of local SSS. It is assumed that increase of SSS is likely an index of an increase of nutrients. The strong coherence for this period was found also in cross-spectral analysis between annual coralline extension and mean summer SSS, and although weaker coherence was still showed in cross-spectral analysis with intra-annual gradient of SSS in Socotra for this period (Fig. 6.13C and D). Instead, cross-spectral analysis between coralline extension and mean winter SSS revealed coherence for this period, but cross-phase analysis showed that winter SSS lags extension rate by 0.7 y, which disprove causality (Fig. 6.13B).

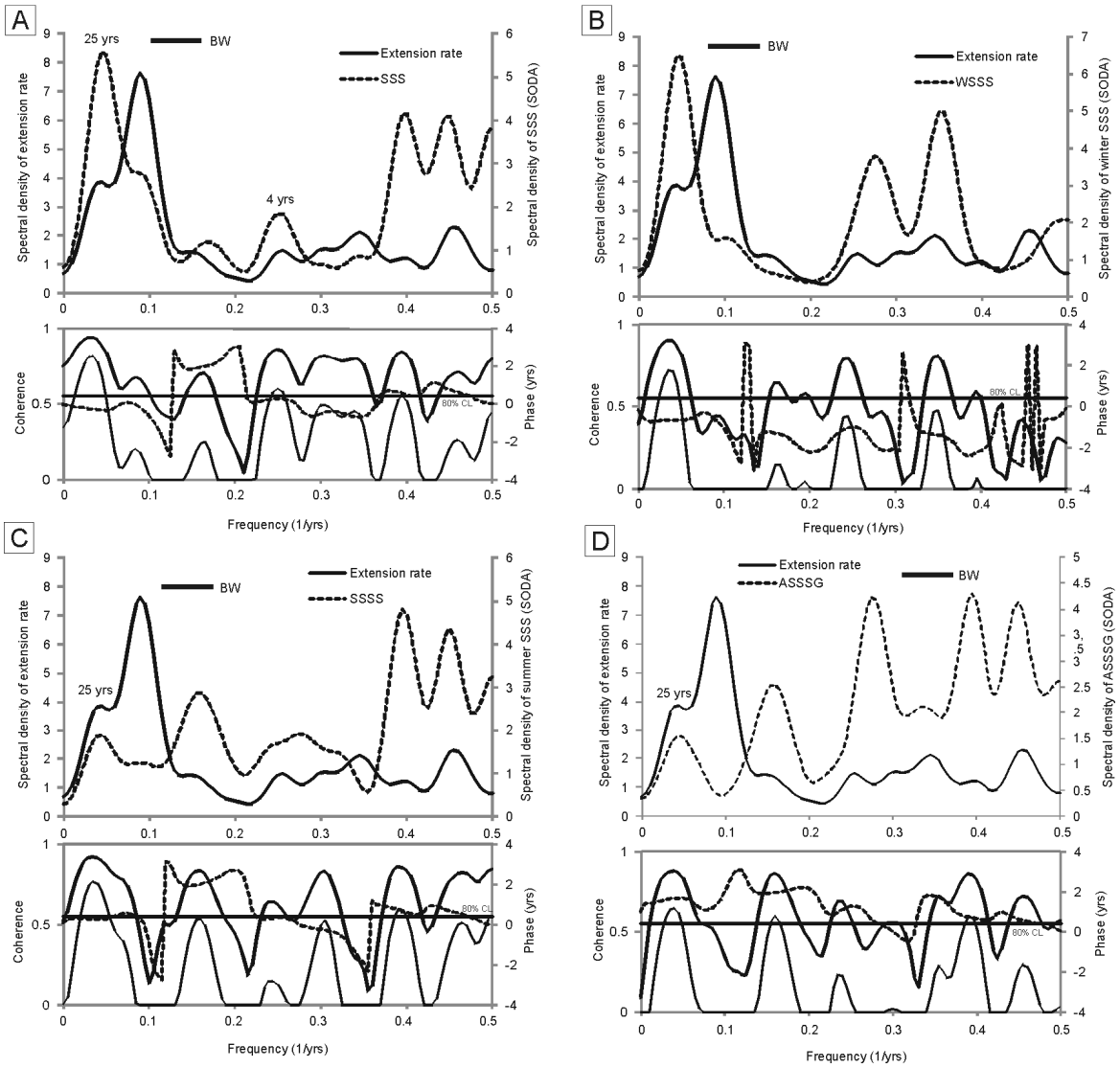

Fig. 6.13 A) cross-spectral analysis of Socotra sample (DB635) extension rates versus SSS (SODA) for 1972-2009; B) corresponding analysis for extension rates versus mean winter SSS (extracted from SODA); C) corresponding analysis for extension rates versus mean summer monsoon SSS (extracted from SODA); D) Cross-spectral analysis of annual algal extension rates versus annual SSS gradient record (ASSSG, difference between mean summer and winter monsoon SSS, extracted from SODA) for 1972-2009. Bandwidth = 0.06, number of lags = 24. See Figure 3.6C for legend.

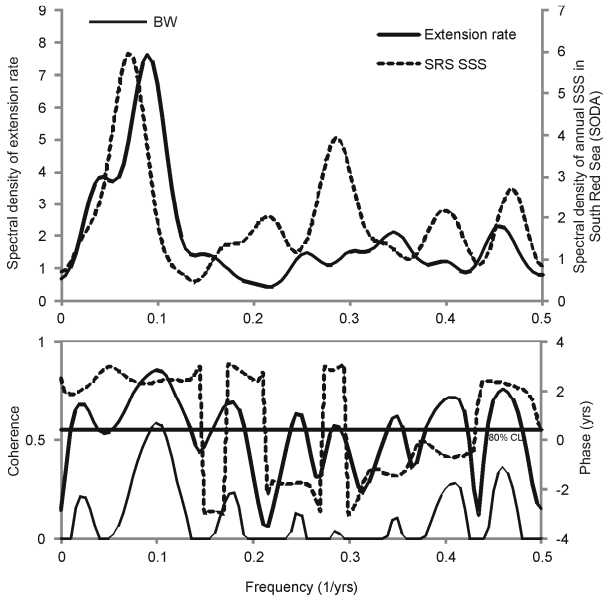

Fig. 6.14 Cross-spectral analysis of Socotra sample (DB635) extension rates versus SSS (SODA) in South Red Sea for 1972-2009. Bandwidth = 0.06, number of lags = 24. See Figure 3.6C for legend.

Cross-spectral analysis between extension rate record and gridded SSS of South Red Sea did not revealed relationship (Fig. 6.14). Moreover, cross-spectral analysis between SSS of Socotra and SIR revealed strong coherence for period centered at ~23.5 yrs (Fig. 6.15A), while cross-spectral analysis between SSS of Socotra and SSS of South Red Sea did not showed link (Fig. 6.15B). Therefore, it is suggested that *Lithopyllum* sp. from Socotra recorded in the extension rate record the Asian monsoon system by local variations of SSS.

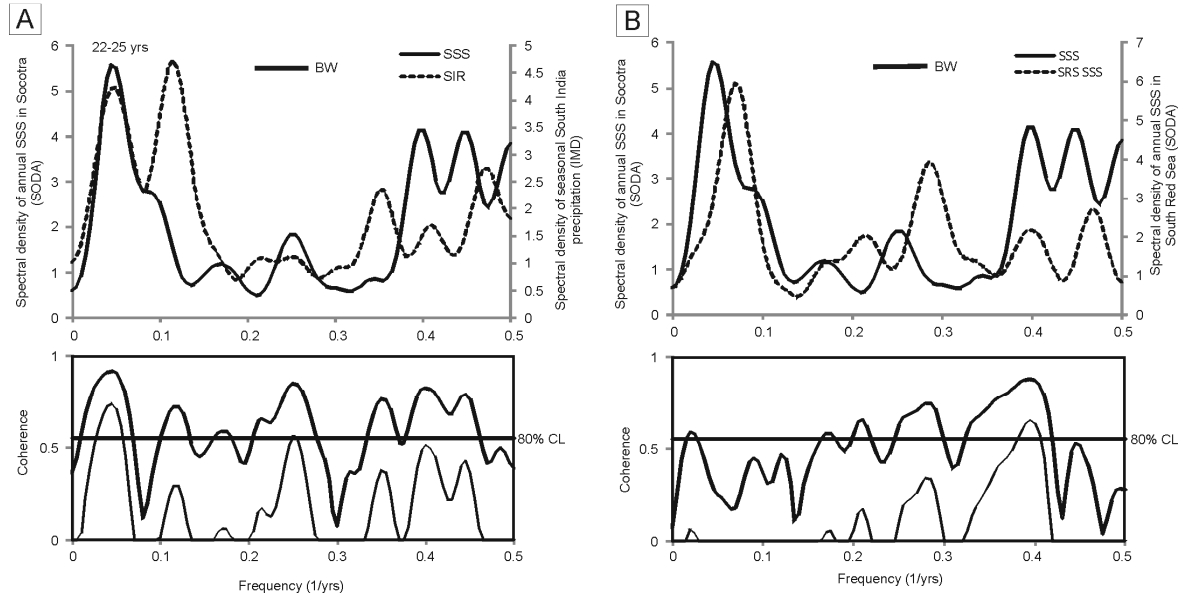

Fig. 6.15 Cross-spectral analysis for 1972-2009 of annual SSS (SODA) in Socotra versus: A) seasonal South India rainfall (IMD); B) annual SSS (SODA) in South Red Sea. Bandwidth = 0.06, number of lags = 24. See Figure 3.6C for legend.

Expectedly, cross-spectral analysis between extension rate and Alexandria precipitation did not revealed relationship (not shown).

6.2.3. Kamaran

The annual extension rate of *L. kotschyanum* f. *affine* of Kamaran for period 1994 to 2008 was variable with a mean of 446.4 µm y^{-1}, and a minimum of 218.9 µm y^{-1} and a maximum of 915.15 µm y^{-1}. In this specimen was observed an higher variability of extension rate than in the samples of Balhaf. As already mentioned, average vertical growth rates of coralline algae were reported to be highly variable, and several factors act on coralline algae growth (chapter 6.2.1.). Adey and McKibbin (1970) assumed that coralline growth is positively correlated with light at higher temperature. The extension rate of the DB576 specimen is lower than reported by the other

authors for coralline algae from subtropic (Adey and Vassar 1975). The rhodolith of Kamaran is strongly affected by endobionts (Fig. 4.6), as well as observed in *L. kotschyanum* f. *affine* from Balhaf and in *Lithophyllum* sp. from Socotra. The *L. kotschyanum* f. *affine* of Kamaran was living close to the coast and in the very shallow water with high level of sediment abating the bright light normally found in shallow water (Fig. 3.13B). Moreover, being a rhodolith, growth cessation can occurred it by burial (Cabioch 1966, Halfar et al. 2011). Hence, out of several factors affecting the coralline growth, it is speculated that mainly light, sedimentation and temporal burial might influence the observed annual extension of *L. kotschyanum* f. *affine* of Kamaran.

6.2.3.1. Extension rate *vs*. SST

Investigations on coralline red algae proxy of the study area have never been conducted. As for *L. kotschyanum* f. *affine* of Balhaf and *Lithophyllum* sp. of Socotra, and in agreement with Kamenos and Law (2010), *L. kotschyanum* f. *affine* of Kamaran did not show relationship with gridded SST (HadiSST1). Although the limitation of gridded datasets used in this study, however, temporal burial of rhodolith from Kamaran may have led to growth cessation, thus to an interrupted environmental record (Cabioch 1966, Halfar et al. 2011). Halfar et al. (2011) found on *C. compactum* from Gulf of Main a poorly but significant relationship between extension rates and SST (ERSST). At the same time the authors suggested the more suitable of attached living (*C. compactum*) than free living algae (rhodoliths) for partial and temporal burial affecting the rhodoliths leading growth cessation. Moreover, Adey and McKibbin (1970) assumed that coralline growth is positively correlated with light at higher temperature, thus the SST is not likely the dominant factor, but light is the mainly factor that influence the observed annual extension of *L. kotschyanum* f. *affine* from Kamaran, as well as of the other subtropical specimen analyzed in this

study.

6.2.3.2. Interannual and decadal climate variability

Studies on coral proxy from Dahlak Archipelago (Klein et al. 1997) and Ras Umm Sidd (South of the Aqaba Gulf, Felis et al. 2000) have demonstrated ENSO-driven interannual climate variability in the Red Sea. Klein et al. (1997) found a weak correlation with local SST on the interannula time-scale, while Felis et al. (2000) still observed in coral skeleton $\delta^{18}O$ record a strong correlation with local SST on interannula time-scale. A cross-spectral analysis between extension rates and gridded SST revealed an interannual peak centered at ~8.3 yrs, but no coherence was found for this period (Fig. 6.16), as well as between extension rate record and Niño3.4 index (not shown). Despite the limitations of the gridded datasets used in this study, *L. kotschyanum* f. *affine* from Kamaran did not record in the extension rates record the periodicity of climate in the Red Sea by local SST variability and even the ENSO-force on the Red Sea climate.

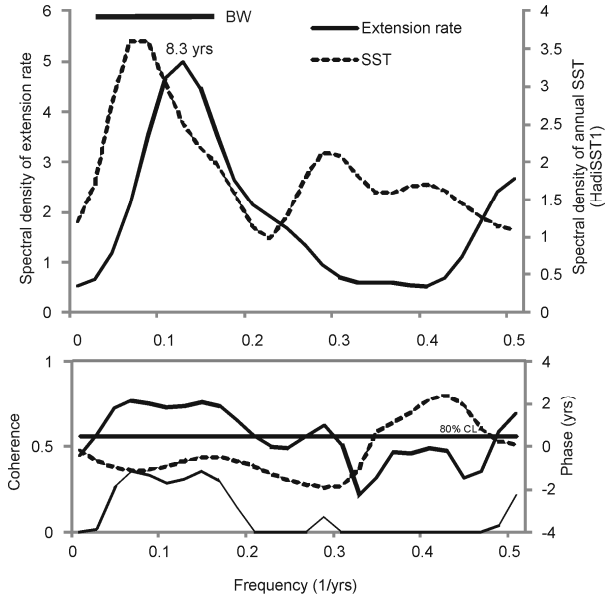

Fig. 6.16 Cross-spectral analysis of Kamaran sample (DB576) extension rates versus annual SST (HadiSST1) for 1994-2008. Bandwidth = 0.14, number of lags = 11. See Figure 3.6C for legend.

Furthermore, cross spectral analysis between alga extension record and zonal current record (SODA) revealed coherence for period 8.3 yrs, but cross-phase analysis showed that current lags the record by 2 yrs, which disprove causality (Fig. 6.17).

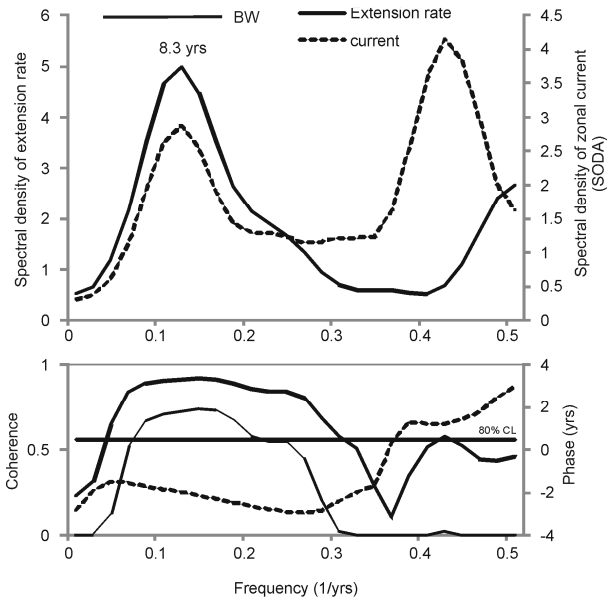

Fig. 6.17 Cross-spectral analysis of Kamaran sample (DB576) extension rates versus zonal current (SODA) for 1994-2008. Note that it shows strong coherence for period centered at ~8.3 yrs, but cross-phase analysis (dashed line in the bottom panel) reveals that there is not causality for this period. Bandwidth = 0.14, number of lags = 11. See Figure 3.6C for legend.

The South Red Sea climate is influence by the climate of the northern part of the Red Sea, and the latter it is subject to greater variability of weather than the south, particularly in winter when it may be influenced by disturbances in the Mediterranean, which leads typical winter rains. Felis et al. (2000) found in coral skeleton $\delta^{18}O$ signal of the Mediterranean climate by Alexandria rainfall variability. Therefore, influence of the North Red Sea on the South Red Sea climate has been investigated in *L. kotschyanum* f. *affine* from Kamaran by Alexandria rainfall variability

recorded in the alga extension rates. Although no correlation was found between alga extension rates and annual Alexandria precipitation, cross-spectral analysis between the two records showed coherence for period of 8.3-10 yrs (Fig. 6.18). Cross-phase analysis revealed that the extension rates lags the Alexandria precipitation by 3 yrs. The phase line rapidly drops to negative values for this period within the Barlett window used, which calls into question the reliability of the causality for this period (Fig. 6.18). However cross-spectral analysis between the Alexandria precipitation and the zonal sea surface current of Kamaran revealed coherence for the period of 5 yrs (Fig. 3.16). The short life span of *L. kotschyanum* f. *affine* from Kamaran, thus its limited temporal resolution seems to have led a reduction of the sensitivity of the statistical analysis used in this study.

Hence, extension rate of *L. kotschyanum* f. *affine* of Kamaran did not show signal of the Red Sea climate variability.

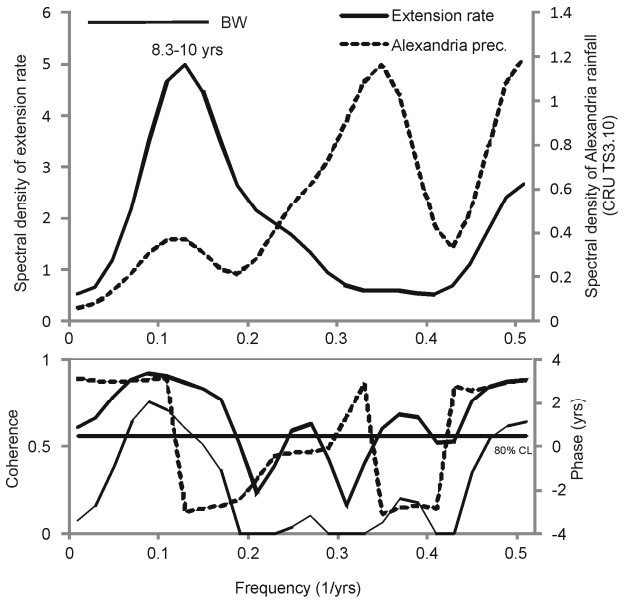

Fig.6.18 Cross-spectral analysis of Kamaran sample (DB576) extension rates versus Alexandria precipitation (CRU TS3.10) for 1994-2008. Note that it shows strong coherence for period centered at ~9 yrs. Bandwidth = 0.14, number of lags = 11. See Figure 3.6C for legend.

6.2.3.3. Asian monsoon system teleconnections

Klein et al. (1997) observed in coral $\delta^{18}O$ of South Red Sea strong correlation with the Indian Ocean SST, especially on the decadal time-scale. Although a strong positive and significant correlation was found between extension rate of rhodolith from Kamaran and SIR (r = 0.57, p-value = 0.03), no coherence was found in cross-spectral analysis between extension rate and SIR (Fig. 6.19).

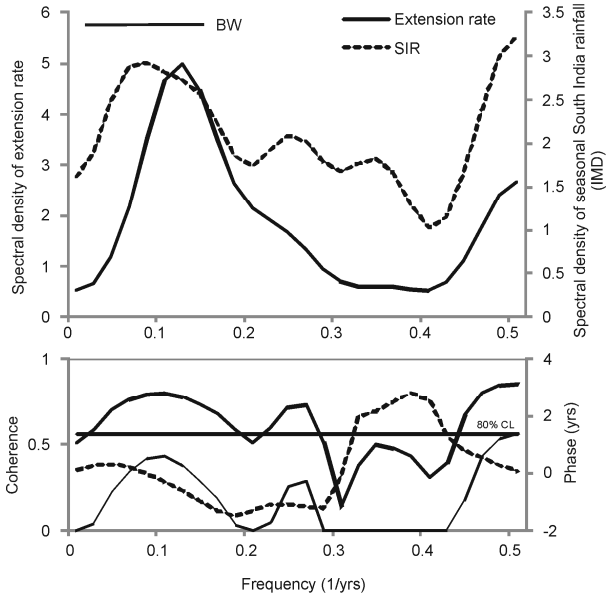

Fig. 6.19 Cross-spectral analysis of Kamaran sample (DB576) extension rates versus seasonal South India rainfall (IMD) for 1994-2008. Bandwidth = 0.14, number of lags = 11. See Figure 3.6C for legend.

The lack of *L. kotschyanum* f. *affine* from Kamaran to detect the climate variability by extension rate record, is likely due to many factors: 1) the limitations of gridded datasets used in this study, 2) alterations on coralline growth due to temporal burial, 2) mainly to its short life span (only 15 yrs), thus its limited temporal resolution. Hence, further long-term studies on coralline red algae of this area are strongly needed.

6.3. Mg/Ca ratio

6.3.1. Balhaf

6.3.1.1. Mg/Ca ratio *vs.* SST

Pioneer investigations reported the Mg content in calcite of rhodoliths ranging between 7.7 and 28.8 mol % $MgCO_3$ (Chave 1954). In *C. compactum* from the Gulf of Maine, this range resulted 9.5 to 14 mol % $MgCO_3$ (Chave and Wheeler 1965). The Mg content in *Lithothamnion* spp. is between 7.7 and 18 mol % in subarctic species, and between 13.2 to 22.4 mol % in subtropical species (Halfar et al. 2000). Samples of *Lithophyllum* spp. from New Zealand, deposit calcite containing 11.6-16.4 mol % $MgCO_3$ (Smith et al. 2012). Although Smith et al. (2012) speculate that latitude (as a proxy for water temperature) had only a minor effect on the Mg content in coralline algae, other authors suggest that the Mg content of coralline algae varies as a function of SST (Chave and Wheeler 1965; Halfar et al. 2000; Kamenos et al. 2008; Hetzinger et al. 2009). It is therefore suggested that within a genera, species sampled in warmer regions should contain higher mol % $MgCO_3$. The mean Mg content measured in *L. kothschyanum* f. *affine* was 20 mol % $MgCO_3$ (SE 0.87), which is significantly higher than 11.6-16.4 mol % $MgCO_3$ found in *Lithophyllum* spp. of New Zealand temperate environment (Smith et al. 2012).

The relationship between Mg and SST in *L. kotschyanum* f. *affine* ranges between 0.62 and 2.06 mol % of $MgCO_3$ $°C^{-1}$ in the same sample (DB659), demonstrating a high intra-specific variability. Moberly (1968) suggested that the Mg content in calcite of coralline red algae depends on growth rates, which is a function of water temperature, light intensity and physiological cycle. The lowest relationship between Mg and SST observed in the specimen with the lowest extension rates (DB659bis), which can be explained by a less Mg variability detected in a low coralline

extension rate. However in specimens with higher extension rates (DB659a and DB659b) this variability still occurred (1.06-2.06 mol % of $MgCO_3$ $°C^{-1}$). The Mg-SST relationship observed is range between half and twice as high as observed in the subarctic species: *L. glaciale* (Henrich et al. 1996; Halfar et al. 2000; Kamenos et al. 2008), *P. calcareum* (Kamenos et al. 2008), *C. compactum* (Moberly 1968), where this relationship was found to be one to one. Chave and Wheeler (1965) reported a relationship close to 0.4 $MgCO_3$ $°C^{-1}$ in *C. compactum*. These differences should be explained by different red algae species from different genera and families (Hapalidiaceae *vs.* Lithophylloideae) used by the different studies, samples from different geographic localities (subarctic *vs*. tropic), the application of different sample techniques (higher sampling resolution of transect than spots; Hetzinger et al. 2010), the sampling of carbonate in lower growth intervals, which resulted in a poorer resolution sampling per year in the studies of the other authors, the quality of SST datasets used in this study in comparison to more reliable data of *in situ* SST datasets used in Kamenos et al. 2008, and the use of different method of analysis (electron microprobe analysis *vs*. LA-ICP-MS). The latter is due to higher resolution, LA-ICP-MS line transect data highlight more fine-scale heterogeneities and are therefore able to better capture seasonal extremes in comparison to electron microprobe analysis (Hetzinger et al. 2010). The correlation between Mg-SST is still lower than found in previous studies, but still significant. Although the limitations of the gridded SST dataset, it is suggested that also in *L. kotschyanum* f. *affine* SST is likely the dominant factor controlling Mg carbonate chemistry in this algae. Smith et al. (2012) found that Mg contents in the genera of *Lithophyllum* and *Mesophyllum* were especially variable. Therefore, although Ries (2006) has shown that in *Neogoniolithon sp*. a vital offset in the process of Mg fractionation is negligible, we suggest to consider possible physiological influence on thallus Mg (Lea 2003). Mg deposition variability in *Lithophyllum* thallus, may explain the significant difference found in the monthly average of Mg/Ca between the two protuberances of the

same alga analyzed. Moreover, since the correlation between Mg-SST drastically decrease in DB659bis specimen (with the lowest extension rates observed), that underlines the limitation of coralline with low extension rates to detect all Mg variability, and so to get a reliable Mg-SST correlation.

Since the samples of DB657 and DB659a-b resulted unsuitable for paleoclimate reconstruction because their short life span and thus their too much limited temporal resolution, the DB659bis specimen, with its age model of 33 years, was the only specimen used in this study to investigate the suitability of *L. kotschyanum* f. *affine* in the reconstruction of climate variability in the Gulf of Aden. Hence, the following discussion regarding to the use of *L. kotschyanum* f. *affine* Mg/Ca ratio as proxy of the climate variability along the Yemen coast, it is only referred to the DB659bis specimen.

6.3.1.2. Interannual and decadal climate variability

The correlation between annual Mg/Ca ratio and gridded SST was weak but significant. For the same geographic, hydrological and climate reasons that characterized the study area and already mentioned in chapter 6.2.1.2, one might expect evidence for ENSO signature in Mg/Ca record. A cross-spectral analysis revealed several peaks from decadal to interannual range, centered at ~17-18 yrs, ~8 and ~5 yrs (Fig. 6.20). Cross-spectral density between annual Mg/Ca record and gridded SST (HadiSST1) revealed weak coherence for period centered at ~17-18 yrs (Fig. 6.20). Almost 90% of Mg/Ca variance is explain in this period. Cross-phase analysis showed that Mg/Ca record lags the SST by 1.5 yrs (Fig. 6.20). This period in the Mg/Ca ratio and SST spectral density appears to be an “endemic” pattern of climate variability in the NW Indian Ocean (Storz and Gischler 2011a-b). Periodicity in the range of 18-19 yrs has been found in annual

extension rates of coral from Maldives, in zonal current and in South India Rainfall variability by Storz and Gischler (2011a-b). Periodicities in this period has been found neither by authors in the annual mean $\delta^{18}O$ record in coral from Maldives, and nor in the annual mean coral $\delta^{18}O$ records of the NW Indian Ocean reported by Charles et al. (1997), Cole et al. (2000), and Pfeiffer and Dullo (2006). Storz and Gischler (2011b) suggested that this is likely due to the fact that variations in monsoon strength are not accompanied by measurable SST and salinity changes. Although a weak or poorly relationship was found between monthly coralline Mg/Ca record and gridded SST, and any correlation was found between annual Mg/Ca ratio and SST, the weak coherence observed between coralline record and SST for period of 18-19 yrs might be due to the fact that variations in monsoon strength are not accompanied in Balhaf by measurable variation in SST.

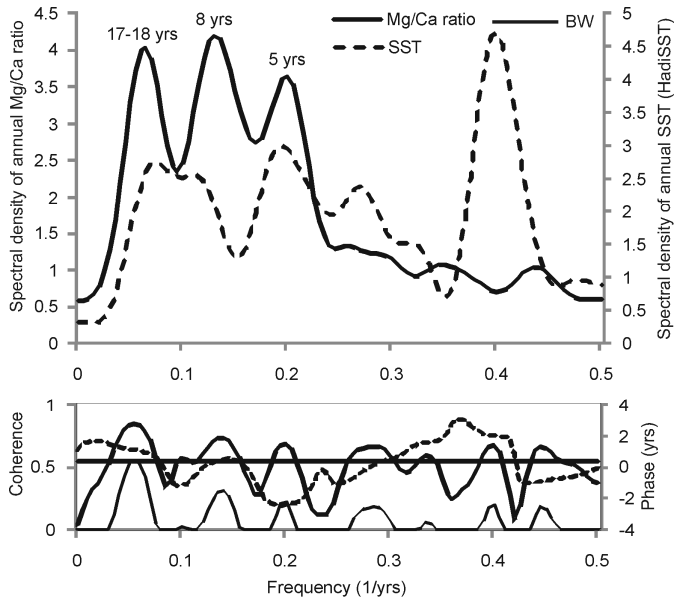

Fig. 6.20 Cross-spectral analysis of DB659bis Mg/Ca ratio versus gridded SST (HadiSST1) for 1974-2008. Note that it reveals weak coherence for period centered at ~18 yrs. Bandwidth = 0.06, number of lags = 24. See Figure 3.6C for legend.

The period of 5 yrs is a typical modes of the ENSO-driven interannual variability, and it has

been also observed in cross-spectral analysis between the Niño 3.4 index and gridded SST (Fig. 3.6C). However cross-spectral analysis between annual Mg/Ca ratio and gridded SST did not reveal coherence for this period, and although cross spectral analysis between Mg/Ca ratio and Niño 3.4 index showed a weak coherence at 5 yrs period, the cross-phase analysis revealed that Niño 3.4 index lags the Mg/Ca ratio by 1.9 yrs, which disproves causality (Fig. 6.21).

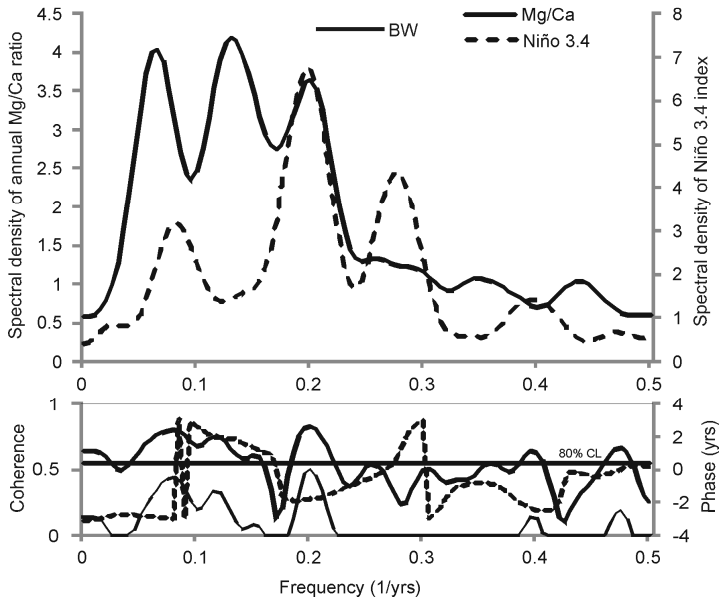

Fig. 6.21 Cross-spectral analysis of DB659bis Mg/Ca ratio versus Niño 3.4 index (from HadiSST1) for 1974-2008. Note that it shows coherence for period centered at ~5 yrs, but cross-phase analysis (dashed line in the bottom panel) reveals that there is not causality for this period. Bandwidth = 0.06, number of lags = 24. See Figure 3.6C for legend.

6.3.1.3. Mg/Ca ratio *vs.* Asian monsoon system

While decadal variability in the Mg/Ca record was link to SST variability, the interannual variability seems to be due to different climatic and environmental factors. As previously discussed, the amount of Mg incorporated in the coralline algae varies as a function of SST, but it might be affected by other factor as growth rates (Moberly 1968) and algal "vital effect" (chapter

6.3.1.1.). Additionally, experiments on marine organisms have shown that this amount in coralline calcitic thallus varies as a function of the Mg/Ca ratio of the seawater in which these organisms are grown (Ries 2006). The NW Indian Ocean is affected by Asian monsoon system, and variations in hydraulic energy is an index of the monsoon strength. Despite Storz and Gischler assumed that variations in monsoon strength are not accompanied by measurable salinity changes, in this study it is found that *L. kotschyanum* f. *affine* from Balhaf recorded SSS variability in extension rates record (see chapter 6.2.1.4.). Hence, although it is assumed that in modern seas the Mg/Ca ratio of seawater is globally constant (mMg/Ca =5.2; Ries 2006), local content of Mg in the surface seawater might change during the SW monsoon when occur upwelling of deeper water that could be rich/poor of Mg. Moreover changes in the local salinity might affect the "partitioning coefficient" leading to changes in the distribution of Mg between bulk solid and aqueous solution (see chapter 2).

Cross spectral analysis between coralline Mg/Ca record and zonal current revealed spectral coherence in the range of 17-18 yrs and ~5-6 yrs (Fig. 6.22).

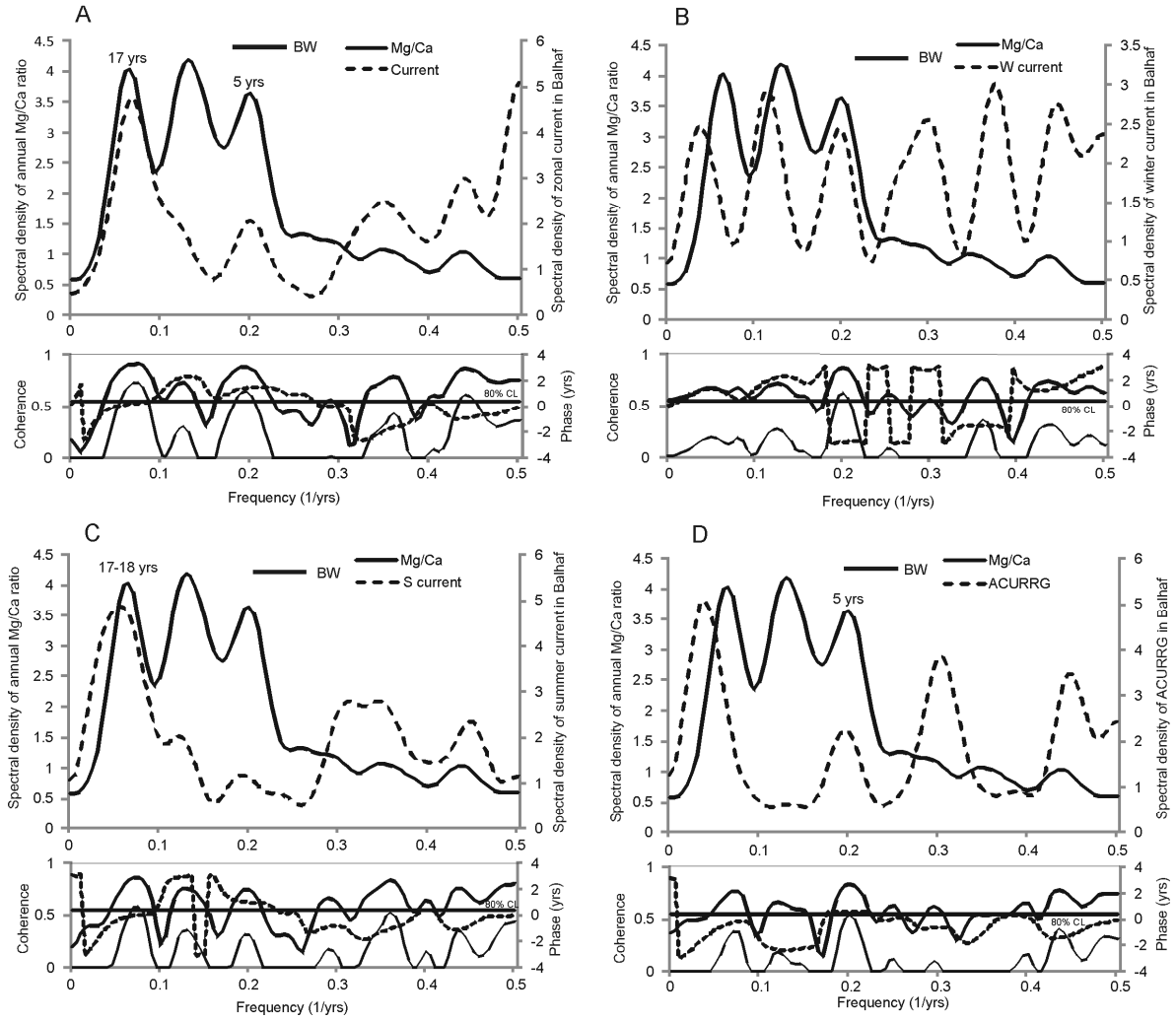

Fig. 6.22 A) cross-spectral analysis of DB659bis annual Mg/Ca ratio versus zonal current (SODA) in Balhaf for 1974-2008; B) corresponding analysis for annual Mg/Ca ratio versus mean winter monsoon current (extracted from SODA); C) corresponding analysis for annual Mg/Ca ratio versus mean summer monsoon current (extracted from SODA); D) cross-spectral analysis of annual Mg/Ca ratio versus annual current gradient record (ACURRG, difference between mean summer and winter monsoon current, extracted from SODA) for 1974-2008. Bandwidth = 0.06, number of lags = 24. See Figure 3.6C for legend.

In order to demonstrate that *L. kotschyanum* f. *affine* records the strength of SW monsoon by Mg/Ca variation recorded in the calcite thallus cross correlations were applied for the annual Mg/Ca record with 1) the mean NE monsoon (November-February) current record, 2) the SW

monsoon (May-September) current record and 3) the difference between NE and SW monsoon currents (ACURRG) as an intra-annual gradient. This analysis led to two conclusions:

1) *No link between NE monsoon currents and Mg/Ca record*. Spectral coherence between Mg/Ca record and NE monsoon current was found for the signal of 5 yrs, but cross-phase analysis showed that zonal current record lags the Mg/Ca record for these period by 2.9 yrs, which disproves causality (Fig. 6.22B).

2) and 3) *Link between SW monsoon and Mg/Ca record*. Expectedly the cross spectrum between the time-series of the SW monsoon current and the Mg/Ca record revealed a coherent peak for period centered at 17-18 yrs (Fig. 6.22C). Almost 90% of the variance of annual Mg/Ca ratio in this range can be explained by the variance in this generated dataset. The Mg/Ca ratio variability with this period can be explained by changes in the strength of the SW monsoon current, that begets SST variability (see chapter 6.3.1.2.). The generated time series of seasonal differences between summer and winter monsoon displayed a weak spectral coherence in the interannula range (Fig. 6.22D). Almost 80% of the variance of annual Mg/Ca ratio in this range can be explained by the variance in this dataset within the range of 5-6 yrs. For this period no link was found with SST, so it suggested that Mg/Ca variability for this period is due to changes in the strength of the SW monsoon currents, linkage to upwelling events, that might have led to changes in seawater Mg. Storz and Gischler (2011) found in their coral proxy study with *P. lutea* from Maldives decadal growth variability with similar periods of 18-19 yrs and 6-7 yrs, that they explained by changes in the strength of SW monsoon currents, but not linked to SST variability. As they themselves suggested, this may be due to the fact that coral was collected in a lagoon, where SST and current variations were likely larger than indicated by gridded instrumental climate records.

Annual Mg/Ca variability in *L. kotschyanum* f. *affine* calcite thallus did not show link with SIR, the other parameter used as index of the monsoon strength. Indeed, cross-spectral analysis

between annual Mg/Ca ratio and SIR revealed strong coherence for periods centered at 17-18 yrs and ~8 yrs, but cross-phase analysis disproved causality for these periods (Fig. 6.23).

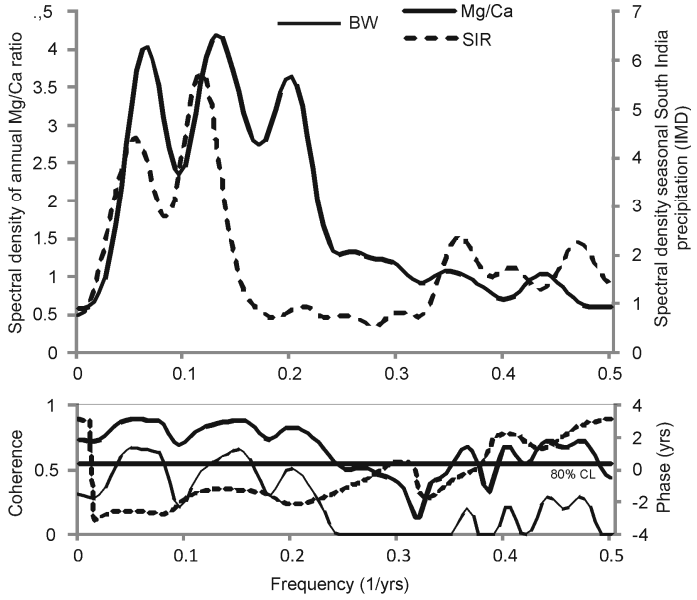

Fig. 6.23 Cross-spectral analysis of DB659bis annual Mg/Ca ratio versus seasonal South India precipitation (IMD) in Balhaf for 1974-2008. Bandwidth = 0.06, number of lags = 24. See Figure 3.6C for legend.

6.3.1.4. Red Sea teleconnections

Albeit interannual fluctuations in algal extension rates can be explained by SSS anomalies driven by current forcing in the South Red Sea, and thus showing teleconnection with the Red Sea climate, the annual Mg/Ca record in the coralline calcite thallus did not revealed signals of Red Sea climate influences. Indeed, cross-spectral analysis between Mg/Ca record and zonal SSS did not reveals connections, as well as between Mg/Ca record and SSS of South Red Sea (not shown). Moreover, cross spectral analysis between Mg/Ca record and current in the South Red Sea revealed spectral coherence for period centered at 17-18 yrs, but cross-phase analysis showed that current lags the Mg/Ca ratio by 1.5 yrs, which disproved causality (Fig. 6.24A). Periodicity in the range of

17-18 has been observed in the cross spectral analysis between the record and the summer current variability in the South Red Sea (Fig. 6.24C). During SW monsoon surface water mass from Red Sea outflow into the Gulf of Aden. The cross spectral showed a weak coherence for this period, and cross-phase analysis did not revealed lags between both time series. This suggested an influence of the hydraulic energy of the Red Sea to the surface circulation of the Gulf of Aden, recorded on the *L. kotschyanum* f. *affine* thallus by Mg/Ca variability.

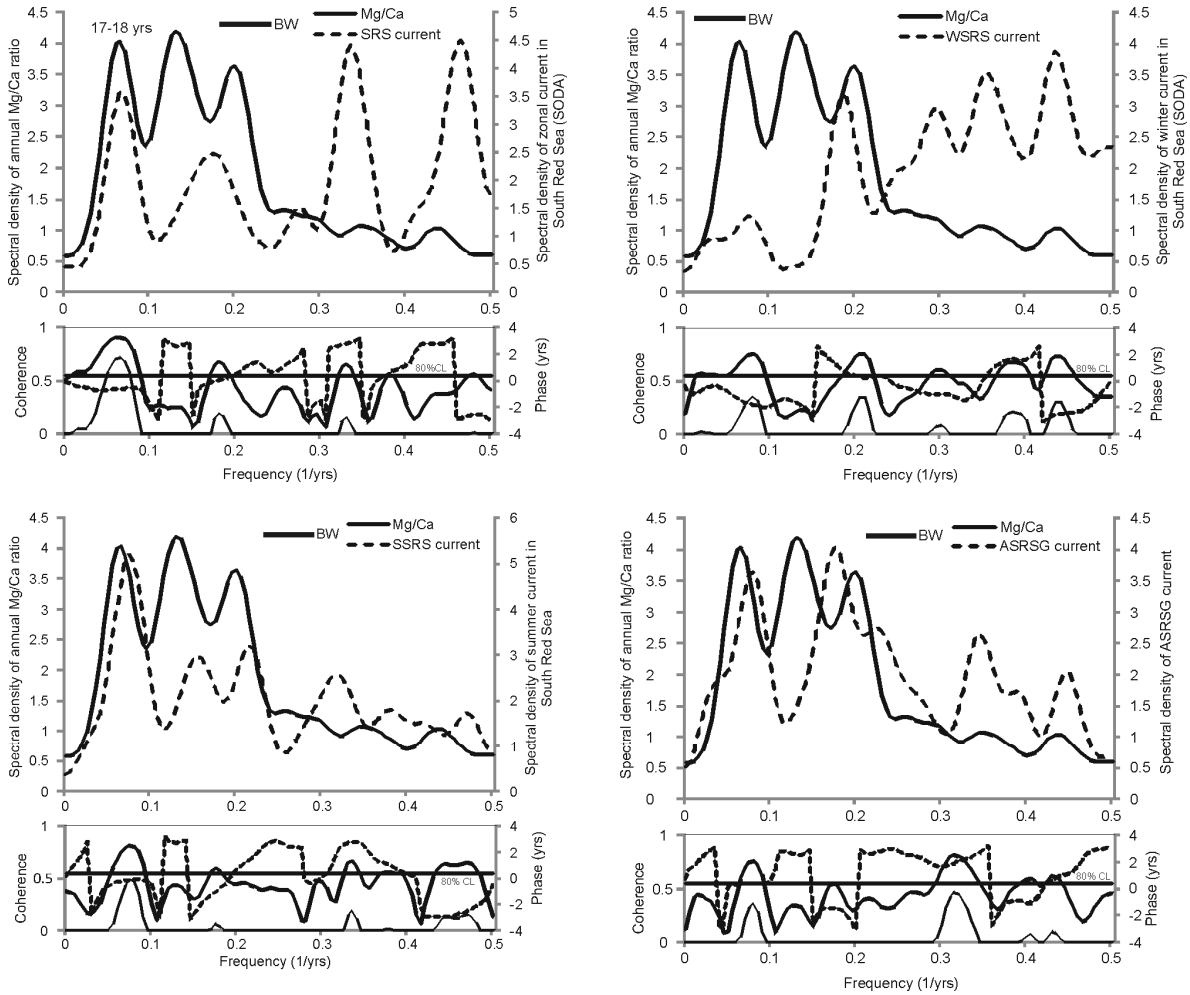

Fig. 6.24 A) cross-spectral analysis of DB659bis annual Mg/Ca ratio versus zonal current (SODA) in South Red Sea for 1974-2008; B) corresponding analysis for annual Mg/Ca ratio versus mean winter monsoon current (extracted from SODA); C) corresponding analysis for annual Mg/Ca ratio versus mean summer monsoon current (extracted from SODA); D) cross-spectral analysis of annual Mg/Ca ratio versus annual current gradient record (ASRSG current, difference between mean summer and winter monsoon current, extracted from SODA) for 1974-2008. Bandwidth = 0.06, number of lags = 24. See Figure 3.6C for legend.

6.3.2. Socotra

6.3.2.1. Mg/Ca ratio *vs*. SST

Expectedly for subtropical coralline sample, the mean Mg content measured in *Lithophyllum* sp. was 20.1 mol % $MgCO_3$ (SD 4.9) which is similar to what found in *L. kothschyanum* f. *affine* of Balhaf.

The relationship between Mg and SST in *Lithophyllum* sp. of Socotra is 1.22 mol % $MgCO_3$ $°C^{-1}$ that fall in the range found in *L. kotschyanum* f. *affine* of Balhaf and it is twice time higher than the DB659bis specimen (the protuberance analyzed in DB659 with the lowest extension rates). As previously discussed the sample from Socotra showed an extension-rate record with low growth rates that was similar to what measured in DB659bis specimen. Despite the limitation of gridded dataset used in this study, the difference between *Lithophyllum* sp. from Socotra and the DB659bis from Balhaf on the Mg/Ca-SST relationship should be explained by different factors: 1) the different species analyzed, 2) the variability of Mg contents in the genera of *Lithophyllum* and *Mesophyllum* (Smith et al. 2012), 3) the vital effect, despite Ries (2006) has shown that in coralline algae a vital offset in the process of Mg fractionation is negligible, 4) the low extension rate has led to a less Mg variability detected in a low coralline extension rate, 5) temporary cessation of rhodolith growth due to temporary burial that led to an interrupted environmental record in the coralline algae (Cabioch 1966, Halfar et al. 2011), 6) different living environment of coralline algae due to different depth (6-8 m of L. kotschyanum f. affine from Balhaf against 22 m of Lithophyllum sp. from Socotra). This could also explain the lower correlation found comparing with previous studies (Kamenos et al. 2008, Hetzinger et al. 2010). Therefore, as already discussed for Balhaf samples (chapter 6.3.1.1.), it is suggested that also in *Lithophyllum* sp. from Socotra SST is likely the dominant factor controlling Mg carbonate chemistry, but the combination of these

factors have led to the low relationship.

6.3.2.2. Interannual and decadal climate variability

The correlation between annual Mg/Ca ratio and gridded SST was weak but significant. For the same geographic, hydrological, climatic and environmental reasons that characterized the study area and already mentioned in chapter 6.2.2.2, one might expect evidence for ENSO signature in Mg/Ca record. A cross-spectral analysis revealed peaks from decadal to interannual range, centered at ~20, ~4.3, ~3 yrs and ~2.4 yrs (Fig. 6.25). Cross-spectral density between annual Mg/Ca record and gridded SST (HadiSST1) showed weak coherence for period centered at ~3 yrs, and cross-phase analysis revealed that the record lags SST by 2 yrs (Fig. 6.25). Only the 45% of the Mg/Ca variance is explained in this period.

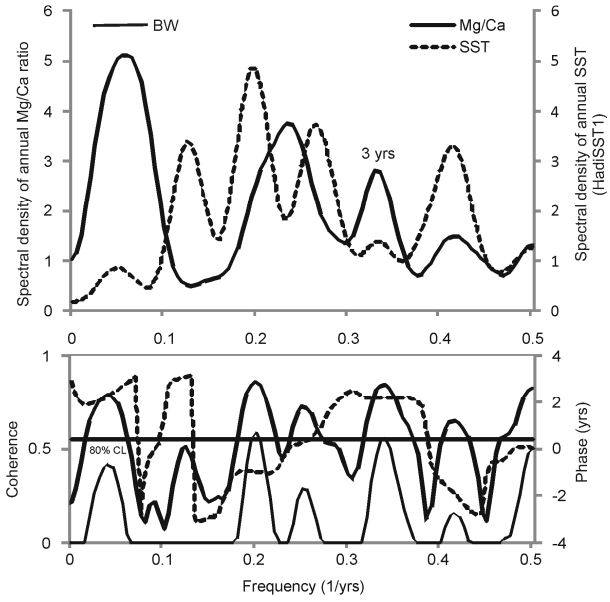

Fig. 6.25 Cross-spectral analysis of Socotra sample (DB635) Mg/Ca ratio versus annual SST (HadiSST1) for 1972-2009. Note that it shows weak coherence for period centered at ~3 yrs. Bandwidth = 0.06, number of lags = 24. See Figure 3.6C for legend.

Albeit a relationship was observed between ENSO and gridded SST for periods 5 yrs and 3.6-3.7 yrs (Fig. 3.12), and a weak but significant correlation was observed between annual Mg/Ca and Niño3.4 index (r = 0.33, p-value = 0.04), no aligned peaks were found in cross-spectral density between Mg/Ca record and Niño3.4 index (Fig. 6.26). Hence the Mg/Ca record on *Lithophyllum* sp. thallus of Socotra did not record any signal of the ENSO-force in the Indian Ocean.

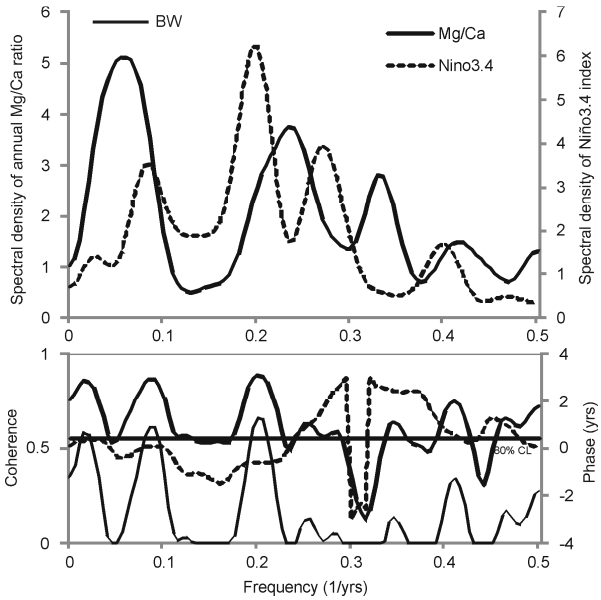

Fig. 6.26 25 Cross-spectral analysis of Socotra sample (DB635) Mg/Ca ratio versus Niño 3.4 index (from HadiSST1) for 1972-2009. Bandwidth = 0.06, number of lags = 24. See Figure 3.6C for legend.

6.3.2.3. Mg/Ca ratio vs. Asian monsoon system

The NW Indian Ocean is affected by Asian monsoon system, and variations in hydraulic energy is an index of the monsoon strength. Despite the Mg/Ca record on *L. kotschyanum* f. *affine* from Balhaf revealed signal of the monsoon strength by local hydraulic variability, the Mg/Ca ratio on *Lithophyllum* sp. thallus from Socotra did not show any relationship with zonal current (not show). As already mentioned in chapter 6.2.2.3., the current dataset used in this study (SODA)

provide data of surface current velocity, thus of the first 5 m depth. Since rhodolith of Socotra lived at 20 m depth, it is reasonable to assume that at this depth, the coralline alga has not recorded the surface current variability caused by monsoonal wind. Thus, the lake of coralline alga from Socotra to record the variation in local hydraulic energy is probably due to the limitation of gridded dataset used in this study, as well as to the temporary cessation of rhodolith growth due to temporary burial that it led to an interrupted environmental record in the coralline alga (Cabioch 1966, Halfar et al. 2011).

However, a positive weak correlation was found between annual Mg/Ca ratio of coralline alga from Socotra and SIR, the other parameter used as index of the monsoon strength ($r = 0.43$, p-value =0.008). Expectedly, cross-spectral density between Mg/Ca record and SIR showed strong coherence for period of 20-22 yrs (Fig. 6.27). This is the typical mode of the Asian monsoon system already found either in extension-rate record of coral from Maldives, and in this study, in Mg/Ca record of *L. kotschyanum* f. *affine* from Balhaf (chapter 6.3.1.3.). While Mg/Ca record of L. kotschyanum f. *affine* from Balhaf did not reveal correlation with SIR, coral extension rates from Maldives showed a negative correlation, explained with a reduction of coral growth during periods of stronger summer monsoon (Storz and Gischler 2011b). The positive relationship found in Mg/Ca record of *Lithophyllum* sp. from Socotra might be explained by the change in salinity due to the variation of the monsoon intensity, that somehow change positively the mechanism of incorporation of Mg into the calcite lattice of the coralline.

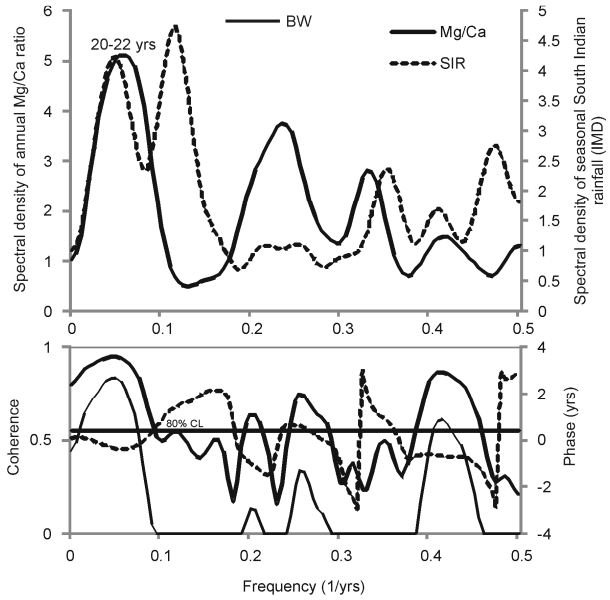

Fig. 6.27 Cross-spectral analysis of Socotra sample (DB635) Mg/Ca ratio versus seasonal South India precipitation (IMD) for 1972-2009. Note that it reveals strong coherence for period centered at ~21 yrs. Bandwidth = 0.06, number of lags = 24. See Figure 3.6C for legend.

6.3.2.4. Red Sea teleconnections

Socotra is bathed by a variety of different water masses, including those originating to the north-west by the Red Sea. The Red Sea water is one of the most saline water masses in the world oceans. Passing through the Gulf of Aden, the water outflows from the Red Sea becomes a part of the intermediate circulation in the Indian Ocean, which has been observed as a mid-depth salinity maximum in the Arabian Sea and even in the southern hemisphere (Mecking and Warner 1999). Therefore, changes in the local SSS and connections with the southern Red Sea SSS were investigated in the Mg/Ca record of *Lithophyllum* sp. from Socotra. Cross-spectral analysis between Mg/Ca record and gridded SSS showed strong coherence for period of 20-22 yrs, and the record lags the SSS by 1.7 yrs (Fig. 6.28).

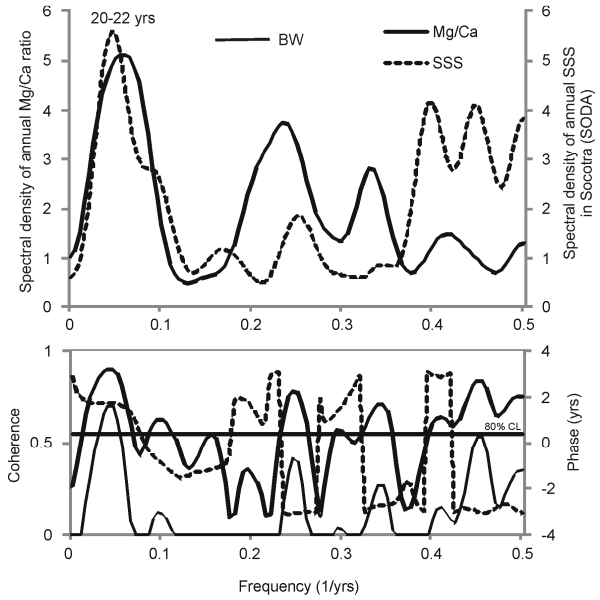

Fig. 6.28 Cross-spectral analysis of Socotra sample (DB635) Mg/Ca ratio versus annual SSS (SODA) for 1972-2009. Note that it shows strong coherence for period centered at ~21 yrs. Bandwidth = 0.06, number of lags = 24. See Figure 3.6C for legend.

Cross-spectral analysis between Mg/Ca record and southern Red Sea SSS revealed strong coherence for period centered at ~16.5 yrs, and the record lags the SSS by 1 yr (Fig. 6.29A).

Strong relationship for the same period was found still with winter and summer SSS of southern Red Sea, with a lag of 1 yr and 1.7 yrs respectively (Fig. 6.29B, C). Since local SSS showed a strong significant correlation with SIR, but not with SSS of the South Red Sea for the period centered at ~23.5 (Fig. 6.15), and Mg/Ca record revealed a strong coherence with SIR for the same period, it is assumed that signal of local SSS variability in the Mg/Ca record for this period is likely due to upwelling of more dense deeper water during monsoon.

While, the period of 3 yrs found in cross-spectral density between Mg/Ca record and SST was still revealed by cross-spectral analysis between the record and zonal current of southern Red Sea (Fig. 6.30).

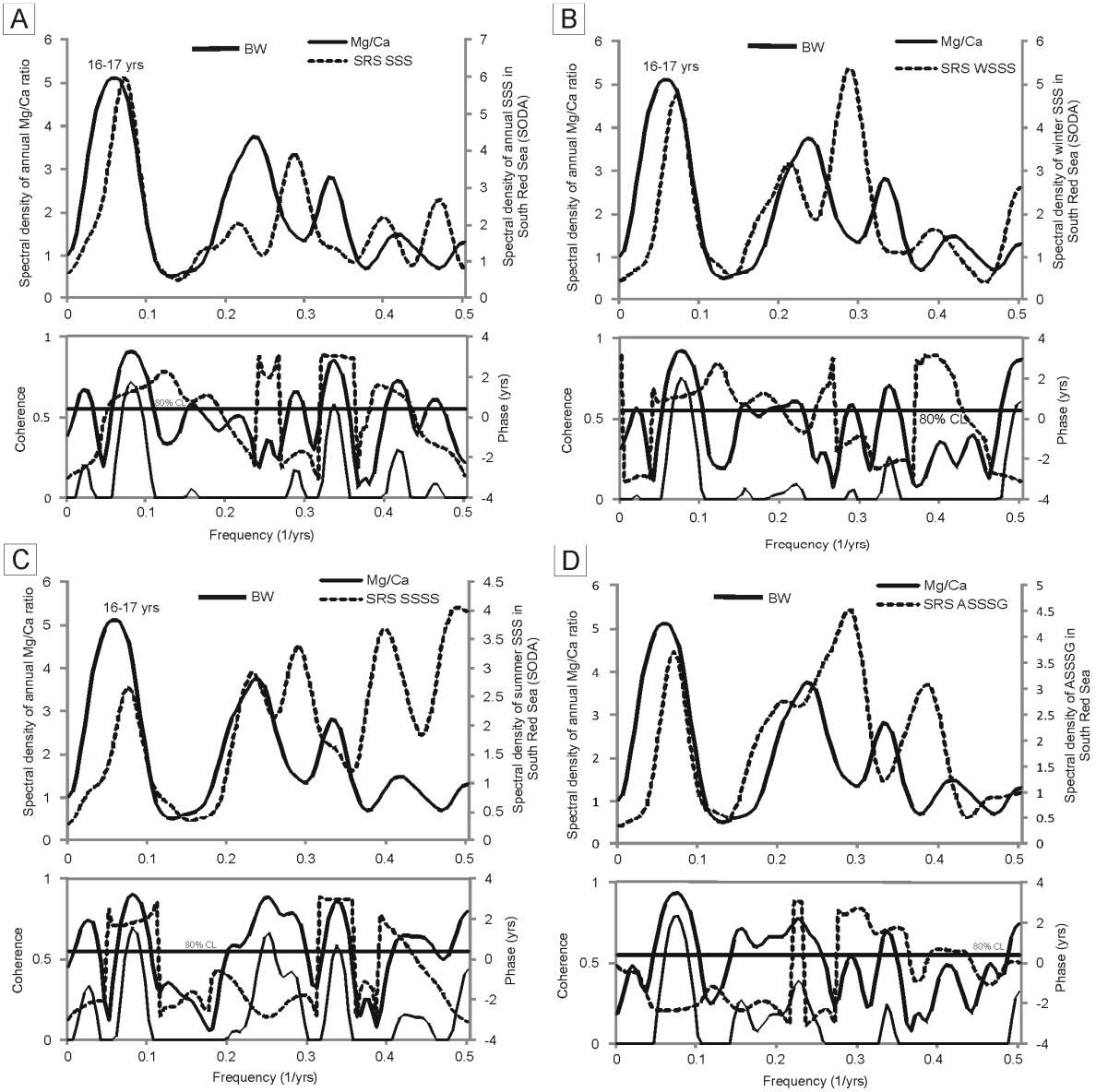

Fig. 6.29 A) cross-spectral analysis of Socotra sample (DB635) Mg/Ca ratio versus SSS (SODA) in South Red Sea for 1972-2009; B) corresponding analysis for annual Mg/Ca ratio versus mean winter SSS (extracted from SODA); C) corresponding analysis for annual Mg/Ca ratio versus mean summer monsoon SSS (extracted from SODA); D) Cross-spectral analysis of annual Mg/Ca ratio versus annual SSS gradient record (ASSSG, difference between mean summer and winter monsoon SSS, extracted from SODA) in South Red Sea for 1972-2009. Bandwidth = 0.06, number of lags = 24. See Figure 3.6C for legend.

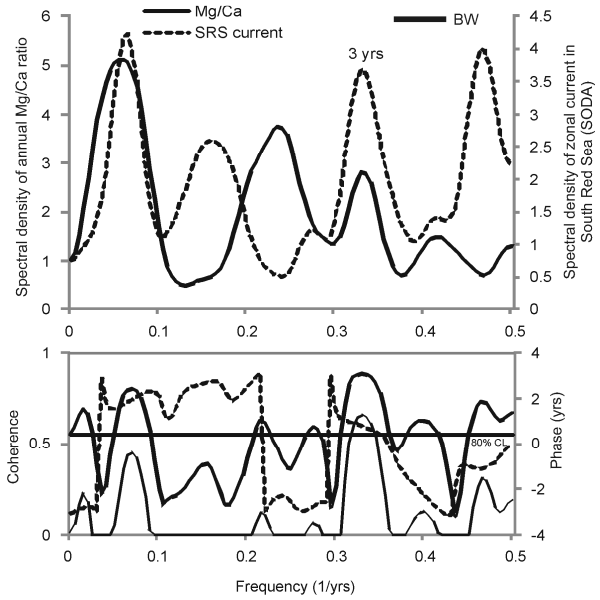

Fig. 6.30 Cross-spectral analysis of Socotra sample (DB635) Mg/Ca ratio versus zonal current (SODA) in South Red Sea for 1972-2009. Note that it shows coherence for period centered at ~3 yrs. Bandwidth = 0.06, number of lags = 24. See Figure 3.6C for legend.

6.3.3. Kamaran

6.3.3.1. Mg/Ca ratio *vs*. SST

Expectedly for subtropical coralline, the mean Mg content measured in *L. kothschyanum* f. *affine* of Kamaran was 19.9 mol % $MgCO_3$ (SD 3.5), similar to the Mg content in the samples of the same species of Balhaf and in *Lithophyllum* sp. of Socotra.

The relationship between Mg and SST in *L. kothschyanum* f. *affine* of Kamaran is 1.4 mol % $MgCO_3$ $°C^{-1}$ that fall in the range found in the samples of the same species from Balhaf and it was similar to what found in *Lithophyllum* sp. of Socotra, although the latter is a different species. Instead it is twice time higher than the DB659bis specimen (the protuberance analyzed in DB659 with the lowest extension rates). As previously discussed difference on Mg/Ca-SST relationship found in *L. kothschyanum* f. *affine* from Kamaran comparing with the other samples analyzed in

this study should be explained by different factors: 1) the different species analyzed (*Lithophyllum* sp. from Socotra), 2) the variability of Mg contents in the genera of *Lithophyllum* and *Mesophyllum* (Smith et al. 2012), 3) the vital effect, despite Ries (2006) has shown that in coralline algae a vital offset in the process of Mg fractionation is negligible, 4) the low extension rate has led to a less Mg variability detected in a low coralline extension rate, 5) temporary cessation of rhodolith growth due to temporary burial that led to an interrupted environmental record in the coralline algae (Cabioch 1966, Halfar et al. 2011), 6) different living environment of coralline algae due to different depth (1.5 m of L. kotschyanum f. affine from Kamaran against 22 m of Lithophyllum sp. from Socotra). This could also explain the lower correlation found comparing with previous studies (Kamenos et al. 2008, Hetzinger et al. 2010). Therefore, as already discussed for Balhaf and Socotra samples (chapter 6.3.1.1. and 6.3.2.1.), it is suggested that also in *L. kotschyanum* f. *affine* from Kamaran SST is likely the dominant factor controlling Mg carbonate chemistry, but the combination of these factors have led to the low relationship.

6.3.3.2. Interannual and decadal climate variability

A Cross-spectral analysis revealed in the Mg/Ca spectral an interannual peak centered at ~7.7 yrs (Fig. 6.31). Albeit extension rate did not show signal of ENSO-force in the South Red Sea, and field correlation between Niño3.4 index and SST in the South of Red Sea did not show significant correlation (Fig. 3.6B), cross-spectral density between Mg/Ca record and Niño3.4 index revealed a weak coherence for period 7.1-8.3 yrs, and 94% of the Mg/Ca variance is explained in this period (Fig. 6.31). Felis et al. (2000) found a coherence preferentially for period of ~5.7, and Klein et al. (1997) in the interannula range. Moreover cross spectral analysis between Niño3.4 index and local SST revealed coherence in the interannula range but in different periods (Fig.

3.20). These factors and coralline's short life span (only 15 yrs), thus its limited temporal resolution further confirm the need of long-term studies on coralline red algae of this area.

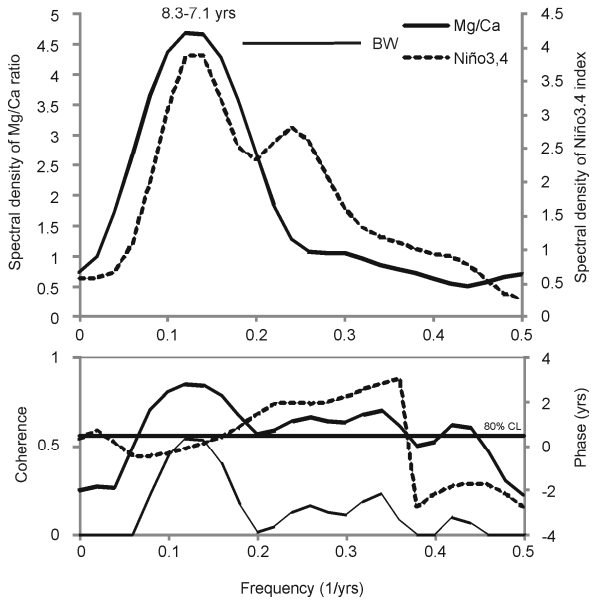

Fig. 6.31 Cross-spectral analysis of Kamaran sample (DB576) Mg/Ca ratio versus Niño 3.4 index (from HadiSST1) for 1994-2008. Note that it shows weak coherence for period centered at ~7.5 yrs. Bandwidth = 0.14, number of lags = 11. See Figure 3.6C for legend.

Cross-spectral analysis between Mg/Ca record and zonal current did not reveal coherence (not shown), but cross-spectral density between the record and the SLP showed coherence for period 7.1-8.3 yrs (Fig. 6.32). Klein et al. (1997) suggested that, on a decadal time-scale, there are simultaneous changes in the phases of the Southern Oscillation, the south Asian monsoon and the Indian Ocean SST, which are recorded in the stable isotope composition of the southern Red Sea corals. Hence, it is suggested here, that likely the Mg/Ca composition in the *L. kotschyanum* f. *affine* of Kamaran recorded on quite decadal time-scale, the ENSO influence on the Red Sea by the SLP variability, rather than by SST variability.

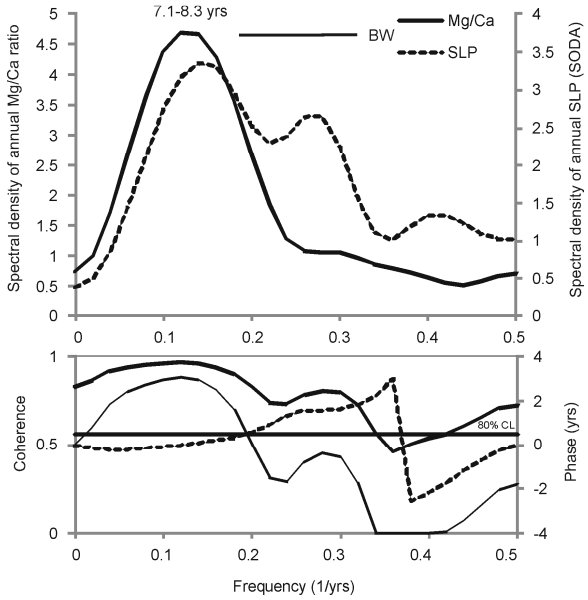

Fig. 6.32 Cross-spectral analysis of Kamaran sample (DB576) Mg/Ca ratio versus annual SLP (SODA) for 1994-2008. Note that it shows weak coherence for period centered at ~7.5 yrs. Bandwidth = 0.14, number of lags = 11. See Figure 3.6C for legend.

No relationship was found with Alexandria precipitation (not shown).

6.3.3.3. Asian monsoon system teleconnections

As for extension rate, also the Mg/Ca did not result a proxy of the influence of the Asian monsoon system on the Red Sea climate.

6.4. Li/Ca ratio

6.4.1. Balhaf

6.4.1.1. Li/Ca ratio *vs.* SST

Li in coralline algae firstly investigated here shows Li/Ca time series following the Mg/Ca curve and strong and significant correlations between both time series in all transects. The mean Li content measured in *L. kothschyanum* f. *affine* was 8.3 µmol % $LiCO_3$ (SE 0.68), and the relationship between Li and SST was 0.46 and 0.57 µmol % of $LiCO_3$ $°C^{-1}$ in the same sample (DB659). That resulted steady respect Mg-SST relationship. In fact, the lowest relationship is found for specimen with the lowest extension rate (DB659bis), which can be explained by a decreased ability to detect Li variability, while in specimen with higher extension rate (DB659a and DB659b) the relationship is found constantly equal to 0.57 µmol %.

Since SST was considered the main factor controlling the incorporation of Mg in coralline algal thallus, a significant correlation was found between monthly average Li/Ca and SST, it is speculated that SST is also the dominant factor controlling Li-carbonate chemistry in *L. kotschyanum* f. *affine* of Balhaf. Studies on skeleton of other marine organisms gave evidence confirming this control (Delaney et al. 1989; Marriott et al. 2004; Montagna et al. 2008), while other provided evidence of the contrary (Delaney et al. 1985; Hell and Chan 2004; Rollion-Bard et al. 2009). In this study, a positive relationship between Li/Ca and SST was found. This is in contrast to studies on other marine skeletal-bearing organisms (Delaney et al. 1989; Marriott et al. 2004; Montagna et al. 2008). This is the first evidence that Li/Ca could be used as a proxy for SST. However, more studies from different environments in different climatic regions and from longer records are needed to fully assess the potential of this elementary ratio as climate proxy.

Since the samples of DB657 and DB659a-b resulted unsuitable for paleoclimate reconstruction because their short life span and thus their too much limited temporal resolution, the DB659bis specimen, with its age model of 33 years, was the only specimen used in this study to investigate the suitability of *L. kotschyanum* f. *affine* in the reconstruction of climate variability in the Gulf of Aden. Hence, the following discussion regarding to the use of *L. kotschyanum* f. *affine* extension rate as proxy of the climate variability along the Yemen coast, it is only referred to the DB659bis specimen.

6.4.1.2. Interannual and decadal climate variability

Since between Mg/Ca and Li/Ca time series showed a strong and significant correlation, and the observed significant Li-SST relationship, one might expect evidence for SST and ENSO signature in Li/Ca record for the same periods found for Mg/Ca record. Cross-spectral analysis between Li/Ca record and gridded SST (HadiSST1) revealed a multi-decadal coherent peak centered at 17-18 yrs, that is more coherent than it found in Mg/Ca record for the same period (Fig. 6.33, Fig. 6.20). The period of 17-18 yrs shared 83% of algal thallus Li/Ca variance. Cross-phase analysis did show lags between the two time series (Fig. 6.33).

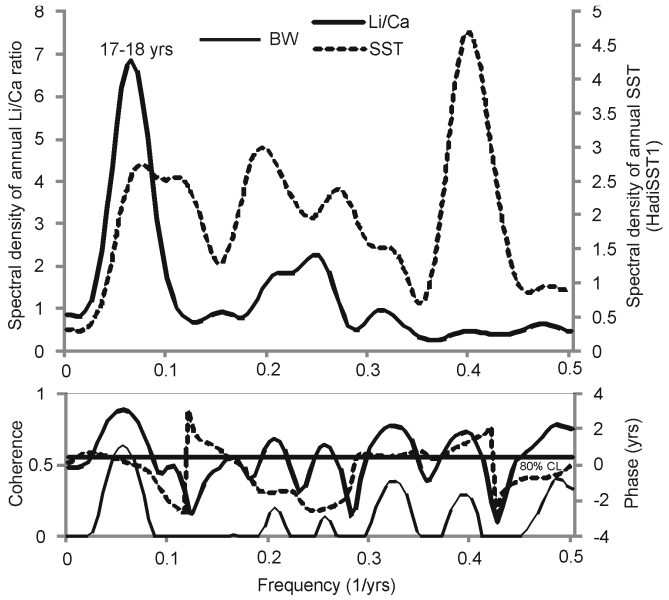

Fig. 6.33 Cross-spectral analysis of DB659bis Li/Ca ratio versus gridded SST (HadiSST1) for 1974-2008. Note that it reveals coherence for period 17-18 yrs. Bandwidth = 0.06, number of lags = 24. See Figure 3.6C for legend.

The interannula variability in the Indian Ocean is characteristic of ENSO force, while decadal and multidecadal response to Pacific influence is under debate. In fact some studies on coral skeleton from Seychelles, Madagascar and Maldives found for decadal variability an expression of the monsoon system (Charles et al. 1997; Zinke et al. 2004; Storz and Gischler 2011a, b), while Cole et al. (2000) in their study on coral from Kenya, suggested that decadal variability in the coral records is primarily a response to Pacific influences. In the present study the cross-spectral analysis between algal Li/Ca record and the Niño 3.4 index showed a weak coherence for period 17-18 yrs (Fig. 6.34), which is not found in Mg/Ca record (Fig. 6.21). Cross-phase analysis showed that Li/Ca record lags the Niño 3.4 index by 2 yrs (Fig. 6.34).

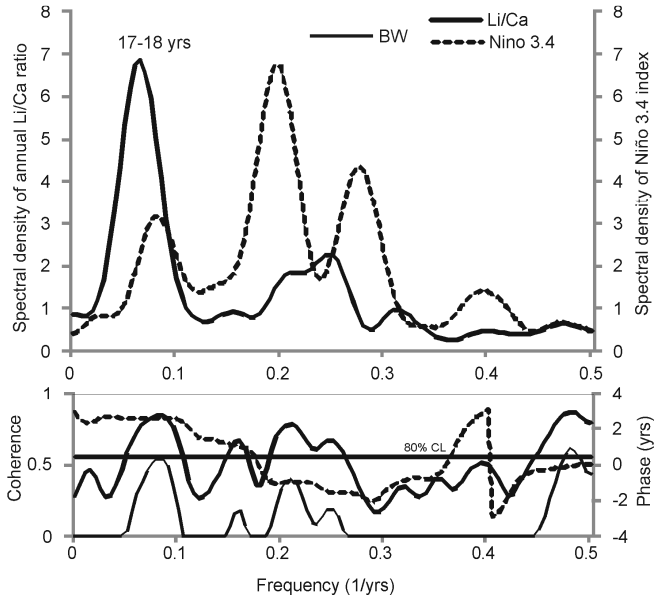

Fig. 6.34 Cross-spectral analysis of DB659bis Li/Ca ratio versus Niño 3.4 index (from HadiSST1) for 1974-2008. Note that it reveals weak coherence for period 17-18 yrs, and cross-phase analysis (dashed line in the bottom panel) shows that Li/Ca record lags the Niño3.4 index by 2 yrs for this period. Bandwidth = 0.06, number of lags = 24. See Figure 3.6C for legend.

6.4.1.3. Li/Ca ratio *vs*. Asian monsoon system

To detect a response to Asian monsoon in the algal Li/Ca record cross-spectral analysis between annual mean of element ratio and the local current was conducted. Strong coherence was found for period centered at 17-18 yrs, but cross-phase analysis revealed that current lags Li/Ca ratio by 0.8 y, which disproves causality (Fig. 6.35).

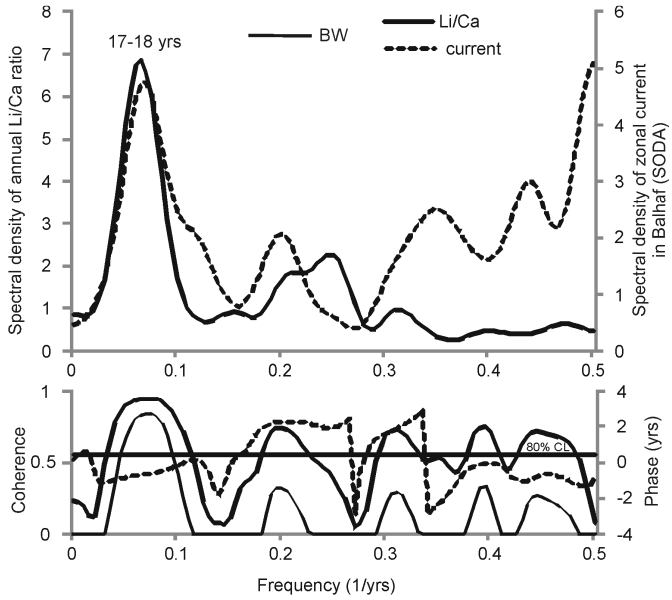

Fig. 6.35 Cross-spectral analysis of DB659bis Li/Ca ratio versus zonal current (SODA) in Balhaf for 1974-2008. Note that it reveals strong coherence for period 17-18 yrs, but cross-phase analysis (dashed line in the bottom panel) shows that there is not causality for these periods. Bandwidth = 0.06, number of lags = 24. See Figure 3.6C for legend.

However, spectral coherence was revealed for the same period between Li/Ca record and SIR, and the Li/Ca record lags the seasonal South India rainfall record by 2.8 yrs (Fig. 6.36). The Li/Ca-SIR showed a weak negative, but significant correlations (r= -0.42, p-value = 0.01). Storz and Gischler (2011b) found a negative relationship between coral extension rate record from Maldives and seasonal South India rainfall, and they explained it by a reduction of coral growth during stronger Asian monsoon due to increase of summer monsoon current. Although extension rates record of *L. kotschyanum* f. *affine* from Balhaf showed negative weak but poorly significant correlation with SIR, the negative and significant relationship found between Li/Ca record and SIR might be explain with a decrease of the coralline extension rate during stronger monsoon probably due to decrease of water transparency and light supply for increase of suspension for upwelling. Therefore the reduction of algal growth rates lead in reduction of Li variability detection.

It is assumed that coralline Li/Ca variability is a signal of the monsoon strength for this

period, and not of the ENSO force, since: 1) Storz and Gischler (2011a, b) observed in coral extension rates from Maldives, coherence with zonal current and SIR for the same period (18-19 yrs); 2) decadal coral $\delta^{18}O$ variability has been linked to Asian monsoon in most studies in the NW Indian Ocean, excepted Cole et al. (2000) who found a decadal signal of ENSO on coral $\delta^{18}O$ variability; 3) in this study the decadal Mg/Ca variability on *L. kotschyanum* f. *affine* thallus has been found to be a signal of zonal current variability for period of 17-18 yrs, 4) the limitation of gridded datasets used in this study, that might cause the lack of signal of zonal current variability in coralline Li/Ca record for this period, 5) limited knowledge on process of Li incorporation into the coralline calcite thallus; that it could only speculate that decadal variability in algal record is primarily a response to monsoon system, which is partially influenced by ENSO force.

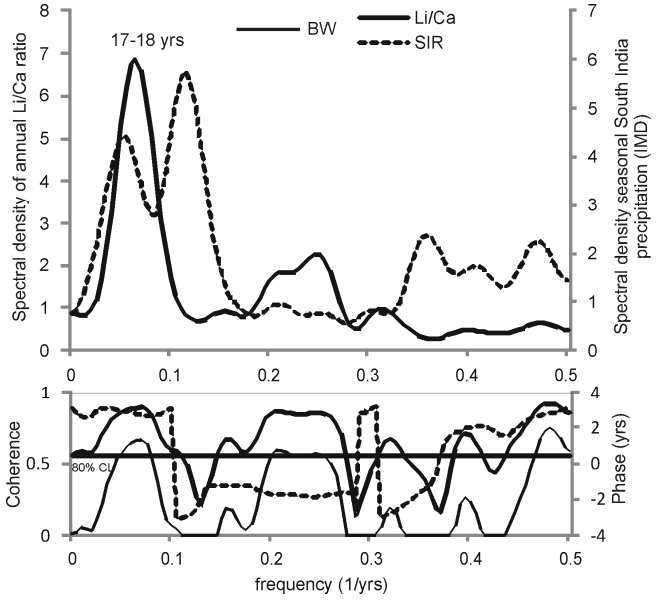

Fig. 6.36 Cross-spectral analysis of DB659bis Li/Ca ratio versus seasonal South India rainfall (IMD) in Balhaf for 1974-2008. Note that it reveals coherence for period 17-18 yrs, and cross-phase analysis (dashed line in the bottom panel) shows that the Li/Ca record lags SIR by 2.8 yrs for this period. Bandwidth = 0.06, number of lags = 24. See Figure 3.6C for legend.

6.4.1.4. Red Sea teleconnections

As for Mg/Ca record no teleconnection with the Red Sea climate was found for Li/Ca record (not shown).

6.4.2. Socotra

6.4.2.1 Li/Ca ratio *vs*. SST

Li/Ca in *Lithophyllum* sp. thallus of Socotra showed a strong positive and significant relationship with Mg/Ca ratio, in agreement with what observed in *L. kotschyanum* f. *affine* of Balhaf. The mean Li content in the rhodolith from Socotra was found lower than that measured in coralline from Balhaf. This can be explain by several factors: 1) unknown of the Li incorporation mechanisms into the calcite lattice of the coralline algae, 2) different species used, 3) temporal cessation of rhodolith growth due to temporary burial that led to an interrupted environmental record in the coralline alga (Cabioch 1966, Halfar et al. 2011), 4) different depths of life of the samples.

Li-SST relationship in *Lithophyllum* sp. was 0.53 µmol % of LiCO3 $°C^{-1}$, that resulted steady respect Li-SST relationship observed in *L. kotschyanum* f. *affine* of Balhaf. Since SST was considered the main factor controlling the incorporation of Mg in coralline algal thallus, a significant correlation was found between monthly average Li/Ca and SST, it is speculated that SST is also the dominant factor controlling Li-carbonate chemistry in *Lihtophyllum* of Socotra, as it has been assumed for *L. kotschyanum* f. *affine* of Balhaf (see chapter 6.4.1.1.).

6.4.2.2. Interannual and decadal climate variability

Since between Mg/Ca and Li/Ca ratio showed a strong and significant correlation, and for significant Li-SST relationship observed, one might expect evidence for SST and ENSO signature in Li/Ca record. A cross-spectral analysis revealed several peaks from decadal to interannual range, centered at ~15, 4.2 yrs and 3 yrs (Fig. 6.37). Although monthly Li/Ca ratio showed significant correlation with SST, annual mean of element ratio did not reveal significant relationship with annual SST. Expectedly cross-spectral analysis between Li/Ca record and gridded SST did not show aligned peaks (Fig. 6.37). However cross-spectral analysis between annual Li/Ca record and Niño3.4 index revealed weak coherence for period centered at ~14.5 yrs (Fig.6.38).

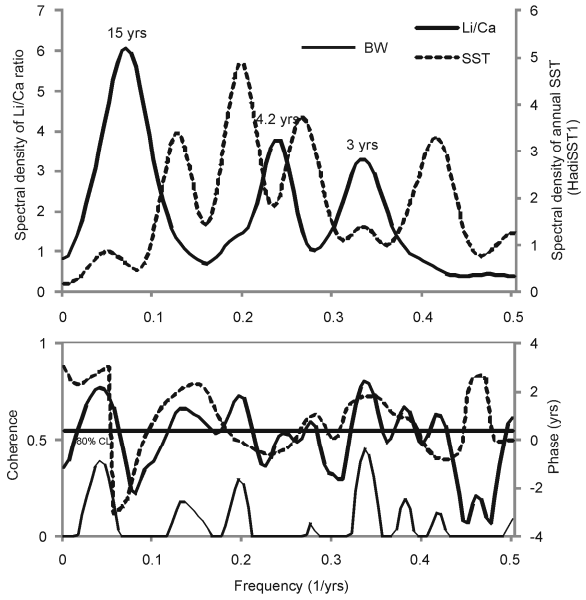

Fig. 6.37 Cross-spectral analysis of Socotra sample (DB635) Li/Ca ratio versus annual SST (HadiSST1) for 1972-2009. Bandwidth = 0.06, number of lags = 24. See Figure 3.6C for legend.

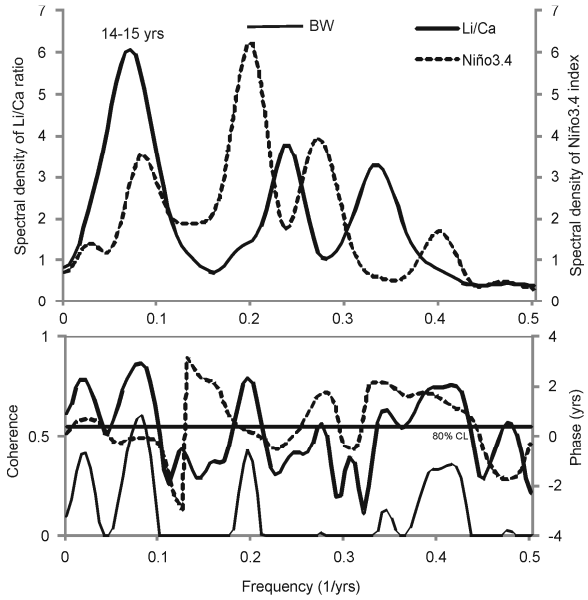

Fig. 6.38 Cross-spectral analysis of Socotra sample (DB635) Li/Ca ratio versus Niño 3.4 index (from HadiSST1) for 1972-2009. Note that it reveals coherence for period centered at ~14.5 yrs. Bandwidth = 0.06, number of lags = 24. See Figure 3.6C for legend.

6.4.2.3. Li/Ca ratio *vs*. Asian monsoon system

The Li/Ca record on *Lithophyllum* sp. thallus from Socotra did not record variation of monsoon intensity neither by hydraulic energy variability, nor by SIR (not shown), despite annual Li/Ca ratio showed positive significant correlation with SIR ($r = 0.49$, p-value = 0.002). However the positive Li/Ca-SIR relationship is in agreement with correlation found between annual Mg/Ca ratio and SIR for *Lithophyllum* sp. from Socotra.

6.4.2.4. Red Sea teleconnections

Socotra is bathed by a variety of different water masses, including those originating to the north-west by the Red Sea. The Red Sea water is one of the most saline water masses in the world

oceans. Passing through the Gulf of Aden, the water outflows from the Red Sea becomes a part of the intermediate circulation in the Indian Ocean, which has been observed as a mid-depth salinity maximum in the Arabian Sea and even in the southern hemisphere (Mecking and Warner 1999). Therefore, changes in the local SSS and connections with the southern Red Sea SSS were investigated in the Li/Ca record of *Lithophyllum* sp. of Socotra. Although Mg/Ca ratio recorded signal of local SSS variability, cross-spectral analysis between Li/Ca record and gridded SSS did not show relationship between both time series (not shown). Therefore, cross-spectral analysis between Li/Ca record and South Red Sea SSS revealed strong coherence in the period of 14-15 yrs (Fig. 6.39A). Almost 90% of Li/Ca variance is explain in this period. Cross-phase analysis showed that Li/Ca lags South Red Sea SSS by 1.3 yrs (Fig. 6.39A). Coherence for the same period was observed in cross-spectral analysis between the record and winter and summer South Red Sea SSS , and cross-phase analysis revealed a similar lag of Li/Ca record on the south Red Sea SSS in this period (Fig. 6.39B and C).

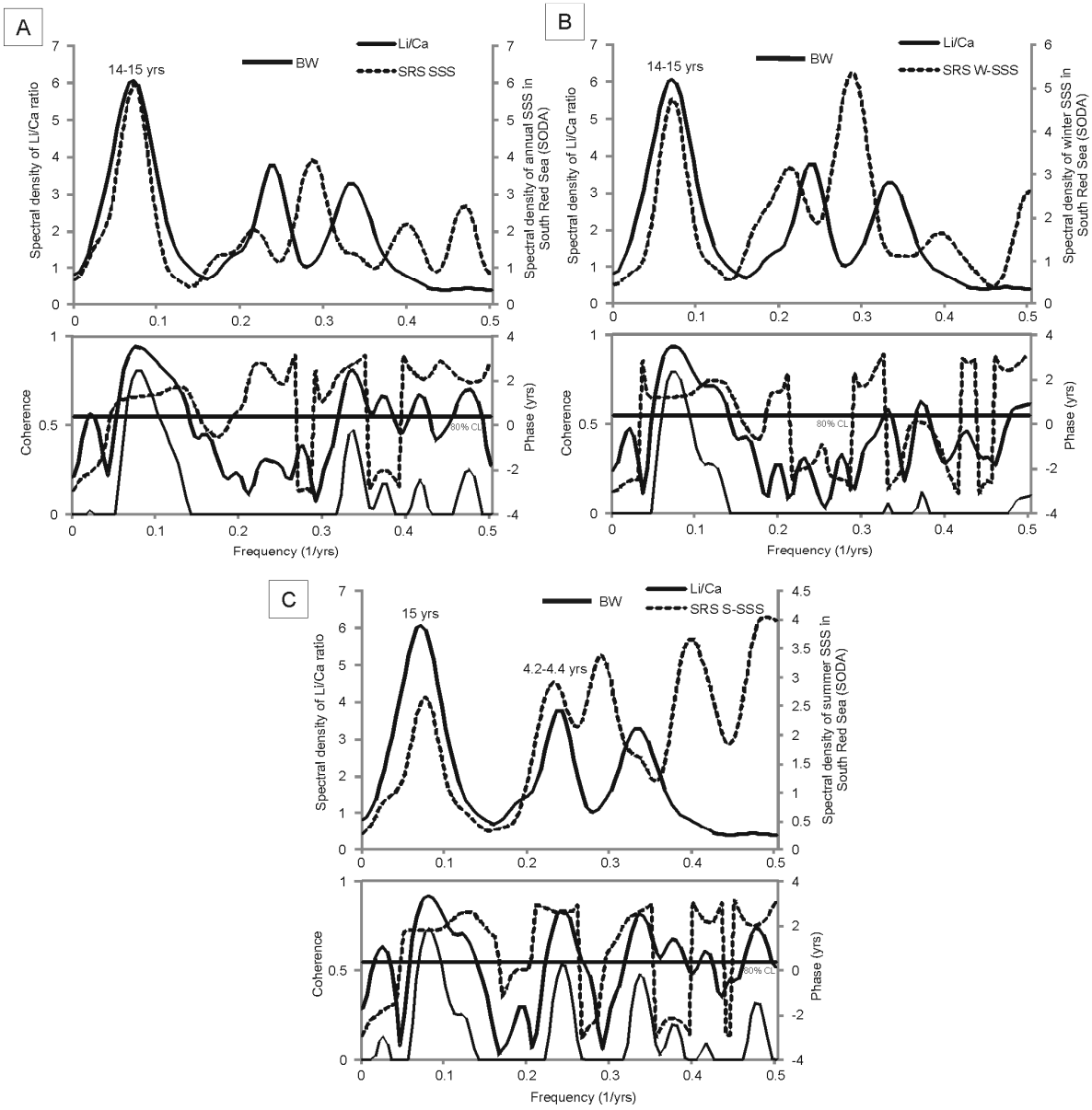

Fig. 6.39 A) cross-spectral analysis of Socotra sample (DB635) Li/Ca record versus SSS (SODA) in South Red Sea (SRS SSS) for 1972-2009; B) corresponding analysis for Li/Ca record versus mean winter SSS (SRS WSSS; extracted from SODA); C) corresponding analysis for Li/Ca record versus mean summer monsoon SSS (SRS SSSS; extracted from SODA). Bandwidth = 0.06, number of lags = 24. See Figure 3.6C for legend.

Moreover, cross-spectral analysis between Li/Ca record and South Red Sea current revealed coherence for the same period (14-15 yrs), and cross-phase analysis showed that Li/Ca record lags South Red Sea current by 2 yrs (Fig. 6.40A). Stronger coherence was observed in

cross-spectral analysis between the record and summer South Red Sea current for the period of 14-15 yrs (Fig. 6.40C), while no coherence was found in cross-spectral density with winter South Red Sea current (Fig. 6.40B). Indeed, passing through the Gulf of Aden, the water outflows from the Red Sea during summer, becomes a part of the intermediate circulation in the Indian Ocean, which has been observed as a mid-depth salinity maximum in the Arabian Sea and even in the southern hemisphere (Mecking and Warner 1999). Hence, the Li/Ca ratio in the *Lithophyllum* sp. of Socotra recorded signal of the Red Sea environmental variability by South Red Sea hydrographic energy and South Red Sea SSS variability.

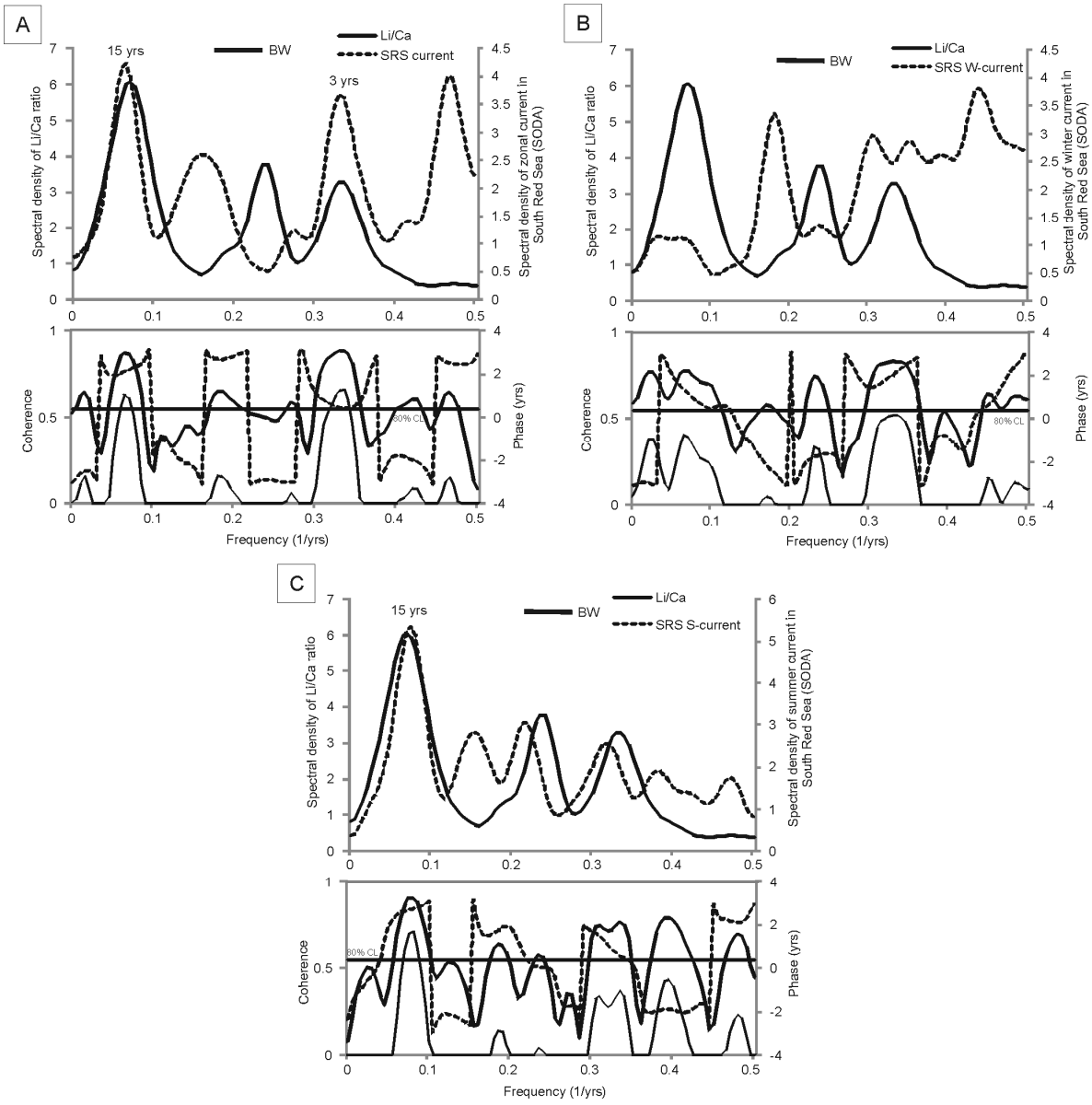

Fig. 6.40 A) cross-spectral analysis of Socotra sample (DB635) Li/Ca record versus zonal current (SODA) in South Red Sea (SRS) for 1972-2009; B) corresponding analysis for Li/Ca record versus mean winter monsoon current (SRS W-current; extracted from SODA); C) corresponding analysis for Li/Ca record versus mean summer monsoon current (SRS S-current; extracted from SODA). Bandwidth = 0.06, number of lags = 24. See Figure 3.6C for legend.

6.4.3. Kamaran

6.4.3.1 Li/Ca ratio *vs*. SST

Li/Ca in *L. kotschyanum* f. *affine* thallus of Kamaran showed the lowest correlation coefficient (r) with Mg/Ca ratio, compared to the other samples analyzed in this study, but it was still positive and significant. The mean Li content in the rhodolith from Kamaran was found to be the lowest compered to *L. kotschyanum* f. *affine* of Balhaf and *Lithophyllum* sp. of Socotra. It was of about 30% less than that measured in *L. kotschyanum* f. *affine* of Balhaf. This difference might be due to different environmental conditions, and even to different coralline form (attached coralline *vs*. rhodolith). Indeed temporal cessation of rhodolith growth due to temporary burial lead to an interrupted environmental record (Cabioch 1966 and Halfar et al. 2011).

Li-SST relationship in *L. kotschyanum* f. *affine* of Kamaran was 0.57 µmol % of LiCO3 $°C^{-1}$, that resulted steady respect the relationship observed in *L. kotschyanum* f. *affine* of Balhaf, and in *Lithophyllum* sp. of Socotra, but higher than in DB659bis (*L. kotschyanum* f. *affine* of Balhaf). This difference with sample from Balhaf might be due to in DB659bis specimen the transect of analysis was divided in four transects to follow the main axis of growth, while in sample from Kamaran the analysis was done along a single transect, and that might has reduced the accuracy of the Li measurement in DB659bis. Since SST was considered the main factor controlling the incorporation of Mg in coralline algal thallus, a significant correlation was found between monthly average Li/Ca and SST, it is speculated that SST is also the dominant factor controlling Li-carbonate chemistry in *L. kotschyanum* f. *affine* of Kamaran, as it has been assumed for *L. kotschyanum* f. *affine* of Balhaf, and for *Lithophyllum* sp. of Socotra.

6.4.3.2. Interannual and decadal climate variability

A cross-spectral analysis revealed two peaks in the interannual range, centered at ~9 yrs and ~2.5 yrs in the spectral of Li/Ca ratio (Fig. 6.41).

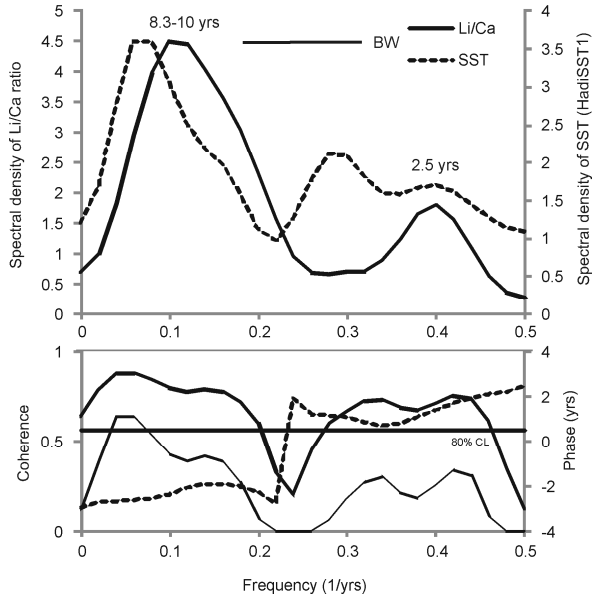

Fig. 6.41 Cross-spectral analysis of Kamaran sample (DB576) Li/Ca ratio versus gridded SST (HadiSST1) for 1994-2008. Bandwidth = 0.14, number of lags = 11. See Figure 3.6C for legend.

The period of ~2.3 yrs in the Blackman Tukey spectrum is the typical mode of the Quasi-biennial oscillation (QBO), a phenomenon that was originally observed between westerly and easterly equatorial stratospheric winds (Baldwin et al. 2001). The QBO significantly influences the Indo-Pacific realm and is found in a variety of meterological records of precipitation, wind-speed and SST (Conversi and Hammed 1998). Tawari and Rao (2004) found the QBO of 2.3 yrs in the coral extension rate from the northern Arabian Sea. The QBO of ~2.5 yrs was observed in coral $\delta^{18}O$ in the South Red Sea by Klein et al. (1997). Although the ENSO-SST relationship for this period was found in the Kamaran area (Fig. 3.20), the cross-spectral density

between algal Li/Ca record and SST did not revealed coherence for this period (Fig. 6.41), as well as between the record and Niño3.4 index (not shown). However, cross-spectral density between Li/Ca record and zonal current revealed coherence for the period of 2.5 yrs (Fig. 6.42). Albeit less than 40% of Li/Ca variance is explained in this period, it is suggested that the QBO-style is recorded in the *L. kotschyanum* f. *affine* of Kamaran Li/Ca record by current variability. Nevertheless, although the limitation of gridded datasets used in this study, it is suggested further coralline analysis on longer time term.

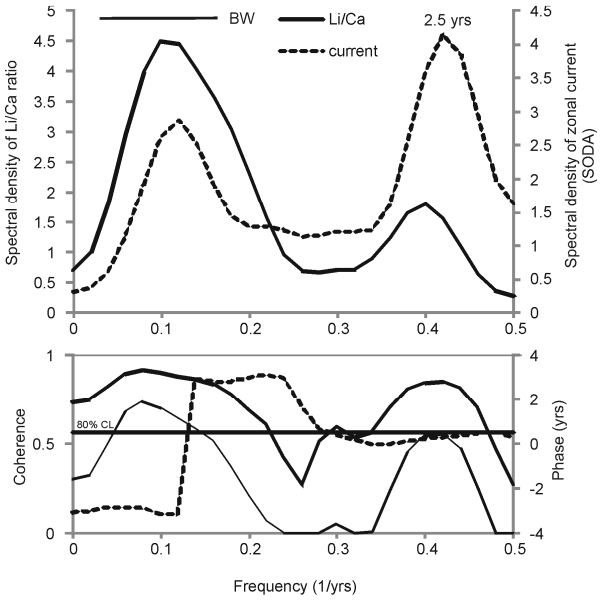

Fig. 6.42 Cross-spectral analysis of Kamaran sample (DB576) Li/Ca ratio versus zonal current (SODA) for 1994-2008. Note that it reveals weak coherence for period centered at ~2.5 yrs. Bandwidth = 0.14, number of lags = 11. See Figure 3.6C for legend.

Felis et al. (2000) found in the coral skeleton of the North Red Sea in the interannual range, link with Alexandria precipitation as signal of influence of the Mediterranean climate on the northern Red Sea. Cross-spectral density between Li/Ca record and Alexandria rainfall showed coherence for period 8.3-10 yr, and cross-phase analysis revealed that the record lags the

Alexandria precipitation by ~2 yrs (Fig. 6.43). Almost 90% of the Li/Ca variance is explained in this period, but only 30% of the Alexandria precipitation variance is expressed in this period. The northern part of the Red Sea is subject to great variability of weather, particularly in winter the weather in the North Red Sea is influenced by disturbances in the Mediterranean, which leads typical winter rains (Edwards 1987). This occur in association with troughs of low pressure which move into the Red Sea from the north and are often accompanied by changes in wind, temperature and humidity and by increased cloud. These fronts may penetrate quite far south.

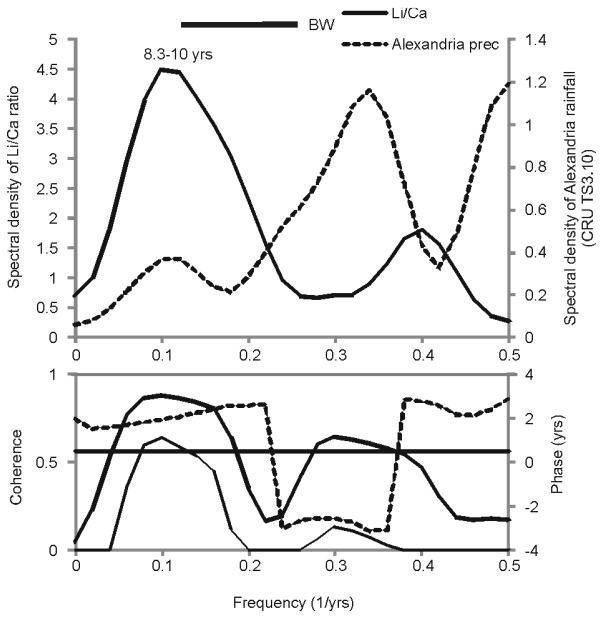

Fig. 6.43 Cross-spectral analysis of Kamaran sample (DB576) Li/Ca ratio versus Alexandria rainfall (CRU TS3.10) for 1994-2008. Note that it reveals coherence for period 8.3-10 yrs. Bandwidth = 0.14, number of lags = 11. See Figure 3.6C for legend.

Cross-spectral density between Li/Ca record and Kamaran precipitation revealed strong coherence for period 8.3-10 yrs and weaker coherence for period 2.5 yrs (Fig. 6.44). Cross-phase analysis showed that Li/Ca ratio lags the Kamaran precipitation by 2.7 yrs for period of 8.3-10 yrs and by 1.4 yrs for period of 2.5 yrs (Fig. 6.44). Klein et al. (1997) suggested that, on a decadal

time-scale, there are simultaneous changes in the phase of the Southern Oscillation, the south Asian monsoon and the Indian Ocean SST, which are recorded in the stable isotope composition of the southern Red Sea corals. Thus, it is suggested here, that *L. kotschyanum* f. *affine* of Kamaran recorded in the Li/Ca ratio the influence of the northern Red Sea to the southern Red Sea climate by precipitation variability, which are likely influenced by ENSO on the decadal range. While it recorded the typical ENSO-style frequency influence to the southern Red Sea climate on the interannual range by hydrographic energy and local precipitation variability.

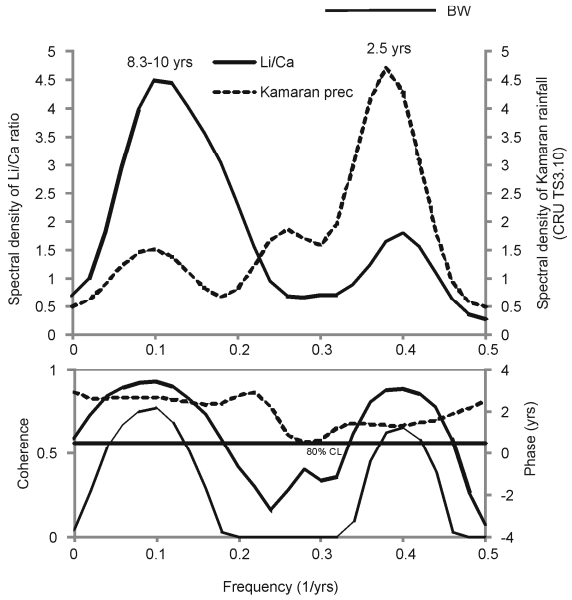

Fig. 6.44 Cross-spectral analysis of Kamaran sample (DB576) Li/Ca ratio versus Kamaran rainfall (CRU TS3.10) for 1994-2008. Note that it reveals strong coherence for periods centered at ~9 and 2.5 yrs.

Bandwidth = 0.14, number of lags = 11. See Figure 3.6C for legend.

6.4.3.3. Asian monsoon system teleconnections

The Li/Ca ratio of *L. kotschyanum* f. *affine* of Kamaran did not recorded signal of the influence of the Asian monsoon system to the Red Sea climate.

6.5. Ba/Ca ratio

6.5.1. Balhaf

6.5.1.1. Ba/Ca ratio *vs.* SST

In Scleractinian corals and planktic foraminifera, Ba/Ca ratios was successfully used as nutrient proxy (Lea and Boyle 1989; Lea et al. 1989). Lea et al. (1989) found that coral Ba/Ca tracks historical SST, because a decrease in SST accompanies the upwelling of cold, nutrient-rich waters to the surface. In coralline algae (*Clathromorphum* spp.) Hetzinger et al (2010) found a low and negative correlations between Ba/Ca and Mg/Ca, and weakly negative or no significant relationship between Ba/Ca and gridded SST. Conversely in L. *kotschyanum* f. *affine* relationship between Ba/Ca and SST, when found, was always positive. The weak or no significant relationship between monthly Ba/Ca and gridded SST suggested that SST plays only a minor role in the incorporation of Ba into algal high-Mg calcite lattice, this is in agreement with the study on the subarctic *Clathromorphum* spp. by Hetzinger et al. (2010). Since values of Ba/Ca ratio increase in spring-summer monsoon (May to September) it is likely that the seasonality of Ba/Ca is linked to the monsoon-induced nutrient introduction of deep water into the shallow water environment. In contrast to the observation by Lea et al. (1989) at the Galapagos Islands, in this case the SST did not work as monsoon intensity index because at the sampling site monthly SST does not vary significantly during the summer monsoon. Additionally as for other elements-SST relationship, it is important to consider the limitation of gridded record comparing to climate *in situ* records. Elementary Ba incorporated in coral skeletons has also been used as tracer for coastal riverine inputs and to monitor long-term increases in sediment from rivers (Alibert et al. 2003; McCulloch et al. 2003). Monthly algal Ba/Ca ratios did not show a relationship with Yemeni precipitation, but

in the year 2007 the highest peak of Ba/Ca ratio was found in two protuberances of DB659 sample (DB659a and DB659b), but not in DB659bis, and DB657. Samples were collected along a small peninsula of the coast (Fig. 6.45) in an area affected by intense building activities. They were sampled in different parts of this peninsula, respectively on the base of it and on the opposite side to the main area of the building work (site B) and along the tip of the peninsula (site C; Fig. 6.45). During this year, dredging and building work took place. The dredging has produced a plume of sediment southeastward (Fig. 6.45), and a sedimentation study done in the 2007, showed higher terrestrial sediment input at location B than in C (unpublished record CREOCEAN). The sediment released by the building activity has been transported in part into Site B by wind, while site C was apparently unaffected.

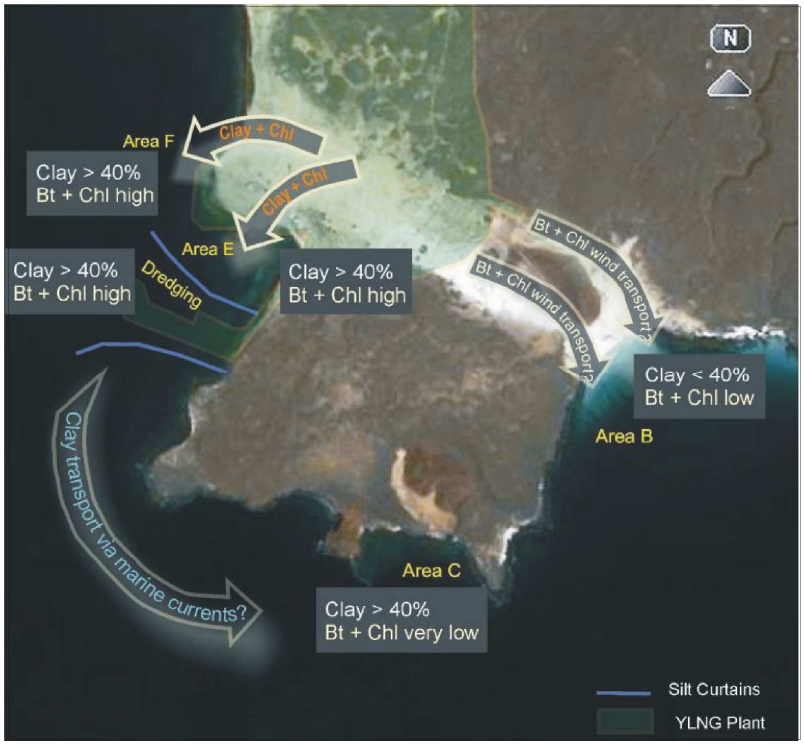

Fig. 6.45 Satellite image of building work area in Balhaf. Schematic representation of clay percentages and Bt + Chl (mica and chlorite) content in the examined samples. The main clay and Bt + Chl sources are represented. (from unpublished CREOCEAN's 2006-2007 report).

In the other protuberance analyzed of the DB659 sample (DB659bis) was not observed the Ba/Ca peak in the year 2007. As for Mg/Ca and Li/Ca ratio, this might be due to the lowest extension rates of this protuberance, which resulted in a poorer resolution sampling per year.

Since the samples of DB657 and DB659a-b resulted unsuitable for paleoclimate reconstruction because their short life span and thus their too much limited temporal resolution, the DB659bis specimen, with its age model of 33 years, was the only specimen used in this study to investigate the suitability of *L. kotschyanum* f. *affine* in the reconstruction of climate variability in the Gulf of Aden. Hence, the following discussion regarding to the use of *L. kotschyanum* f. *affine* extension rate as proxy of the climate variability along the Yemen coast, it is only referred to the DB659bis specimen.

6.5.1.2. Interannual and decadal climate variability

Due to weakly or no significant relationship between monthly Ba/Ca and SST suggested the missed of the Ba/Ca time series in reconstructing SST interannual and decadal variations. A cross-spectral analysis revealed a spectral peak for period 9-13 yrs (Fig. 6.46). Although, cross spectral analysis between Ba/Ca record and SST did not show coherence for this period, cross spectral analysis between the record and Niño 3.4 index revealed coherence for this period (Fig. 6.47). Cross-phase analysis showed that Ba/Ca record lags Niño 3.4 record by 2 yrs (Fig. 6.47). Cole et al. (2000) in their study on coral from Kenya, suggested that decadal variability in the coral records is primarily a response to Pacific influences. Therefore, Ba/Ca variability in the *L. kotschyanum* f. *affine* thallus result apparently a signal of ENSO-force in the Indian Ocean for period 9-13 yrs.

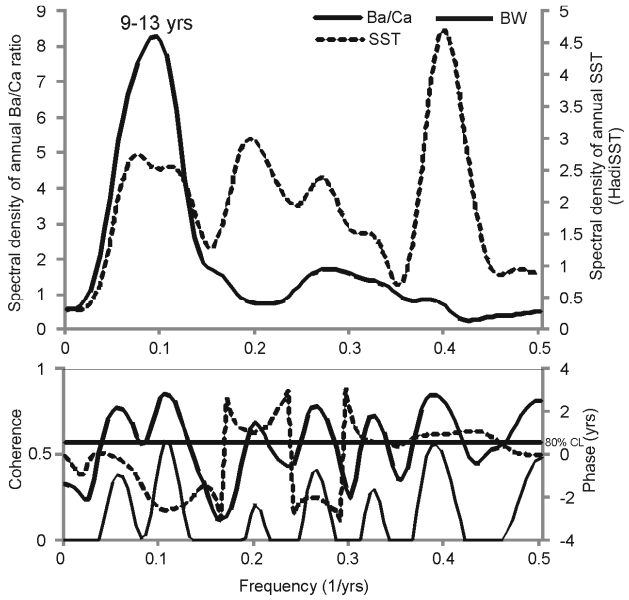

Fig. 6.46 Cross-spectral analysis of DB659bis Ba/Ca record versus SST (HadiSST1) for 1974-2008. Bandwidth = 0.06, number of lags = 24. See Figure 3.6C for legend.

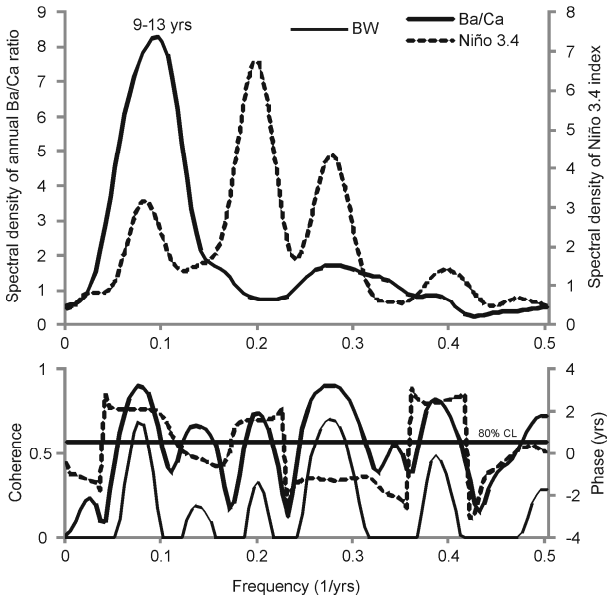

Fig. 6.47 Cross-spectral analysis of DB659bis Ba/Ca record versus Niño 3.4 index (from HadiSST1) for 1974-2008. Note that it reveals coherence for period centered at ~11 yrs. Bandwidth = 0.06, number of lags = 24. See Figure 3.6C for legend.

6.5.1.3. Ba/Ca ratio *vs*. Asian monsoon system

Tudhope et al. (1996) in coral from the close Arabian Sea (Oman coast) found that coral did not show a simple response to the strength of SW monsoon upwelling. They suggested that Ba maxima may not only be a direct response to increased surface water Ba but might also reflect site-specific factors in organism-Ba incorporation such as inclusion of organically bound particulate Ba. Moreover, another important issue pointed out by authors was the incomplete understanding of the processes of barium incorporation, which hinders the use of the coral-Ba-results in reconstructing interannual variations in upwelling intensity in this particular settings. Cross-spectral analysis between Ba/Ca record and annual current revealed a strong coherence for period 9-13 yrs, but cross-phase analysis showed that current lags Ba/Ca record, which disprove causality (Fig. 6.48).

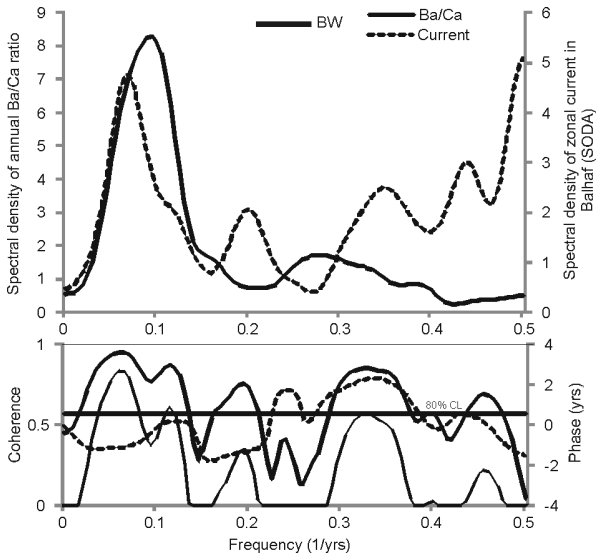

Fig. 6.48 Cross-spectral analysis of DB659bis Ba/Ca record versus zonal current (SODA) in Balhaf for 1974-2008. Bandwidth = 0.06, number of lags = 24. See Figure 3.6C for legend.

Annual Ba/Ca ratio on L. kotschyanum f. affine from Balhaf showed a strong negative

correlation with SIR (r = -0.54, p-value<0.0001). Cross-spectral analysis between Ba/Ca and SIR revealed coherence for period 9-11 yrs, and cross-phase analysis showed that Ba/Ca record lags SIR by ~3 yrs (Fig. 6.49). Since a correlation was found between Ba/Ca and Niño3.4 index for the same period, it is speculated that strength monsoon variability for this period, is likely influence by ENSO. Moreover, in agreement with Tudhope et al. (1996), Ba maxima may not only be a direct response to increased surface water Ba but might also reflect site-specific factors, as observed in the year 2007 on the two protuberances analyzed of DB659 sample (DB659a and DB659b). However, the negative and significant relationship found between Ba/Ca record and SIR is in agreement with the Li/Ca-SIR relationship found here for the same sample. As explicate in chapter 6.4.1.3. this negative correlation might be explain with a decrease of the coralline extension rate during stronger monsoon, that lead to a reduction of Ba variability detection. The decrease on coralline growth is probably due in Balhaf to decrease of water transparency and light supply for increase of suspension for upwelling.

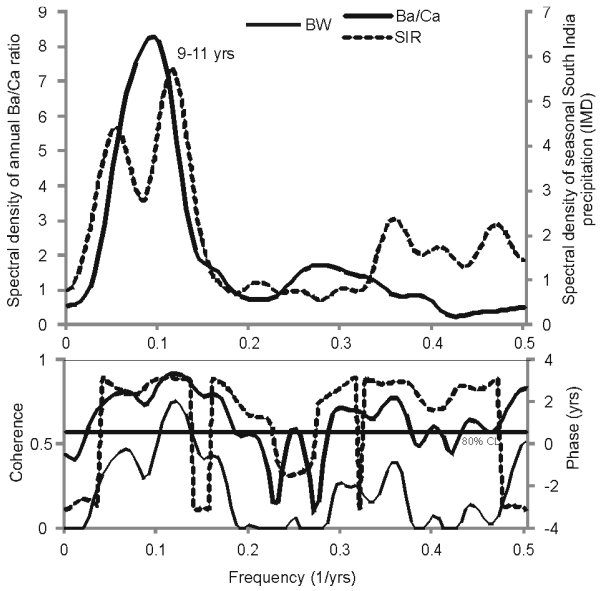

Fig. 6.49 Cross-spectral analysis of DB659bis Ba/Ca record versus seasonal South India rainfall (IMD) for 1974-2008. Bandwidth = 0.06, number of lags = 24. See Figure 3.6C for legend.

6.5.1.4. Red Sea teleconnections

As for Mg/Ca and Li/Ca records no teleconnection with the Red Sea climate was found for Ba/Ca record (not shown).

6.5.2. Socotra

6.5.2.1. Ba/Ca ratio *vs*. SST

The Ba content in *Lithophyllum* sp. of Socotra resulted lower than in *L. kotschyanum* f. *affine* of Balhaf, likely due to different species considered. Although Lea et al. (1989) found in scleractinian corals that Ba/Ca tracks historical SST, and Hetzinger et al. (2010) observed a low, negative but significant correlation between *Clathromorphum* spp. Ba/Ca and gridded SST, as observed in *L. kotschyanum* f. *affine* of Balhaf, as well as Ba/Ca record in *Lithophyllum* sp. of Socotra showed a seasonality, but significant relationship was found neither between monthly Ba/Ca and Mg/Ca, nor between monthly Ba/Ca and gridded SST. In contrast to the observations by Lea et al. (1989) at the Galapagos Islands, in this study the SST did not work as monsoon intensity index, although in Socotra during the summer monsoon is recorded the lowest SST of the year (Fig. 3.11C). In scleractinian corals and planktic foraminifera, Ba/Ca ratios was successfully used as nutrient proxy (Lea and Boyle 1989; Lea et al. 1989). Additionally, elementary Ba incorporated in coral skeletons has also been used as tracer for coastal riverine inputs and to monitor long-term increases in sediment from rivers (Alibert et al. 2003; McCulloch et al. 2003). The lack of relationship between Ba/Ca record and SST in *Lithophyllum* sp. of Socotra as well as *L. kotschyanum* f. *affine* of Balhaf, might be due either to the limitation of gridded dataset used and to the low growth rates, which result in the decrease ability to detect Ba variability and to an

interrupted environmental record (Cabioch 1966, Halfar et al. 2011).

6.5.2.2. Interannual and decadal climate variability

Tudhope et al. (1996) observed that in coral skeleton from Arabian Sea, although annual Ba/Ca ratio displayed strong annual cycles, the record did not appear to directly record interannual climatic/oceanographic variability. They observed in the outer few millimeters of the coral skeleton (i.e. tissue not completely removed by the initial field treatment with bleach) small barite crystal, that confirmed elevated Ba content. They found , that the barium was concentrated in pores between coral trabeculae and between individual aragonite fibres. In the end the authors suggested of release through time of barium incorporated into the skeleton, in a phase distinct from aragonite (i.e. a refractory, slowly decomposing organic compound and/or barite), at the time of growth. These have been observed in elevated barium levels in coral skeleton. However in *Lithophyllum* sp. of Socotra elevated annual Ba levels were only found since 1988 to 1996, but this time range also showed an higher annual Mg and Li content. Hence, this suggested that the Ba content measured in *Lithophyllum* sp. was not affected by factors mentioned by Tudhope et al. (1996).

Nevertheless, cross-spectral analysis between Ba/Ca record and SST showed an interannual peak for the period centered at 6.4 yrs, but any aligned peak in the spectral density of gridded SST (Fig. 6.50). Expectedly, cross-spectral analysis between Ba/Ca record and Niño3.4 index did not reveal coherence. Hence, in coralline thallus, the record appeared to neither directly record interannual SST variability, nor ENSO-force.

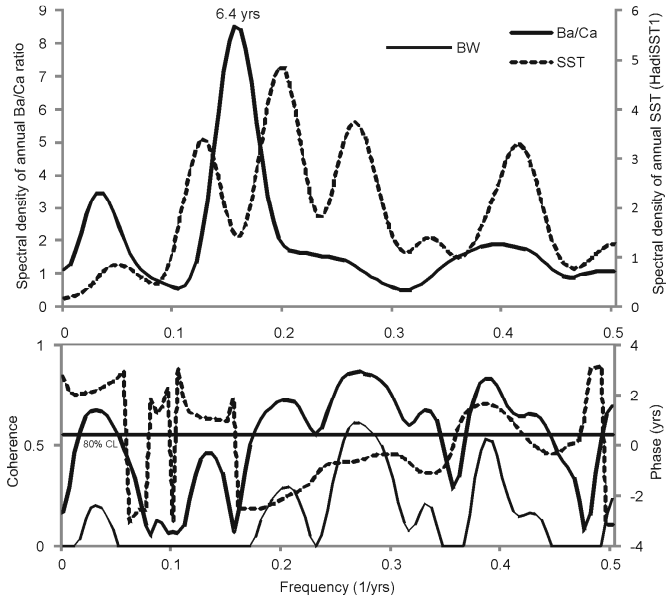

Fig. 6.50 Cross-spectral analysis of Socotra sample (DB635) Ba/Ca ratio versus annual SST (HadiSST1) for 1972-2009. Bandwidth = 0.06, number of lags = 24. See Figure 3.6C for legend.

6.5.2.3. Ba/Ca ratio *vs*. Asian monsoon system

Although annual Ba/Ca ratio revealed positive and significant correlation with SIR (r = 0.49, p-value = 0.002), cross-spectral analysis between the two records did not show coherent peaks (not shown). However, cross-spectral analysis between Ba/Ca record and zonal current showed weak, but significant coherence for period of 6.4 yrs (Fig. 6.51). This is the typical mode of Asian monsoon system in agreement with Storz and Gischler (2011b). The 94% of the Ba/Ca variance is explain in this period, and cross-phase analysis showed that Ba/Ca lags current by 1.9 yrs (Fig.6.51). The positive correlation found between the annual Ba/Ca ratio and SIR is in agreement with its feature to track variation on nutrient content in water by upwelling of deep, nutrient-rich waters to the surface during the summer monsoon.

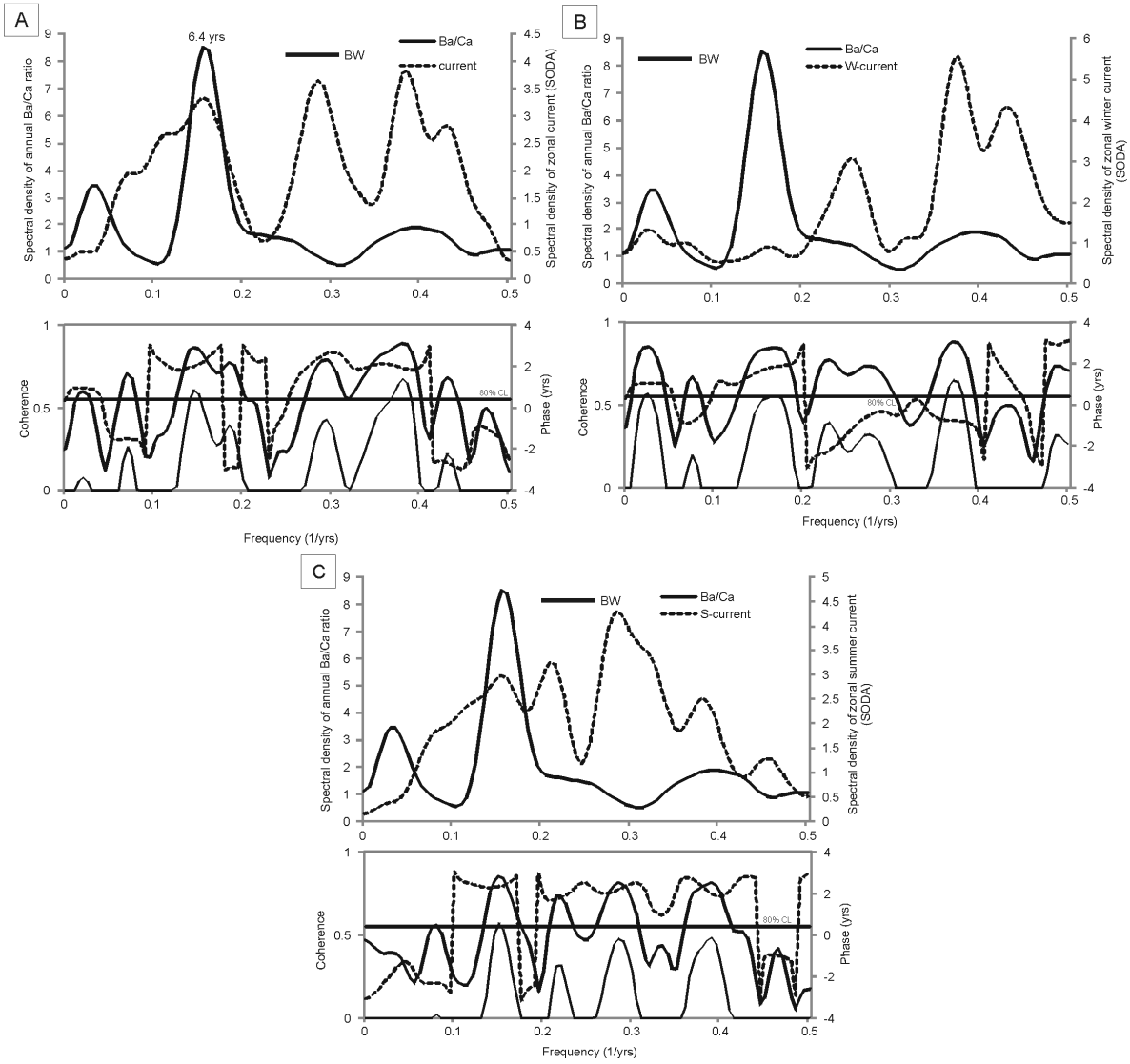

Fig. 6.51 A) cross-spectral analysis of Socotra sample (DB635) Ba/Ca ratio versus zonal current (SODA) for 1972-2009; B) corresponding analysis for Ba/Ca ratio versus mean winter monsoon current (extracted from SODA); C) corresponding analysis for Ba/Ca ratio versus mean summer monsoon current (extracted from SODA). Bandwidth = 0.06, number of lags = 24. See Figure 3.6C for legend.

During the SW monsoon occur the upwelling of deeper colder and rich in nutrient water. This bottom water is also rich in organic matter that may therefore contain high levels of barite crystals which come from tissues of decomposed organisms. Thus, in this case the SSS variability can be an index of the monsoon strength. Cross-spectral analysis between Ba/Ca record and local

SSS revealed weak coherence for the period of 6.4 yrs (Fig. 6.52A). In order to demonstrate that coralline Ba/Ca recorded the Asian monsoon system by SSS variability, correlations were applied for the annual record with 1) the mean winter (November-February) SSS (WSSS) of Socotra, 2) the mean summer (May-September) SSS (SSSS) of Socotra, 3) the difference between winter and summer SSS (ASSSG) of Socotra, as inter-annual gradient. This analysis led to:

1) *No link between Winter SSS of Socotra and Ba/Ca ratio.* Expectedly, the spectrum between the time series of winter SSS and Ba/Ca record did not reveal coherence for the period of 6.4 yrs (Fig. 6.52B).

2) and 3) *Link between SW monsoon and Ba/Ca record.* Cross-spectral analysis between Ba/Ca record and summer SSS of Socotra revealed coherence for period 6.4 yrs (Fig. 6.52C). Cross-phase analysis did not show lags between the two time series for the same period (Fig. 6.52C). Stronger coherence was observed for the same period in cross-spectral analysis between Ba/Ca record and ASSG for the period 6.4 yrs (Fig. 6.52D).

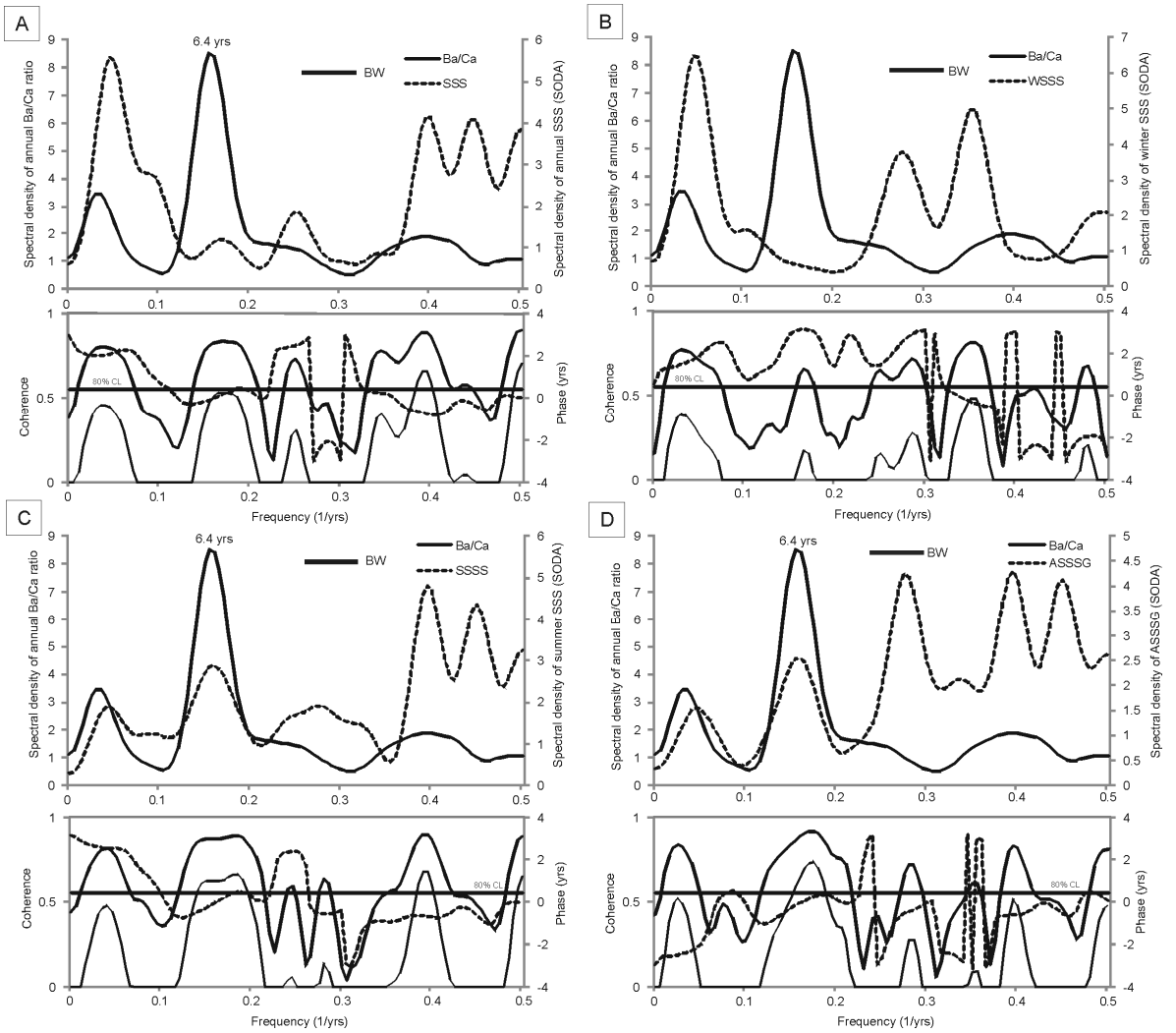

Fig. 6.52 A) cross-spectral analysis of Socotra sample (DB635) Ba/Ca ratio versus local SSS (SODA) for 1972-2009; B) corresponding analysis for Ba/Ca ratio versus mean winter monsoon SSS (extracted from SODA); C) corresponding analysis for Ba/Ca ratio versus mean summer monsoon SSS (extracted from SODA); D) Cross-spectral analysis of annual Ba/Ca ratio versus annual SSS gradient record (ASSSG, difference between mean summer and winter monsoon SSS, extracted from SODA) for 1972-2009. Bandwidth = 0.06, number of lags = 24. See Figure 3.6C for legend.

6.5.2.4. Red Sea teleconnections

During summer water mass outflow from the Red Sea into the Gulf of Aden, and in the Indian Ocean. Although, cross-spectral analysis between Ba/Ca record and South Red Sea SSS did not show aligned peaks (not shown), and cross-spectral analysis between Ba/Ca record and South Red Sea current did not reveal coherence (Fig. 6.53A), coherence between the record and summer South Red Sea current was observed in cross-spectral analysis for period of 6.4 yrs (Fig. 6.53B). Cross-phase analysis showed that Ba/Ca record lags the summer South Red Sea current by 2.4 yrs (Fig. 6.53B). Hence, Ba/Ca ratio in *Lithophyllum* sp. of Socotra recorded signal of the Red Sea influence by South Red Sea hydrographic variability.

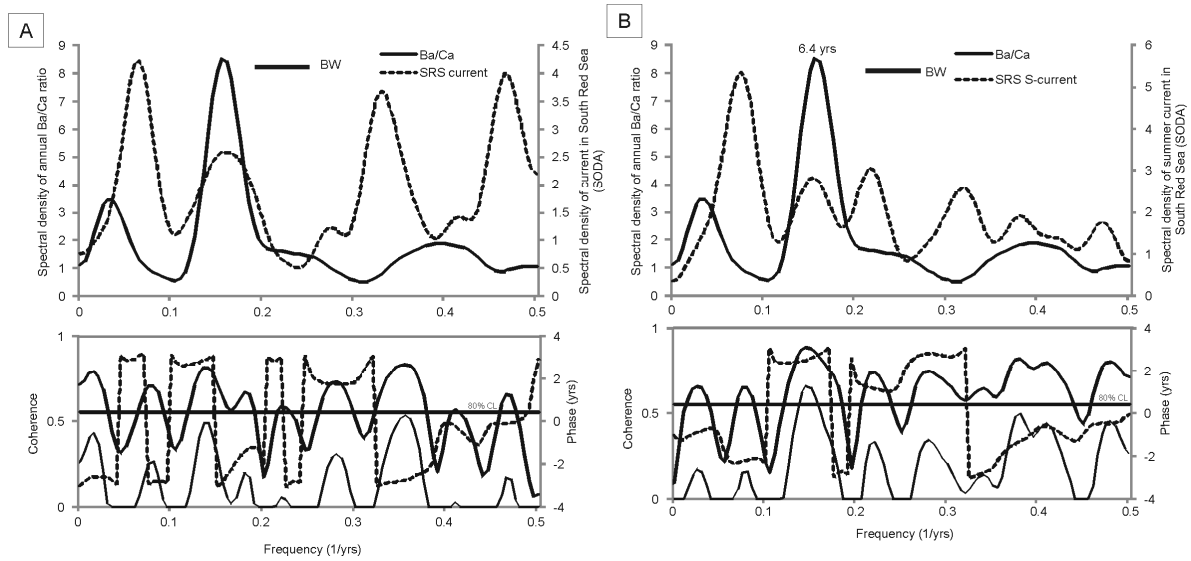

Fig. 6.53 A) cross-spectral analysis of Socotra sample (DB635) Ba/Ca ratio versus zonal current (SODA) in South Red Sea for 1972-2009; B) corresponding analysis for Ba/Ca ratio versus mean summer monsoon current (extracted from SODA). Bandwidth = 0.06, number of lags = 24. See Figure 3.6C for legend.

6.5.3. Kamaran

6.5.3.1. Ba/Ca ratio *vs*. SST

The Ba content in *L. kotschyanum* f. *affine* of Kamaran was found lower than the other samples of the same species from Balhaf, but similar to the Ba content in *Lithophyllum* sp. of Socotra. Lea et al. (1989) found in scleractinian corals that Ba/Ca tracks historical SST, and Hetzinger et al. (2010) observed a low, negative but significant correlation between *Clathromorphum* spp. Ba/Ca and gridded SST. Indeed although the Ba/Ca ratio in *L. kotschyanum* f. *affine* of Kamaran showed a seasonality, a significant relationship was found neither between monthly Ba/Ca and Mg/Ca, nor between monthly Ba/Ca and gridded SST as well as observed in *L. kotschyanum* f. *affine* of Balhaf, and in *Lithophyllum* sp. of Socotra.

In scleractinian corals and planktic foraminifera, Ba/Ca ratios was successfully used as nutrient proxy (Lea and Boyle 1989; Lea et al. 1989). Additionally, elementary Ba incorporated in coral skeletons has also been used as tracer for coastal riverine inputs and to monitor long-term increases in sediment from rivers (Alibert et al. 2003; McCulloch et al. 2003). The lack of relationship between Ba/Ca record and SST in *L. kotschyanum* f. *affine* of Kamaran as well as in the other samples analyzed in this study, might be due either to the limitation of gridded dataset used and to the low growth rates, which result in the decrease ability to detect Ba variability and to an interrupted environmental record (Cabioch 1966, Halfar et al. 2011).

6.5.3.2. Interannual and decadal climate variability

A cross-spectral analysis revealed peaks from decadal to interannula range, centered at ~8.5 yrs and 2.9 yrs (Fig. 6.54).

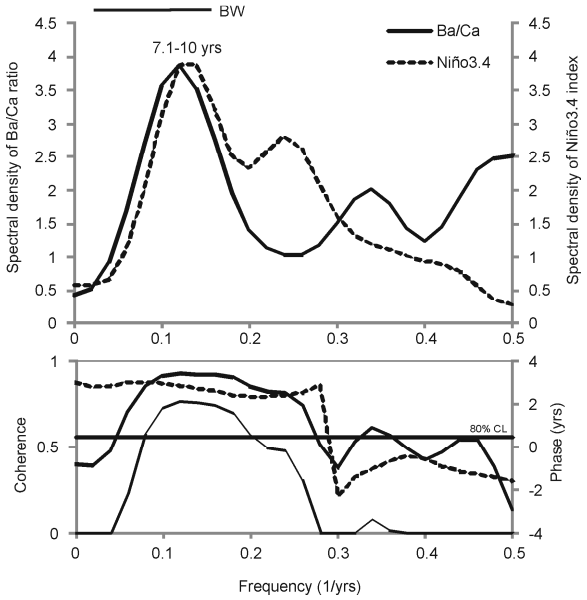

Fig. 6.54 Cross-spectral analysis of Kamaran sample (DB576) Ba/Ca ratio versus Niño 3.4 index (from HadiSST1) for 1994-2008. Note that it shows strong coherence for period centered at ~8.5 yrs.

Bandwidth = 0.14, number of lags = 11. See Figure 3.6C for legend.

Expectedly, no link was found between Ba/Ca record and gridded SST (not show). Since the period of 2.9 yrs is the typical ENSO-style frequencies, one might expect coherence between Ba/Ca record and the Niño3.4 index for this period. Instead, cross-spectral density between both the two time series did not showed aligned peaks for this period, but a strong coherence for the period 7.1-10 yrs (Fig. 6.54). Almost 90% of the Ba/Ca variance in the *L. kotschyanum* f. *affine* of Kamaran is explained in this period, and cross-phase analysis revealed that Ba/Ca record lags the Niño3.4 index by 2.7 yrs (Fig. 6.54). Hence *L. kotschyanum* f. *affine* of Kamaran recorded in the Ba/Ca composition the ENSO on a decadal time-scale in agreement with what observed by Klein et al. (1997) in the stable isotope composition of the southern Red Sea coral.

The *L. kotschyanum* f. *affine* of Kamaran did not record in the Ba/Ca composition the other climate and oceanography features of the study area used here.

6.5.3.3. Asian monsoon system teleconnections

Although the annual Ba/Ca revealed strong and significant correlation with SIR (r = 0.5, p-value = 0.04), cross-spectral analysis between Ba/Ca record of *L. kotschyanum* f. *affine* from Kamaran and SIR did not show coherent peaks.

7. Summary and conclusions

The results of this study provide the records of the elementary ratio of Mg/Ca, Li/Ca and Ba/Ca measured for the first time on coralline red algae thalli from the NW Indian Ocean (South Red Sea, Gulf of Aden, and South-west Arabian Sea). In particular, the elementary ratios were investigated for the first time in the Lithophylloideae thallus (*Lithophyllum kotschyanum* f. *affine* and *Lithophyllum* sp.). The seasonal fluctuations of Mg/Ca also provide information on thalli annual extension rates, on the $MgCO_3$ present in the carbonate lattice of coralline Mg-calcite thalli, and on algal biology, such as the season of reproduction.

Banding due to different growth rates of alternating thick-walled short cells *versus* thin-walled long cells has been revealed by longitudinal section of histological and calcite thallus of *L. kotschyanum* f. *affine* from Balhaf, Yemen. Banding in longitudinal sections of coralline red algae thalli has been well described in species from high and medium latitudes (Cabioch 1966; Adey and McKibbin 1970; Agegian 1981; Freiwald and Henrich 1994; Basso 1994; Basso et al. 1997; Halfar et al. 2000; Blake and Maggs 2003). To date, the reasons for different growth rates are poorly understood, and more samples of this species from a wider geographical range and a control of growth pattern over longer periods are needed to unravel the origin of banding in *L. kotschyanum* f. *affine*.

The LA-ICP-MS measured on *L. kotschyanum* f. *affine* from Balhaf of Mg/Ca cycles revealed that carposporangial conceptacles are produced in this alga in late winter shortly before the rise of SST in spring corresponding to those described for *Lithophyllum* from the British Isles (Irvine and Chamberlain 1994) and *Clathromorphum* spp. From the Gulf of Main (Adey 1965).

The annual extension rate resulted highly variable in all samples. In *L. kotschyanum* f. *affine* it ranges from a minimum of 185.46 µm y^{-1} to a maximum of 1700 µm y^{-1}, and in *Lithophyllum* sp. of Socotra it ranges from a minimum of 67.38 µm y^{-1} to a maximum of

410.43 µm y^{-1}. Although growth rate is generally affected by different environmental factors it is speculated that light mainly influences the growth rate of these coralline red algae. Moreover, all specimens were found to be affected by endobionts that in addition of dichotomization of branch in fruticose coralline algae (attached *L. kotschyanum* f. *affine* of Balhaf) has led to changes in the direction of the main axis of growth, thus to an irregular internal structure, that could explain the observed intra-specimen variability. Consequently, it is suggested that rhodoliths (*L. kotschyanum* f. *affine* of Kamaran and *Lithophyllum* sp. of Socotra) have been affected by temporal burials leading to growth cessation.

Expectedly for subtropical coralline algae, the mean Mg content measured in *L. kotschyanum* f. *affine* was compatible with the definition of high Mg-calcite, namely 20 mol % $MgCO_3$ (SE 0.7), and 20.1 mol % $MgCO_3$ (SD 4.9) in *Lithophyllum* sp. of Socotra.

Results showed a positive and strong relationship between monthly coralline Mg/Ca and gridded SST in *Lithophyllum* spp. with an higher annual extension rates, while it decreases and it was found weak but significant with decreasing annual extension rate. Instead, no correlation was found between annual Mg/Ca and gridded SST. The relationship between Mg and SST in *L. kotschyanum* f. *affine* ranges between 0.62 mol % $MgCO_3$ C^{-1} and 2.06 mol % $MgCO_3$ C^{-1}, and in *Lithophyllum* sp. of Socotra is 1.22 mol % $MgCO_3$ C^{-1}. Hence, it is suggested that despite the limitations of the gridded SST dataset used in this study, the SST is the dominant factor controlling Mg carbonate chemistry in these algae, and that the low growth rate or cessation of growth due to temporal rhodolith burial have likely resulted in interrupted environmental record. Moreover, since in attached *L. kotschyanum* f. *affine* with highest extension rates and, thus, more detailed record of the Mg-SST relationship, the variability still occurs (from 1.06 to 2.06 mol % $MgCO_3$ C^{-1}), it is assumed an algal physiological influence of unknown origin on thallus Mg incorporation.

The mean Li content in *L. kotschyanum* f. *affine* was 7.8 µmol % $LiCO_3$ (SE 1.2), and in *Lithophyllum* sp. of Socotra was 6.9 µmol % $LiCO_3$ (SD 2.5). A positive and strong

relationship was found between coralline Mg/Ca and Li/Ca. Since Mg/Ca ratios are temperature-controlled, and given the positive correlation between Li/Ca and SST, it is firstly suggested here that seawater temperature plays an important role in the incorporation of Li into coralline thallus. As for Mg-SST relationship, also the Li/Ca correlations with gridded SST was strong based on monthly means in algae with the highest annual extension rate, but it became weak with decreasing annual growth rate. No correlation was found between annual mean Li/Ca and SST. The Li-SST relationship in *L. kotschyanum* f. *affine* ranges between 0.46 to 0.57 µmol % $LiCO_3$ C^{-1}, and in *Lithophyllum* sp. of Socotra it was 0.53 µmol % $LiCO_3$ C^{-1}. It is assumed that this variability might be due to an algal physiological influence as mentioned above for the Mg-SST relationship.

The relationship between coralline Ba/Ca ratio and SST was not significant. It is assumed that the SST is not the dominant factor controlling the Ba carbonate chemistry in these algae, but nutrient and sedimentation rate are the main factors affecting the Ba variability in the coralline thalli analyzed in this study. The mean Ba content in *L. kotschyanum* f. *affine* was 0.48 µmol % $BaCO_3$ (SE 0.04), and in *Lithophyllum* sp. of Socotra was 0.4 µmol % $BaCO_3$ (SD 0.1).

In this study a different phyletic line (Lithophylloideae) from that of the species investigates to date (Hapalidiaceae), was studied as potential paleoclimatic archive. For the first time it has been demonstrated that variations in annual extension rates and elementary ratio of Mg/Ca, Li/Ca and Ba/Ca on Lithophylloideae thallus record historical climate and oceanographic variations of the NW Indian Ocean. Coralline red algae proxy records from the Gulf of Aden, South Red Sea and South Arabian Sea do not exist, and they differently recorded the climatic and oceanographic connections between the three studied areas, and even the ENSO teleconnections.

The *L. kotschyanum* f. *affine* from Balhaf recorded the quasi-multidecadal oscillations (~18 yrs) of the Asian monsoon system in the annual extension rate, Mg/Ca and Li/Ca

variability. The interannual variability (~5-6 yrs) of the monsoon system was recorded in the coralline Mg/Ca record by local hydrographic energy variability. Such periodicity of the Asian monsoon system on quasi-multidecadal and interannual time-scales was also recorded in the annual extension rates of the central Maldives corals (Storz and Gischler 2011a,b). Teleconnections with the Red Sea was recorded in the interannual range in the coralline extension rate by local SSS variation and southern Red Sea hydrographic energy variations. The coralline Li/Ca variations recorded, on a quasi-multidecadal time-scale, either the ENSO-force and the Asian monsoon variability. The coralline Ba/Ca ratio recorded on decadal time-scale (centered at 11 yrs) the signal of the Asian monsoon variability and the ENSO-force. Therefore, it is suggested that on the decadal time-scale, Li/Ca and Ba/Ca composition of the north-east Gulf of Aden coralline algae recorded simultaneous changes in the phase of the ENSO and the Asian monsoon.

The *Lithophyllum* sp. from Socotra recorded the decadal (11-12.5 yrs) ENSO-force in the annual extension rate variations, corresponding to those found in stable isotope composition of corals from Kenya by Cole et al. (2000). A multidecadal oscillation (centered at 23.5 yrs) of the Asian monsoon system has been recorded in the annual extension rate and Mg/Ca records by local SSS and south Indian rainfall variability. Moreover, the influence of the Red Sea oceanography on decadal time-scale (centered at 16.5 yrs) was found in the Mg/Ca and Li/Ca records by South Red Sea SSS and south Red Sea hydrographic energy variability. Simultaneous interannual (6.4 yrs) oscillations of the local hydrographic energy, local SSS and of the South Red Sea hydrographic energy were recorded in the Ba/Ca variability.

The growth rate and Ba/Ca ratio in *L. kotschyanum* f. *affine* from Balhaf increased with the increasing current and decreasing seasonal South India Rainfall (SIR), mirroring the variability of the Asian monsoon system and its consequences in term of water transparency, nutrient supply by upwelling, and rainfall regime. While Ba/Ca ratio in *Lithophyllum* sp. from

Socotra increase with the increasing seasonal South India Rainfall, mirroring the variability of the Asian monsoon system and its consequences in term of nutrient supply by upwelling. It is suggested that, on decadal time-scale, there are simultaneous changes in the South Red Sea oceanography, Asian monsoon system, and ENSO-force which are recorded in the annual extension rates and in the elementals ratio composition of the north-east Gulf of Aden and of the south-west Arabian Sea coralline red algae.

The extension rate and elementals ratio composition of *L. kotschyanum* f. *affine* from Kamaran recorded the quasi-decadal simultaneous variation of ENSO-force, oceanography and climate of southern Red Sea and rainfall of northern Red Sea. Thus, it is suggested that on a decadal time scale the coralline algae of Kamaran recorded the influence of the northern Red Sea and the ENSO-force on the oceanography and climate of the southern Red Sea. Klein et al. (1997) suggested that, on decadal time-scale, there are simultaneous changes in the phase of the Southern Oscillation, the south Asian monsoon and the Indian Ocean SST, which are recorded in the stable isotope composition of the southern Red Sea corals. Moreover, the Li/Ca variability on the coralline thallus recorded the interannual (2.5 yrs) ciclicity of southern Red Sea climate and oceanography by hydrographic energy and local precipitation variability.

Concluding, gridded datasets as used in this study resulted to be a limitation for historical climate and oceanography reconstructions. The simultaneous study of coralline algae climate proxies and of oceanographic variables by *in situ* instrumental datasets is crucial to an unequivocal and more detailed environmental reconstruction. Attached coralline algae resulted more suitable than rhodoliths for paleoclimate reconstruction, in agreement with Halfar et al. (2011), likely due to the occurrence of rhodolith growth cessation by temporary burial. The sample from Kamaran, southern Red Sea, was the less suitable for paleoclimate reconstruction because of its short life span and, thus, its limited temporal resolution. Hence, further long-term studies on coralline red algae of this area are strongly needed.

References

Adey WH (1965) The genus *Clathromorphum* (Corallinaceae) in the Gulf of Maine. Hydrobiologia 26:539-572

Adey WH, McKibbin DL (1970) Studies on the Maerl species *Phymatolithon calcareum* (Pallas) nov. comb. and *Lithothamnium coralloides* Crouan in the Ria de Vigo. Botanica Marina 13:100-106

Adey WH, Vassar JM (1975) Colonization, succession and growth rates of tropical crustose coralline algae (Rhodophyta, Cryptonemiales). Phycologia 14:55-69

Aiki H, Takahashi K, Yamagata T (2006) The Red Sea outflow regulated by the Indian monsoon. Continental Shelf Research 26:1448-1468

Alibert C, Kinsley L, Fallon SJ, McCulloch MT, Berkelmans R, McAllister F (2003) Source of trace element variability in Great Barrier Reef corals affected by the Burdekin flood plumes. Geochim Cosmochim Acta 67:231-246

Al Saafani MA (2008) Physical Oceanography of the Gulf of Aden. PhD Thesis, Goa University, India 213 pp

Al Saafani MA, Shenoi SSC (2004) Seasonal cycle of hydrography in the Bab el Mandab region, southern Red Sea. Proc. Indian Acad. Sci 3:269-280

Al Saafani MA, Shenoi SSC (2007) Water masses in the Gulf of Aden. Journal of Oceanography 63:1-14

Alverson K, Bradley R, Briffa K, Cole J, Hughes M, Larocque I, Pedersen T, Thompson L, Tudhope S (2001) A global paleoclimate observing system. Scienve 293:47-48

Baldwin MP, Grey LJ, Dunkerron TJ, Hamilton K, Haynes PH, Randel WJ, Holton JR, Alexander MJ, Hirota I, Horinouchi T, Jones DBA, Kinnersley JS, Marquardt C, Sato K, Takahashi M (2001) The quasi-biennial oscillation. Reviews of Geophysics 39:179-229

Basso D (1994) Study of living calcareous algae by a paleontological approach: the non-geniculate Corallinaceae (Rhodophyta) of the soft bottoms of the Tyrrhenian Sea (Western Mediterranean). The genera *Phymatolithon* Foslie nom. cons. and *Mesophyllum* Lemoine. Riv It Paleont Strat 100:575-596

Basso D, Fravega P, Vannucci G (1997) The taxonomy of *Lithothamnium ramosissimum* (Gümbel non Reuss) Conti and *Lithothamnium operculatum* (Conti) Conti (Rhodophyta, Corallinaceae). Facies 37:167-182

Basso D, Nalin R, Nelson CS (2009) Shallow-water *Sporolithon* rhodoliths from North Islands (New Zealand). PALAIOS 24:92-103

Basso D (2012) Carbonate production by calcareous red algae and global change. Geodiversitas 34:13-33

Benzoni F, Bianchi CN, Morri C (2003) Coral communities of the North western Gulf of Aden (Yemen): variation in framework building related to environmental factors and biotic conditions. Coral Reefs 22:475-484

Benzoni F, Basso D, Caragnano A, Rodondi G (2011) *Hydrolithon* spp. (Rhodophyta, Corallinales) overgrow live corals (Cnidaria, Scleractinia) in Yemen. Mar Biol 158:2419-2428

Bhatt US (1989) Circulation regimes of rainfall anomalies in the African-South Asian monsoon belt. J Climate 2:1133-1144

Blake C, Maggs CA (2003) Comparative growth rates and internal banding periodicity of maerl species (Corallinales, Rhodophyta) from northern Europe. Phycologia 42:606-612

Blakman RB, Tukey JW (1958) The measurement of power spectra from the point of view communication engineering. Dover publication, New York

Bressan G (1974) Rodoficee calcaree dei mari italiani. Boll Soc Adr Sc 59:1-132

Brock JC, McClain CR, Hay WW (1992) A southwest monsoon hydrographic climatology for the northwestern Arabian Sea. Journal of Geophysical Research 97:9455-9465

Brock J, Sathyendranath S, Platt T (1993) Modelling the seasonality of subsurface light and primary production in the Arabian Sea. Marine Ecology Progress Series 101:209-221

Cabioch J (1966) Contribution à l'étude morphologique anatomique et systématique de deux Mélobésiées: *Lithothamnium calcareum* (Pallas) Areschoug et *Lithothamnium corallioides* Crouan. Botanica Marina 9:33-53

Cabioch J, Giraud G (1986) Structural spects of biomineralization in the coralline algae (calcified Rhodophyceae). *In*: Biomineralization in lower plants and animals, (*ed*) BSC Leadbeater & R Reading. Clarendon press, Oxford

Caragnano A, Colombo F, Rodondi G, Basso D (2009) 3-D distribution of nongeniculate Corallinales: a case study from a reef crest of South Sinai (Red Sea, Egypt). Coral Reefs 28:881-891

Carton JA, Giese BS (2008) A reanalysis of ocean climate using Simple Ocean Data Assimilation (SODA), Mon. Weather Rev. 136:2999-3017

Charles CD, Hunter DE, Fairbanks RG (1997) Interaction between the ENSO and the Asian monsoon in a coral record of tropical climate. Science 277:925-928

Chave KE (1954) Aspects of biogeochemistry of magnesium. a: calcareous marine organisms. J. Geol. 62:266-283

Chave KE, Wheeler BDJr (1965) Mineralogic change during growth in the red alga, *Clathromorphum compactum*. Science 621

Cheung C, DeVantier L (2006) Socotra - A natural history of the islands and their people. Van Damme K (Science Editor). Odyssey Books and Guides. Airphoto International Ltd., Hong Kong

Cole JE, Dunbar RB, McClanahan TR, Muthiga NA (2000) Tropical Pacific forcing of decadal SST variability in the western Indian Ocean over the past two centuries. Science 287:617-619

Conversi A, Hammed S (1998) Common signals between physical and atmospheric variables and zooplankton biomass in the subarctic Pacific. ICES J Mar Sci 55:739-747

Crueger T, Zinke J, Pfeiffer M (2009) Patterns of Pacific decadal variability recorded by Indian Ocean corals. Int J Earth Sci 98:42-52

Davis RA (1991) Oceanography: an introduction to the marine environment. 2nd Ed, Dubuque, Brown WmC Publishers

Delaney ML, Bé AWH, Boyle EA (1985) Li, Sr, Mg, and Na in foraminiferal calcite shells from laboratory culture, sediment traps, and sediment cores. Geochim Cosmochim Acta 49:1327-1341

Delaney ML, Popp BM, Lepzelter CG, Anderson TF, (1989) Lithium-to-calcium ratios in modern, Cenozoic and Paleozoic articulate brachiopod shells. Paleoceanography 4:681-691

Dethier MN, Steneck R (2001) Growth and persistence of diverse intertidal crusts: survival of the slow in a fast-paced world. Mar Ecol Prog Ser 223:89-100

Edmond JM, Measures C, McDuff RE, Chan LH, Collier R, Grant B, Gordon LI, Corliss JB (1979) Ridge crest hydrothermal activity and the balances of the major and minor elements in the ocean: the Galapagos data. Earth Planet Sci Lett 46:1-18

Edwards FJ (1987) Climate and Oceanography. *In*: Red Sea (Key Environment), Pergamon press,

Oxford
Eshel G, Cane MA, Blumenthal MB (1994) Model of sub-surface, intermediate, and deep water renewal in the Red Sea. J Geophys Res 99:15,941-15,952
Fabricius K, De'ath G (2001) Environmental factors associated with the spatial distribution of crustose coralline algae on the Great Barrier Reef. coral Reefs 19:303-309
Feldman G, Kuring NNgC, Esaias W, McClaine C, Elrod J, Maynard N, Endres D, Evans R, Brown J, Walsh S, Carle M, Podesta G (1989) Ocean-color: availability of the global data set. EOS (Trans Am Geophys Un) 70:634
Felis T, Pätzold J, Loya Y, Fine M, Nawar AH (2000) A coral oxygen isotope record from the northern Red Sea documenting NAO, ENSO, and North Pacific teleconnections on Middle East climate variability since the year 1750. Paleoceanography 15:679-694
Foster M (2001) Rhodoliths: between rocks and soft places. J. Phycol. 37:659-667
Fragoso D, Ramírez-Cahero F, Rodríguez-Galván A, Hernández-Reyes R, Heredia A, Rodríguez D, Aguilar-Franco M, Bucio L, Basiuk VA (2010) Characterization of the $CaCO_3$ biomineral in coralline red algae (Corallinales) from the Pacific coast of Mexico. Cenc. Mar. 36:41-58
Frantz BR, Kashgarian M, Coale KH, Foster MS (2000) Growth rate and potential climate record from a rhodolith using ^{14}C accelerator mass spectrometry. Limnol. Oceanogr. 45:1773-1777
Freiwald A, Henrich R (1994) Reefal coralline algal build-ups within the Arctic Circle: morphology and sedimentary dynamics under extreme environmental seasonality. Sedimentology 41:963-984
Goodwin DH, Schöne BR, Dettman DL (2003) Resolution and fidelity of oxygen isotopes as paleotemperature proxies in bivalve mollusk shells: Models and observations. Palaios 18:110-125
Halfar J, Zack T, Kronz A, Zachos JC (2000) Growth and high-resolution paleoenvironmental signals of rhodoliths (coralline red algae): a new biogenic archive. Journal of Geophysical research 105:22,107-22,116
Halfar J, Steneck R, Schöne BR, Moore GWK, Joachimski M, Kronz A, Fietzke J, Estes J (2007) Coralline alga reveals first marine record of subarctic North Pacific climate change. Geophysical Research Letters 34 LO7702, doi:10.1029/2006GL028811
Halfar J, Steneck RS, Joachimski M, Kronz A, Wanamaker ADJr (2008) Coralline red algae as high-resolution climate records. Geology 36:463-466
Halfar J, Hetzinger S, Adey W, Zack T, Gamboa G, Kunz B, Williams B, Jacob DE (2011) Coralline algal growth-increment widths archive North Atlantic climate variability. Palaeogeography, Palaeoclimatology, Palaeoecology 302:71-80
Hall JM, Chan LH (2004) Li/Ca in multiple species of benthic and planktonic foraminifera: thermocline, latitudinal, and glacial-interglacial variation. Geochim Cosmochim Acta 68:529-545
Head SM (1987) Introduction. *In*: Red Sea (Key Environment), Pergamon press, Oxford
Henrich R, Freiwald A, Wehrmann A, Schäfer P, Samtleben C, Zankl H (1996) Nord cold-water carbonates:occurences and controls. In Global and Regional Controls on Biogenic Sedimentation (*Eds*) Reitner J, Neuweiler F, Gunkel F, Göttinger Arbeiten Geol. Paläontol., Sb 2, Göttinger, Germany
Hetzinger S, Halfar J, Kronz, A, Steneck RS, Adey W, Lebednik PA, Schöne BR (2009) High-resolution Mg/Ca ratios in a coralline red alga as a proxy for bering sea temperature variations from 1902 to 1967. PALAIOS 24:406-412

Hetzinger S, Halfar J, Zack T, Gamboa G, Jacob DE, Kunz BE, Kronz A, Adey W, Lebednik PA, Steneck RS (2011) High resolution analysis of trace elements in crustose coralline algae from the North Atlantic and North Pacific by laser ablation ICP-MS. Palaeogeography, Palaeoclimatology, Palaeoecology 302:81-94

Irvine LM, Chamberlain YM (1994) Seaweeds of the British Isles. Volume 1 *Rhodophyta* Part 2B *Corallinales, Hildenbrandiales*. HMSO, London

James RH, Austin WEN (2008) Biogeochemical controls on palaeoceanographic environmental proxies: a review. *In*: Biogeochemical controls on palaeoceanographic environmental proxies, (*eds*) Austin WEN & James RH. Geological Society, London, Special Publications 303:3-32

Jochum KP, Nohl U, Herwig K, Lammel E, Stoll B, Hofmann AW (2006) GeoReM: a new geochemical database for reference materials and standards. Geostandards and Geoanalytical Research 29:333-338

Johansen HW (1981) Coralline algae, a first synthesis. CRC Press, Boca Raton, FL

Kamenos NA, Cusack M, Moore PG (2008) coralline algae are global palaeothermometers with bi-weekly resolution. Geochim Cosmochim Acta 72:771-779

Kamenos NA, Law A (2010) Temperature controls on coralline algal skeletal growth. Journal of Phycology 46:331-335

Klein R, Tudhope AW, Chilcott CP, Pätzold J, Abdulkarim Z, Fine M, Fallick AE, Loya Y (1997) Evaluating southern Red Sea corals as a proxy record for the Asian monsoon. Earth and Planetary Science Letters 148:381-394

Kucharski F, Molteni F, and Yoo JH (2006) SST forcing of decadal Indian Monsoon rainfall variability. Geophys Res Lett doi:10.1029/2005GL025371

Kuffner IB, Andersson AJ, Jokiel PL, Rodgers KS, Mackenzie FT (2007) Decreased abundance of crustose coralline algae due to ocean acidification. Nature doi:10.1038/ngeo100

Lea DW (2003) Elemental and isotopic proxies of marine temperatures. In The Oceans and Marine Geochemistry (Elderfield H Ed). Vol 6, Treatise on Geochemistry:Elsevier-Pergamon, Oxford

Lea DW, Shen GT, Boyle EA (1989) Coralline barium records temporal variability in equatorial Pacific upwelling. Nature 340:373-376

Lea DW, Boyle EA (1993) Determination of carbonate-bound barium in foraminifera and corals by isotope dilution plasma-mass spectrometry. Chemical Geology 103:73-84

Lea DW, Martin PA (1996) A rapid mass spectrometric method for the simultaneous analysis of barium, cadmium, and strontium in foraminifera shells. Geochim Cosmochim Acta 60:3143-3149

Le Gall L, Payri CE, Bittner CE, Saunders GW (2009) Multigene polygenetic analyses support recognition of the Sporolithales, ord. nov. Molecular Phylogenetics and Evolution 54:302-305

Mann S (1983) Mineralization in biological systems. Structural Bonding 54:125-174

Marriott CS, Henderson GM, Belshaw NS, Tudhope AW (2004) Temperature dependence of δ^7Li, δ^{44}Ca and Li/Ca during growth of calcium carbonate. Earth and Planetary Science Letters 222:615-624

Mecking S, Warner MJ (1999) Ventilation of Red Sea water with respect to chlorofluorocarbons. Journal of Geophysical Research 104:11087-11097

McConnaughey T (1989) ^{13}C and ^{18}O isotopic disequilibrium in biological carbonates: I. Patterns. Geochim Cosmochim Acta 53:151-162

McCulloch M, Fallon S, Wyndham T, Hendy E, Lough J, Barnes D (2003) Coral record of

increased sediment flux to the inner Great Barrier Reef since European settlement. Nature 421:727-730
Mertz-Kraus R, Brachert TC, Reuter M (2008) *Tarbellastraea* (Scleractinia): a new stable isotope archive for Late Miocene paleoenviroments in the Mediterranean. PALAEO 257:294-307
Moberly RJ (1968) Composition of magnesian calcites of algal and pelecypods by electron microprobe analysis. Sedimentology 11:61-82
Montagna P, McCuloch M, Mazzoli C, Silenzi S, Odorico R (2007) The non-tropical coral *Cladocora caespitosa* as the new climate archive for the Mediterranean: high-resolution (~weekly) trace element systematics. Quaternary Science Reviews 26:441-462
Montagna P, López Correa M, Rüggeberg A, McCulloch M, Rodolfo-Metalpa R, Dullo WC, Ferrier-Pagès C, Freiwald A, Henderson GM, Mazzoli C, Russo S, Silenzi S, Taviani M (2008) Coral Li/Ca in micro-structural domains as a temeprature proxy. In: Geochim. Cosmochim. Acta. 72, pp. A645 Supplement 1. Pergamon-elsevier Science Ltd, 2008.
O'Brien TP, McCully ME (1981) The study of plant structure Principles and selected methods. Melbourne, Australia: Termacarphi.
Paillard D, Labeyrie L, Yiou P (1996) Macintosh program performs time series analysis. Eos Trans AGU 77:379
Pfeiffer M, Dullo WC (2006) Monsoon-induced cooling of the western equatorial Indian Ocean as recorded in coral oxygen isotope records from the Seychelles covering the period of 1840-1994 AD. Quat Sci Rev 25:993-1009
Pfeiffer M, Dullo WC, Eisenhauer A (2004a) Variability of the intertropical convergence zone recorded in coral isotopic records from the central Indian Ocean. Quat Res 61:245-255
Pfeiffer M, Timm O, Dullo WC (2004b) Oceanic forcing of interannual and multidecadal climate variability in the southwestern Indian Ocean: evidence from a 160 year coral isotopic record (La Réunion, 55°E, 21°S) Paleoceanography doi:10.1029/2003PA000964
Philippi RA (1837) Beweis, dass die Nulliporen Pflanzen sind. Archiv für Naturgeschichte 3:387-393
Pueschel CM, Cole KM (1982) Rhodophycean pit plugs: an ultrastructural survey with taxonomic implications. Am J Bot 69:703-720
Qasim SZ (1982) Oceanography of the northern Arabian Sea. Deep Sea Research 29:1041-1068
Rayner NA, Parker DE, Horton EB, Folland CK, Alexander LV, Rowell DP, Kent EC, Kaplan A (2003) Global analyses of sea surface temperature, sea ice, and night marine air temperature since the late nineteenth century. J. Geophys. Res. 108/(D14), 44017, doi:10.1029/2002JD002670
Ries JB (2006) Mg fractionation in crustose coralline algae:geochemical, biological and sedimentological implications of secular variation in Mg/Ca ratio of seawater. Geochim. Cosmochim. Acta 70:891-900
Rollion-Bard C, Vigier N, Meibom A, blamart D, Reynaud S, Rodolfo-Metalpa R, Martin S, Gattuso J-P (2009) Effect of environmental conditions and skeletal ultrastructure on the Li isotopic composition of scleractinian corals. Earth and Planetary Science Letters 286:63-70
Rudolf B, Schneider U (2005) Calculation of gridded precipitation data for the global land-surface using in-situ gauge observations. Proceeding of the 2ndworkshop of the International Precipitation Working Group IPWG, Monterey October 2004,EUMETSAT, ISBN 92-9110-070-6, ISSN 1727-432X, 231-247
Schöne BR, Zhang Z, Gillikin DP, Jacob D, Tütken T, Garbe-Schönberg D, McConnaughey T, Soldati A (2010) Effect of organic matrices on the determination of minor elements (Mg, Sr) and Mg/Ca and Sr/Ca ratios of aragonitic bivalves shells (*Arctica islandica*) - comparison of

ICP-OES and LA-ICP-MS data. Geochemical journal 44:23-37
Schöne BR, Zhang Z, Radermacher P, Thébault J, Jacob DE, Nunn EV, Maurer AF (2011) Sr/Ca and Mg/Ca ratios of old-grown, long-lived bivalve shells (*Arctica islandica*) and their function as paleotemperature proxies. Palaeogeography, Palaeoclimatology, Palaeoecology 302:52-64
Sheppard C, Price A, Roberts C (1992) Marine ecology of the Arabian region. Patterns and processes in extreme tropical environments. Academic Press, London
Smith AM, Sutherland JE, Kregting L, Farr TJ, Winter DJ (2012) Phylomineralogy of the coralline red algae: correlation of skeletal mineralogy with molecular phylogeny. Phytochemistry http://dx.doi.org/10.1016/j.phytochem.2012.06.003
Sontakke NA, Singh N, Singh HN (2008) Instrumental period rainfall series of the Indian region (1813-2005): revised reconstruction, update and analysis. The Holocene 18:1055-1066
Spötl C, Vennemann T (2003) Continuous-flow isotope ratio mass spectrometric analysis of carbonate minerals. Rapid Communications inMass Spectrometry 17:1004-1006
Steneck RS (1983) Escalating herbivory and resulting adaptive trends in calcareous algae. Paleobiology 9:45-63
Steneck RS, Adey WH (1976) The role of environment in control of morphology in *Lithophyllum congestum*, a Caribbean algal ridge builder. Botanica Marina 19:197-215
Stoffyn-Egli P, Mackenzie FT (1984) Mass balance of dissolved lithium in the oceans. Geochim Cosmochim Acta 48:859-872
Storz D, Gischler E (2011a) Coral extension rates in the NW Indian Ocean I: reconstruction of 20th century SST variability and monsoon current strength. Geo-Mar Lett 31:141-154
Storz D, Gischler E (2011b) Coral extension rates in the NW Indian Ocean II: reconstruction of 20th centuary Indian monsoon strength and rainfall over India. Geo-Mar Lett 31:155-162
Tiwari K, Rao KNN (2004) Signature of ENSO signals in the coral growth rate record of Arabian Sea and Indian Monsoon. Pure and Applied Geophysics 161:413-427
Torrence C, Webster PJ (1999) Interdecadal changes in the ENSO-monsoon system. J Clim 12:2679-2690
Tourre YM, White WB (1995) ENSO signals in global upper ocean temperature. Journal of Physical Oceanography 25:1317-1332
Trenberth KE (1997) The definition of El Niño. Bull Am Meteorol Soc 78:2771-2777
Tudhope AW, Lea DW, Shimmield GB, Chilcott CP, Head S (1996) Monsoon climate and Arabian Sea Coastal upwelling recorded in massive corals from southern Oman. PALAIOS 11:347-361
Van Oldenborgh GJ, Burgers G (2001) The effects of El Niño on precipitation and temperature, an update. KNMI preprint 2001-07. The KNMI Climate Explorer is available at http://climexp.knmi.nl
Vecchi GA, Xie S-P, Fischer AS (2004) Ocean-atmosphere covariability in the western Arabian Sea. Journal of Climate 17:1213-1224
Zinke J, Dullo WC, Heiss GA, Eisenhauer A (2004) ENSO and Indian Ocean subtropical dipole variability is recorded in a coral record off southwest Madagascar for the period 1659-1995. Earth Planet Sci Lett 228:177-194
Walker R, Moss B (1984) Mode of attachment of six epilithic crustose Corallinaceae (Rhodophyta). Phycologia 23:321-329
Webster PJ, Magaña VO, Palmer TN, Shukla J, Tomas RA, Yanai M, and Yasunari T (1998) Monsoon: processes, predictability, and the prospects for prediction. J Geophys Res 103:14451-14510

Webster PJ, Moore MA, Loschnigg JP, Leben RR (1999) Coupled ocean-atmosphere dynamics in the Indian Ocean during 1997-98. Nature 401:356-359

Woelkerling J (1988) The coralline red algae: an analysis of the genera and subfamilies of Nongeniculate Corallinaceae. British Museum (Natural History) Oxford University Press, London

Weiner S, Dove PM (2003) An overview of biomineralization processes and the problem of the vital effect. *In*: Dove PM, De Yoreo JJ, Weiner S (*eds*) Biomineralization. Reviews in Mineralogy and Geochemistry 54:1-29

Woodruff SD, Woewy SJ, Lubker ZJi, Freeman JE, Berry DI, Brohan P, Kent EC, Reynolds RW, Smith SR, Wilkinson C (2011) ICOADS Release 2.5: extension and enhancements to the surface marine meteorological archive. Int. J. Climatol 31:951-967